1976

Determination of the blade-element performance of a small transonic rotor.

Hawkins, Wayne Randolph

Monterey, California. Naval Postgraduate School

http://hdl.handle.net/10945/17727

DETERMINATION OF THE BLADE-ELEMENT PERFORMANCE OF A SMALL TRANSONIC ROTOR

Wayne Randolph Hawkins

NAVAL POSTGRADUATE SCHOOL
Monterey, California

THESIS

DETERMINATION OF THE BLADE-ELEMENT
PERFORMANCE OF A SMALL TRANSONIC ROTOR

by

Wayne Randolph Hawkins

December 1976

Thesis Advisor: R. P. Shreeve

Approved for public release; distribution unlimited.

SECURITY CLASSIFICATION OF THIS PAGE (When Data Entered)

REPORT DOCUMENTATION PAGE		READ INSTRUCTIONS BEFORE COMPLETING FORM
1. REPORT NUMBER	2. GOVT ACCESSION NO.	3. RECIPIENT'S CATALOG NUMBER
4. TITLE (and Subtitle) Determination of the Blade-Element Performance of a Small Transonic Rotor		5. TYPE OF REPORT & PERIOD COVERED Master's Thesis December 1976
		6. PERFORMING ORG. REPORT NUMBER
7. AUTHOR(s) Wayne Randolph Hawkins		8. CONTRACT OR GRANT NUMBER(s)
9. PERFORMING ORGANIZATION NAME AND ADDRESS Naval Postgraduate School Monterey, California 93940		10. PROGRAM ELEMENT, PROJECT, TASK AREA & WORK UNIT NUMBERS
11. CONTROLLING OFFICE NAME AND ADDRESS Naval Postgraduate School Monterey, California 93940		12. REPORT DATE December 1976
		13. NUMBER OF PAGES 114
14. MONITORING AGENCY NAME & ADDRESS(if different from Controlling Office)		15. SECURITY CLASS. (of this report) Unclassified
		15a. DECLASSIFICATION/DOWNGRADING SCHEDULE

16. DISTRIBUTION STATEMENT (of this Report)

Approved for Public Release; Distribution Unlimited

17. DISTRIBUTION STATEMENT (of the abstract entered in Block 20, if different from Report)

18. SUPPLEMENTARY NOTES

19. KEY WORDS (Continue on reverse side if necessary and identify by block number)

Compressor measurements
Transonic compressor
Flow probes
Pneumatic probes
Blade-element performance

20. ABSTRACT (Continue on reverse side if necessary and identify by block number)

The blade-element performance of a small transonic compressor rotor operating at high subsonic speeds is reported. Measurements were made downstream using a small calibrated pneumatic probe, with simultaneous measurements of total pressure, velocity, turning angle, and temperature. In addition, a program is presented to calculate blade-element performance based on empirical data contained in NASA SP-36.

Determination of the Blade-Element Performance of a Small Transonic Rotor

by

Wayne Randolph Hawkins
Lieutenant, United States Navy

Submitted in partial fulfillment of the requirements for the degree of

MASTER OF SCIENCE IN AERONAUTICAL ENGINEERING

from the

NAVAL POSTGRADUATE SCHOOL

December 1976

ABSTRACT

The blade-element performance of a small transonic compressor rotor operating at high subsonic speeds is reported. Measurements were made downstream using a small calibrated pneumatic probe, with simultaneous measurements of total pressure, velocity, turning angle, pitch angle, and temperature. In addition, a program is presented to calculate blade-element performance based on empirical data contained in NASA SP-36.

TABLE OF CONTENTS

LIST OF TABLES

LIST OF ILLUSTRATIONS

TABLE OF SYMBOLS

Latin

a	Speed of sound based on stagnation conditions, ft./sec.
C	Chord length
D	Diffusion factor
F_ϕ	Combination probe calibration factor
F_θ	Combination probe calibration factor
D_m	Diameter of rotor profile
E	Chord with sharp leading and trailing edges
H	Angle of cone through stacking radius
i	Incidence angle; angle between inlet-air direction and tangent to blade mean aamber line at leading edge, degrees.
$(i_o)_{10}$	Zero-camber reference minimum-loss incidence angle
$(i_{ref})_{2-D}$	Two-dimensional reference incidence angle
i_{3-D}	Three-dimensional reference incidence angle
$(K_\delta)_{SH}$	Correction for blade shape
$(K_i)_t$	Correction for blade thickness
$(K_i)_t$	Correction for the effect of blade thickness for zero-camber reference minimum-loss incidence
$(K_\delta)_t$	Correction for effect of blade thickness for zero-camber reference deviation angle
m	Slope factor for circular-arc-mean line blades
M	Mach number
M_u	Relative Mach number
n	Slope factor in incidence-angle relation
P	Pressure

R	Blade
S	Blade spacing
t	Blade maximum profile thickness
T	Temperature
U	Tangential rotor velocity
V	Velocity
W	Relative Velocity
W^*	Referred flow rate
X	Non-dimensional or limiting velocity

<u>Greek</u>

Δ	Finite difference
α	Angle of attack, angle between inlet-air direction and blade chord; or, flow angle with respect to axis
β	Air angle, angle between air velocity and axial direction.
γ	Stagger angle
γ'	Ratio of specific heats
δ	Deviation angle, angle between outlet-air direction and tangent to blade mean camber line at trailing edge
$(\delta_{ref})_{2-D}$	Reference two-dimensional deviation angle
δ_{3-D}	Three-dimensional deviation angle
ϵ	Fractional error
ϕ	Flow pitch angle
ϕ'	Blade camber angle
ρ	Density of air
σ	Blade solidity
Φ	Flow function

$\bar{\Phi}$	Normalized flow function
$\bar{\omega}'$	Rotor loss coefficient

<u>Subscripts</u>

C_L	Centerline value
i	i^{th} value
ref	Reference
t	Total or Stagnation value
1	Upstream of the rotor
2	Downstream of the rotor

ACKNOWLEDGMENT

The experimentation and analysis reported in this paper would not have been possible without the endless counseling and guidance of my thesis advisor, Associate Professor R. P. Shreeve. I wish to express my gratitude for his seemingly infinite patience and genuine interest in this field.

The preparation of experiments, calibration of equipment, and overall technical expertise were provided by Mr. J. E. Hammer. His practical knowledge, coupled with an engineering background, made the transition from theory to application a much simpler process.

I. INTRODUCTION

The study reported here is part of an ongoing program at the Naval Postgraduate School to determine the performance of a transonic compressor stage. The overall goal of the program is to develop the knowledge necessary to design compressors with multiple transonic stages which are efficient, light in weight, and free of flutter problems. It has long been appreciated that increasing the wheel speed and relative air velocities in axial compressors would result in fewer stages for a given energy addition. However, in order to achieve high overall efficiencies in multiple axial stages, the ability to predict the behaviour of a single stage correctly must be shown. The purpose of this study was to measure the blade-element performance of a transonic compressor rotor operating at high subsonic speeds and to compare the measurements with the performance calculated according to the method given in Reference 1.

The transonic compressor and drive turbine were designed by Dr. M. H. Vavra. The program is supported by the Naval Air System Command, Code 310, through the office of Dr. H. J. Mueller.

To determine the blade-element performance of a compressor blade row, it is necessary to evaluate radial velocity and angle distributions into and out of the blade row. In a transonic compressor, at or near design speed, the unsteady nature of the flows with large pressure amplitudes

complicates the problem. In addition, the possibility that wakes might induce vibrations in the highly stressed blades prohibit the use of probes upstream of the rotor. Measurements can be made downstream of the rotor; however, since the flow area is small, boundary effects on probe measurements can be significant.

In order to carry out the present study, a small combination temperature-pneumatic probe was designed by Dodge (Ref. 2) specifically to be used immediately downstream of the rotor. In previous work, the flow upstream of the rotor was determined at different flow rates (Ref. 3). It was left to the present work to represent the inlet flow field analytically, to calibrate the combination probe for boundary effects, and both to measure and to calculate the rotor blade element performance.

In this report the transonic compressor and test rig are first described in Section II. The method of approach and program of measurements are described in Section III.

The results of the measurements are then described and discussed in Section IV, and conclusions are given in Section V. In order to maintain a clear presentation of the relevant results, the details of the calculations and of the calibration measurements are given in separate Appendices.

II. THE TRANSONIC COMPRESSOR

A. DESCRIPTION

A drawing of the compressor test rig is shown in Fig. 1. The test rig consists of an air-turbine drive unit and an induction section containing a filter, a throttle, a settling chamber and a flow measuring nozzle. The air turbine is designed to deliver 450 horsepower at 30,000 RPM. The relative blade tip Mach number of the rotor at design point is 1.5. The compressor flow rate is controlled by an electric-hydraulic rotating throttle plate. Power is provided by a compressed air supply from an Allis-Chalmers multi-stage axial compressor. A complete description of the Turbopropulsion Laboratory and test facilities is contained in Ref. 4. A drawing of the transonic compressor is shown in Fig. 2.

The blade design for the transonic compressor rotor was derived from circular-arc elements wrapped on six conical surfaces. The outer surface (at the case wall) is a cylinder. The blading geometry is given in Fig. 3. The blade pressure side is flat and the suction side is a circular-arc. The solidity is fairly constant with a value of 1.35 at the mid-streamline. The outer diameter of the rotor blade is 11 inches with a channel height of 1.92 inches downstream and a radius ratio at the inlet face of 0.5.

B. INSTRUMENTATION

The transonic compressor is equipped with stationary probes to provide routine performance data. Triple redundancy is provided in the measurement of the power; either the mass flow rate and temperature drop through the drive turbine, or the mass flow rate and temperature increase through the compressor, or the speed and the measurement of torque can be used. The torque is measured by strain gauges on flexures against which the stator assembly is free to rotate. Flow straighteners before and after the stage ensure that the stator and rotor torques are equal. The method based on torque and speed is the most accurate since it is independent of flow profiles. Static pressure taps were installed on both outer and inner walls of the compressor casing. The rotative speed of the test rotor was determined by a magnetic flux cutter and electronic counter. The fixed instrumentation will not be described further. It was used in the present tests only to provide the reference conditions for the survey measurements. The compressor cylindrical casing was modified to accommodate a variety of probes and sensors which may be required in the program of steady state and unsteady flow pressure measurements. The casing can be rotated to position probes in the peripheral direction.

The rotor exit survey measurements reported here were obtained using a combination probe (Fig. 4) designed by Lt. F. J. Dodge (Ref. 2). The combination probe, following

calibration, was used to determine total pressure rise, total temperature rise, and flow velocity in magnitude and direction. In addition, static pressure was measured using the wedge static probe shown in Fig. 5, which was based on a NASA design provided by Mr. Lloyd N. Krause of NASA Lewis Research Center. Each probe had two "static pressure" sensors which, if the probes were rotated until the indicated static pressures were equal, allowed the probes to be aligned with the flow direction. It was determined that better accuracy could be attained, however, by aligning both probes to the flow direction sensed by the combination probe. This was because the sensors on the wedge probe were separated in the radial direction. A chromel-constantan fine-wire thermocouple in the combination probe was used in conjunction with a similar sensor mounted upstream of the rotor to measure, differentially, the total temperature rise.

Radial surveys were taken at a fixed peripheral case angle by manually positioning the probe in the flow using a United Sensor traverse unit, manually rotating the combination probe to balance indicated static pressures, and adjusting the wedge probe to the same angle. All pressures were measured by a calibrated transducer in a Scanivalve arrangement. (A capability exists to remotely control probe movement and balancing through the use of a programmable microprocessor and a probe traversing mechanism designed by Lt. D. D. Patton (Ref. 5). Remote operations will be needed as higher operational speeds are developed.)

C. DATA ACQUISITION AND REDUCTION

Pressures, temperatures, rotational speed and other data were scanned and punched onto paper tape by a B & F Model 24133 solid state data acquisition system. A complete description of this system is contained in Ref. 4. The punched tape data was processed using Hewlett-Packard Model 9830A programmable calculator data system. The data was transferred to a Model 9867B mass memory disk unit for storage prior to data reduction. The data facilities are shown in Fig. 6.

A program, designated "WH001" was written to transfer raw data from tapes to the mass memory. A second program "HAWK1" was written to calculate temperature, corrected non-dimensional velocity, turning angle, total pressure, and static pressure. Two other programs, used in sequence ("REPRO1" and "RA5C") completed the data reduction process. Plotting routines developed by Dr. R. P. Shreeve were adapted to plot distributions of Mach number, pressure rise, temperature rise, flow angle, and loss coefficients, using the X-Y plotter.

In reducing the probe measurements to obtain velocities and loss data, the thermocouple calibration reported in Ref. 2 was used. However, new pneumatic calibrations were performed and corrections were derived as described in Appendix B.

III. METHOD OF APPROACH

A. METHOD

The usual approach to the design of axial compressors is described in Ref. 1. The method involves combining an axi-symmetric through-flow analysis, which prescribes the stream surfaces, with a two-dimensional cascade performance calculation which determines the required blading geometry on those surfaces. The blading is generally layed out on conical approximations of the prescribed stream surfaces.

When a new machine is built, the opportunity is there to compare the actual blade element performance established by measurement with that which can be calculated by applying the design approach. The comparison can be used to derive corrections for use in future designs, and it is particularly useful to obtain data for new blade profiles.

The transonic compressor investigated here was designed using the above approach, and the resulting blading is shown in Fig. 3. It is to be noted that the rotor blading is not typical in design. In order to establish the blade element performance of a rotor experimentally, measurements should be made of the flow into and out of the rotor on the stream surfaces on which the blading profiles are prescribed. However, it is desirable not to operate at high wheel speeds with strong wakes from upstream probes, and so in the present work a method of prescribing the inlet flow field from measurements of only total flow rate and wheel speed was derived. The method is given in the following section.

The flow downstream of the rotor was determined using two calibrated probes. The calibration and corrections required for the probes are described in Appendix B. From the rotor exit flow measurements, the blade element loss coefficient and the local deviation angle were calculated.

Finally, as described in Appendix A. the method of calculating deviation angle and loss coefficient given in Chapter 7 of Reference 1 was programmed for the Hewlett-Packard Model 9830A calculator so that these quantities could be computed for four blade element surfaces at any given compressor flow rate and operating speed.

B. INLET FLOW FIELD REPRESENTATION

The flow field ahead of the rotor was measured in early tests using a calibrated pneumatic probe (Ref. 3). The measurements were compared with the results of a compressible finite difference calculation reported in Reference 6, and blockage factors were derived to relate the inviscid calculations to the measured flow field.

The method adopted here was based only on Anderson's measured data. As described in Appendix C a polynomial relation was found to correlate the measured velocity distributions away from the hub and tip regions. The flow function in this region was therefore calculated using Eq. C(3) and Eq. C(7).

C. USE OF FLOW PROBES

Pressure probes are designed to exploit the distribution of pressure which occurs over a body immersed in a moving fluid. These pressure variations depend mainly on the flow velocity so that with a carefully selected choice of body shape, having multiple sensors, a probe can be calibrated to determine flow velocity. The relationship between pressure and velocity must be established over a range of Mach numbers. In addition to flow velocity in magnitude and direction, the distributions of stagnation temperature, and total and static pressure are usually required. The probe designed by Dodge and reported in Ref. 2 is a small lightweight probe of aerodynamic design which allows these quantities to be determined at any position in the flow.

In order to provide an independent measurement to compare with the combination probe, the static pressure distribution was measured with a second probe, and static pressures were also recorded at hub and tip wall taps. The wedge static probe shown in Fig. 5 has the favorable characteristic that when it is aligned with the flow in the yaw plane (by balancing the pressures measured on the wedge surfaces) the indicated static pressure is relatively insensitive to angle variation in the pitch plane. As reported in Ref. 7 this type of probe has been used successfully up to a Mach number of 1.6. Further, for measurements in the transonic regime the probe has favorable characteristics. If the leading edge is sharp and the wedge is small, Ref. 7 states that the

calibration is also independent of Mach number. This was found to be the case for the probe used in the present work.

D. PROGRAM OF MEASUREMENTS

The combination probe and the wedge static probe were mounted at the exit of the rotor with a peripheral separation of 120 degrees. Four surveys were conducted at 50 percent of design speed, at throttle conditions varying from near surge to maximum flow rate. Case angle for the first survey was 345 degrees. Subsequent surveys were conducted at a case angle of 357 degrees because it was determined that peripheral variations induced by the stator blading were felt least at this setting. RPM was the same (15,230 ± 30) for all four runs.

The procedure in each survey was to move the probes inward simultaneously, balance the combination probe to sense the flow angle, and then set the wedge probe to the measured angle. A data scan was taken, and the procedure was repeated at 0.1 inch intervals. Because of the hooked geometry of the wedge probe, measurements with this probe of static pressure could not be made closer than .6 inches to the outer wall boundary. Static pressures were derived for the complete passage through the use of the combination probe calibration. Wall static pressure measurements at the hub and tip were also recorded. Yaw angle and linear displacement were recorded manually. All other data were automatically recorded by the data recording system. Pressures were recorded to an accuracy of .1 inches of water.

V. RESULTS AND DISCUSSION

A. TIME-AVERAGED FLOW FIELD

The distributions of total pressure rise, total temperature rise, Mach number and flow angle measured using the combination probe downstream of the rotor are shown in Figs. 7, 8, 9, and 10.

The total pressure rise was nearly constant with radius, whereas the temperature rise was indicated to be larger toward the tip. The larger indicated temperature rise near the case wall might be caused by higher temperatures in the incoming case wall boundary layer. Both the Mach number and the flow angle increase toward the hub, so that the through-flow velocity tends to remain constant. The results for the flow angle are qualitatively consistent; however, a large decrease can be observed in the magnitude of the flow angle for the open throttle case (Fig. 8). No definitive explanation was found, but as will be shown later this measurement leads to inconsistencies in the correlation of blade element performance.

The velocity and pitch angle distributions, which were derived from the probe calibration and corrected for boundary effects (Appendix B), are shown in Fig. 11 and Fig. 12. The pitch angle shows a smooth variation between the values of the wall slopes at the hub and tip boundaries. It is shown in Appendix B that the pitch angle is determined to only $1\frac{1}{2}^{\circ}$ accuracy, so that the variations in pitch angle indicated in Fig. 12 might be exaggerated.

A sensitive test of the accuracy of the combination probe measurements was to examine the static pressure distribution inferred from the measured velocity and probe impact pressure measurement. Fig. 13 shows the distribution of static pressure calculated in this way. Also included in Fig. 13 are the values of static pressure measured at the hub and tip wall static taps. It can be seen that agreement near the case wall was excellent. The comparison near the hub wall was not as good; however, very similar results were obtained from the wedge probe as shown in Fig. 14. While no readings were possible near the outer wall using the wedge probe, the two probes gave very similar results near the hub wall, and gave almost identical results for the survey at open throttle.

As shown in Appendix B, the effect of flow boundaries on the readings of the combination probe is small. The magnitude of the correction which was included in the above results can be seen in Fig. 15. The correction is less than 1% in velocity over the useful range of the survey.

Velocity diagrams near the mean radius (0.55 of the channel height) are shown in the four parts of Fig. 16.

B. DEVIATION ANGLES

The design procedure for calculating the deviation angles for a given blade profile, with corrections for three-dimensional effects, is described in Appendix A. Blade profiles are known on four conical surfaces in the

flow field, on which the blading dimensions are those given in Fig. 3. Using relative flow angle β_2 from the velocity diagram data (Fig. 16 for example), the flow deviation angle (δ) can be calculated from the stagger angle (γ) and camber angle (ϕ') using the relation

$$\delta = \beta_2 - \gamma + \frac{\phi'}{2}$$

The results for the four probe surveys are shown in Fig. 17 in comparison with the results of calculations following Ref. 1.

Departures from values predicted using Ref. 1 are quite large. However, the design procedure strictly applies only to the case where the operation is at the point of minimum loss for the given blade element. A closer correlation might be expected as the higher operating levels are achieved and closer to design conditions are attained. (Ref. 1 states that at transonic inlet Mach number levels, the point of minimum loss should constitute the desired design setting.) It is noted that the through-flow velocity is considerably increased through the rotor at the 50% design speed setting, and this would effect the deviation angle. No explanation was found for the indication of negative values of deviation angle near the hub, although a careful check was made on the accuracy of the probe yaw angle measurements and on the accuracy of the data reduction program. It must tentatively be concluded that there are strong three-dimensional effects present which can lead to the indication (locally) of negative deviation angles. More data must be obtained to investigate this speculation.

C. LOSSES

Loss coefficients for the flow over the blade elements, assuming that the stream surfaces were the conical surfaces given in Fig. 3, were calculated from the probe measurements using the methods described in Appendix D. The calculated loss coefficient ($\bar{\omega}'$) was consistent with the definition of loss coefficient used in Ref. 1. Of the two methods described in Appendix D, Method 1 uses both the stagnation pressure rise and stagnation temperature rise measurements of the probe. Method 2 does not use the stagnation temperature rise measurement, but uses a temperature rise calculated from the velocity and angle measurements, through Euler's turbine equation.

The results are shown in Fig. 18. Good agreement was obtained between the two methods of calculating the loss coefficient, however negative values were calculated for the inner stream surface. It should be noted that all measured data and all blade properties varied smoothly with radius, so that smooth curves between the individual data values could be drawn. The distributions are in qualitative agreement with earlier measurements, and it is noted that negative values of losses were previously reported by Dodge (Ref. 2) from measurements made with the same combination probe.

A negative value of the loss coefficient can result only from a measurement of stagnation pressure rise which is too high, or a measurement of stagnation temperature rise which

is too low. This can be seen if Eq. D(13) is rewritten in the form

$$\bar{\omega}' = \frac{\left[1 + X_{u2}^2\right]^{\gamma/(\gamma-1)}}{\left[1 + X_{u2}^2\right]^{\gamma/(\gamma-1)} - \left[1 - X_1^2\right]^{\gamma/(\gamma-1)}} \left\{ 1 - \frac{\dfrac{P_{t2}}{P_{t2}}}{\Psi^{\frac{2\gamma}{(\gamma-1)}}} \right\}$$

where Ψ is the ratio of total temperatures, (T_{t_2}/T_{t_1}). Clearly, since X_{u_2} and X_{u_1} are positive, $\bar{\omega}'$ is negative only if $\Psi^{\frac{2\gamma}{\gamma-1}} > (P_{t_2}/P_{t_1})$. Since the prediction of Method 1 and Method 2 agree, and because a favorable comparison with earlier unreported measurements of temperature rise was made, it is tentatively concluded that the impact pressure rise measurement is too large. A positive error in impact pressure could result from the pneumatic integration of the periodic unsteadiness of the flow from the rotor. All parts of the probe are the open ends of continuous tubing. It is known that pneumatic probes of different designs integrate differently in periodic flow conditions. An investigation of the pneumatic averaging characteristics of the probe is required in order to correct the measurements of losses. It should be noted that the velocity and pitch angle calculated from the time-averaged probe readings should not be as sensitive to the averaging behaviour of the probe. This is because all parts are made from similar tubing and will average in a similar way. The loss coefficient, however, is very sensitive to errors in impact pressure measurement alone.

While the magnitude of the loss coefficients is clearly in error, it is of interest to attempt to correlate the measurements on the basis of diffusion factor as defined in Ref. 1. The result of this attempt is shown in Fig. 19. The diffusion factor (D) was calculated from the definition

$$D = 1 - \frac{W_2}{W_1} + \frac{R_1 W_{u1} + R_2 W_{u2}}{\sigma (R_1 + R_2)\, W_1}$$

where W denotes the relative velocity, R is the radius, σ is the solidity and subscripts 1 and 2 denote stations upstream and downstream of the rotor. W_u is the peripheral component of the relative velocity. The "total loss parameter", ($\bar{\omega}' \cos \beta_2 / 2\sigma$) is consistent with that shown in Fig. 203 of Ref. 1 and was calculated from probe measurements.

It can be seen in Fig. 19 that a reasonable correlation of the loss coefficient data on the basis of diffusion factor was obtained for three of the four sets of data. The data for full open throttle departed significantly from the data from three other test conditions. It should now be recalled that the flow angles measured for this test were also inconsistent. More data is again needed, and a correction must be devised for unsteady flow effects on the probe measurements before a complete correlation can be obtained.

VI. CONCLUSIONS

The attempt was made here to determine the blade element performance of an "impulse" rotor designed for transonic flow (design point) but operating at high subsonic (off-design) conditions. The results were preliminary, but served to define the problems involved in obtaining necessary design data from empirical correlations of measurements made in actual machines.

The results obtained depended on the performance of a particular combination probe when used downstream of the rotor. The following conclusions were drawn concerning the probe measurements :

(i) The effect of the presence of flow boundaries on the probe measurements was small, but corrections were derived and applied in the present work. Static pressure derived from the probe measurements, static pressure from wedge probe measurements and wall static pressures were in reasonable agreement.

(ii) The temperature rise across the rotor measured by the probe, using the probe calibration, was consistent with the rise deduced from Euler's turbine equation. All indications were that the probe provided an accurate measurement of the temperature rise.

(iii) The impact pressure measured by the probe in the unsteady flow downstream of the rotor was probably too high. An investigation of the unsteady response of the tubing used

in the probe design is required in order to correct the data obtained so far.

(iv) The flow velocity derived from the probe measurements was probably not as sensitive to unsteady flow effects since all the pressure sensors on the probe were constructed from the same tubing. The derived velocity depends mainly on differences between the pressures registered by the sensors. In steady flow the velocity was determined to better than 1.0% accuracy, to nearly sonic speeds.

(v) The pitch angle was determined by the same probe to within $1\frac{1}{2}^{\circ}$.

(vi) The wedge probe provided a good measurement of static pressure in the compressor when rotated to a pre-measured flow angle.

As a result of (iii), the loss coefficients determined from probe measurements were too small, becoming negative over the blading near to the hub. A correction to the impact pressure measurements and more data are needed before a useful correlation of the losses can be obtained. However, it was found that the present results from three tests and four different blade-element surfaces correlated reasonably well in terms of the NASA diffusion factor.

The deviation angles measured in the present tests departed significantly from the values predicted using NASA SP-36. No explanation was found for the negative values measured near to the hub, although the possibility exists that they could be caused by three-dimensional effects in the

flow through the rotor. More data are needed to confirm the trends in the deviation angles. Agreement with the predicted values was not expected since the blade profiles were unusual, and were operating well away from the design condition.

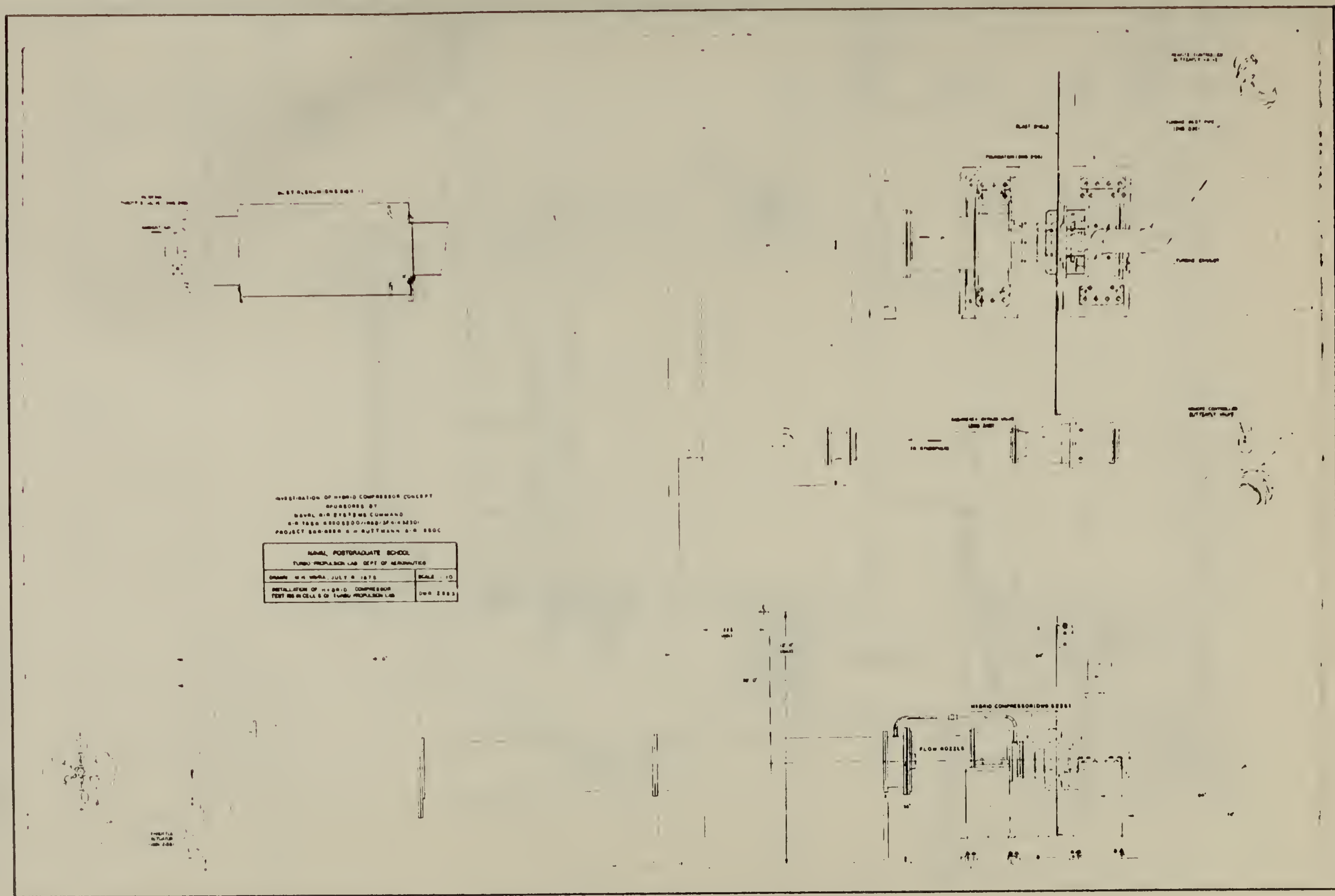

FIG. 1 THE COMPRESSOR TEST RIG

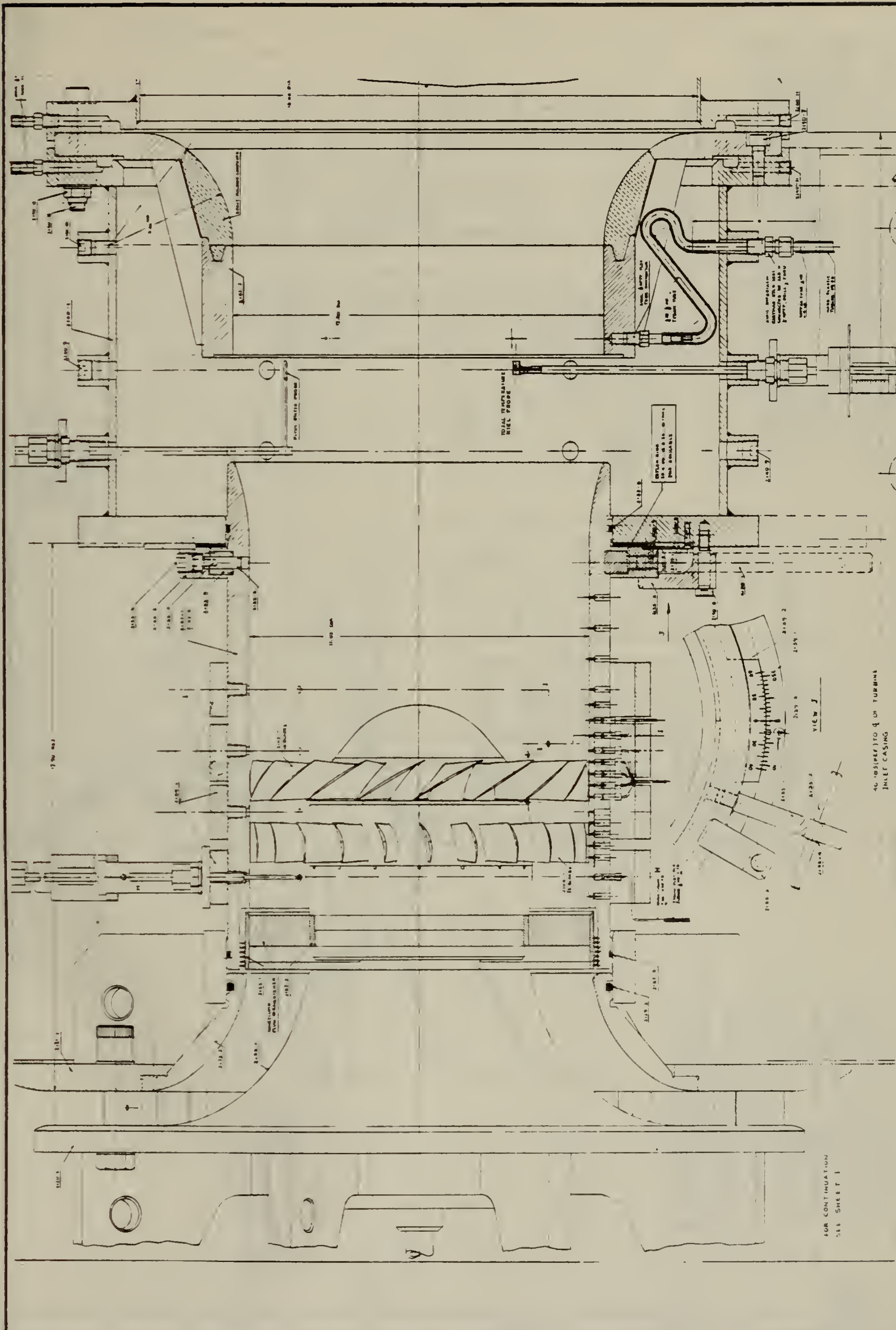

FIG. 2 TRANSONIC COMPRESSOR ASSEMBLY

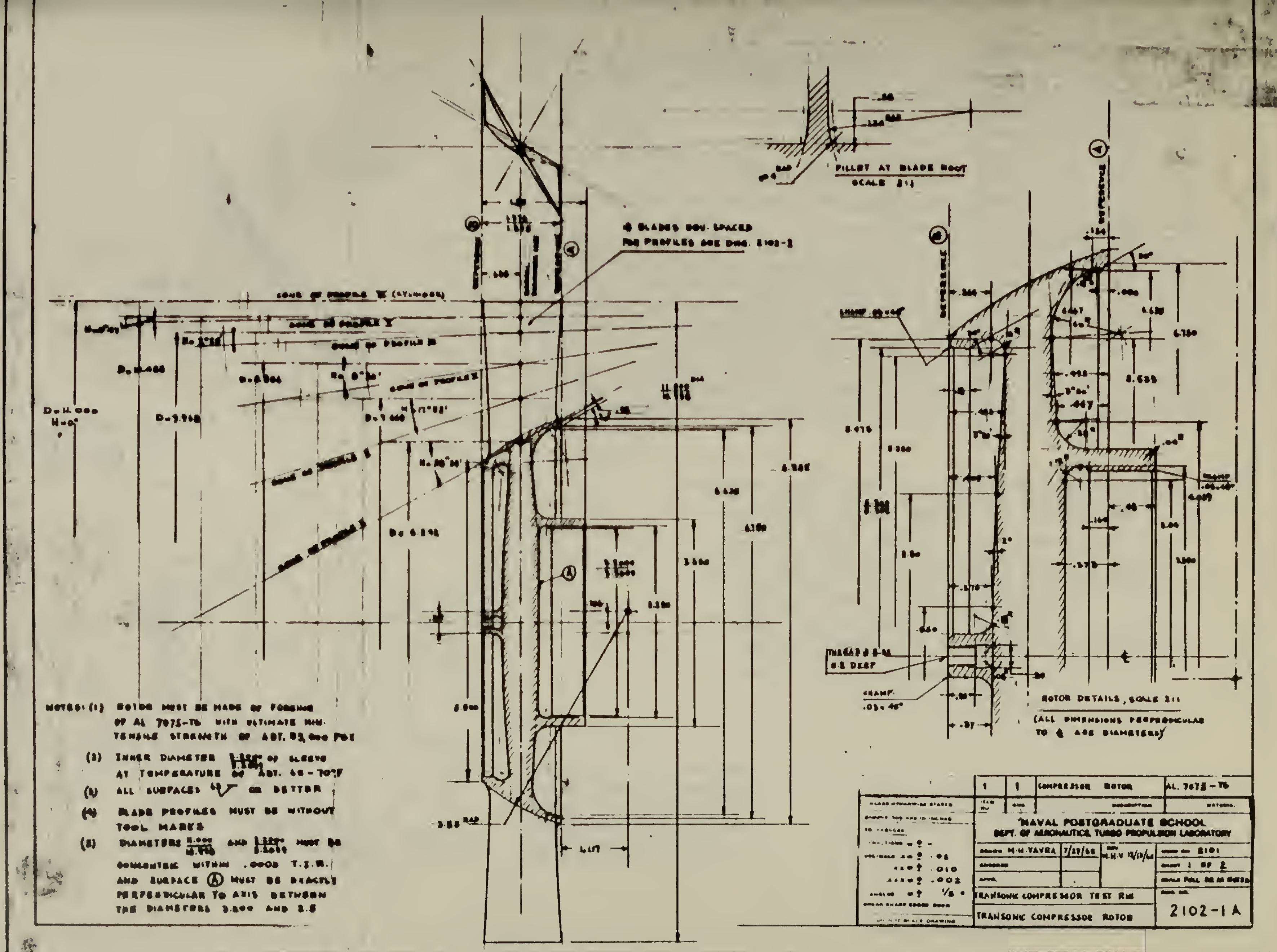

FILLET AT BLADE ROOT
SCALE 2:1
18 BLADES EQU. SPACED
FOR PROFILES SEE DWG. 2102-2
ROTOR DETAILS, SCALE 2:1
(ALL DIMENSIONS PERPENDICULAR
TO ℄ ARE DIAMETERS)
NOTES: (1) ROTOR MUST BE MADE OF FORGING
OF AL 7075-T6 WITH ULTIMATE MIN.
TENSILE STRENGTH OF ABT. 83,000 PSI
(2) INNER DIAMETER OF SLEEVE
AT TEMPERATURE OF ABT. 68-70°F
(3) ALL SURFACES OR BETTER
(4) BLADE PROFILES MUST BE WITHOUT
TOOL MARKS
(5) DIAMETERS AND MUST BE
CONCENTRIC WITHIN .0005 T.I.R.
AND SURFACE (A) MUST BE EXACTLY
PERPENDICULAR TO AXIS BETWEEN
THE DIAMETERS 3.800 AND 2.5
NAVAL POSTGRADUATE SCHOOL
DEPT. OF AERONAUTICS, TURBO PROPULSION LABORATORY
COMPRESSOR ROTOR
AL. 7075-T6
M.H. VAVRA
TRANSONIC COMPRESSOR TEST RIG
TRANSONIC COMPRESSOR ROTOR
2102-1A

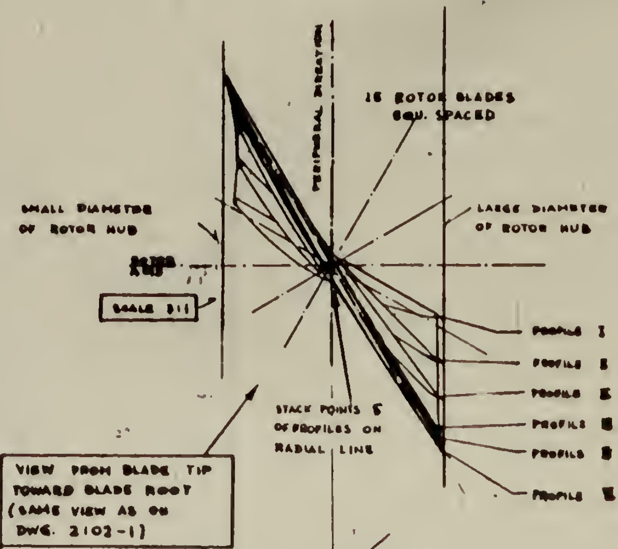

SYMBOL	PROFILE	I	II	III	IV	V	VI
D	DIAMETER OF CONE THRU STACKING RADIUS (SEE DWG. 2102-1)	5.342	7.449	8.806	9.956	10.488	11.000
H	ANGLE OF CONE THRU STACKING RADIUS (SEE DWG. 2102-1)	28° 52'	17° 52'	8° 52'	3° 38'	0° 47'	0
G	ANGLE BETWEEN PROFILE CHORD AND ROTOR AXIS	30° 05'	40° 06' 59"	53° 36' 10"	68° 46' 38"	79° 21' 40"	89° 47' 35"
C	PROFILE CHORD	1.465	1.792	2.100	2.389	2.657	2.938
R	RADIUS OF PROFILE CONTOUR	1.950	2.173	5.811	9.221	11.442	16.330
E	CHORD WITH SHARP LEADING & TRAILING EDGES	1.553	1.920	2.269	2.564	2.701	2.911
A	DISTANCE OF STACK POINT S FROM PROFILE CHORD	.067	.061	.050	.036	.032	.025
T	MAX. PROFILE THICKNESS	.168	.150	.135	.090	.080	.065
ER	LEADING AND TRAILING EDGE RADIUS	.015	.012	.014	.007	.005	.005
X1	DISTANCE OF PROFILE EDGE FROM S IN AXIAL DIRECTION	.609	.605	.589	.598	.655	.680
X2	DISTANCE OF PROFILE EDGE FROM S IN AXIAL DIRECTION	.661	671	.655	646	.671	696
Y1	DISTANCE OF PROFILE EDGE FROM S IN PERIPHERAL DIRECTION	.328	605	.887	1.007	1.070	1.185
Y2	DISTANCE OF PROFILE EDGE FROM S IN PERIPHERAL DIRECTION	.419	676	874	1.037	1.106	1.1732
P1	DISTANCE OF POINT LE FROM S IN AXIAL DIRECTION	.681	630	.527	.539	661	.709
P2	DISTANCE OF POINT TE FROM S IN AXIAL DIRECTION	.716	.924	709	.701	.715	.754
Q1	DISTANCE OF POINT TE FROM S IN PERIPHERAL DIRECTION	.339	640	867	1.086	1.146	1.245
Q2	DISTANCE OF POINT LE FROM S IN PERIPHERAL DIRECTION	.488	.788	907	1.134	1.178	1.271

NOTES: (1) BLADE SECTIONS SHOWN ARE TO BE WRAPPED ON CONES WITH THE DIAMETER 'D' IN THE PLANE THRU THE RADIAL STACKING LINES. THESE CONES HAVE THE ANGLES 'H' WITH THE ROTOR AXIS AS SHOWN IN DWG 2102-1.

(2) THE BLADE PROFILES BETWEEN THE ONES SPECIFIED ON THE CONES ARE OBTAINED BY SMOOTH FAIRING.

(3) THE ACTUAL HUB PROFILE IS OBTAINED BY THE INTERSECTION OF THE BLADE WITH THE SURFACE OF REVOLUTION OF THE HUB (SEE RADIUS) SPECIFIED IN DWG. 2102-1

(4) THE FILLET SHOWN IN DWG. 2102-1 MUST EXIST ALL AROUND THE HUB PROFILE AND ALSO FORWARD OF THE LEADING EDGE, AND DOWNSTREAM OF THE TRAILING EDGE, IN DIRECTION OF THE CHORD LINE.

(5) TOLERANCES: FOR THICKNESS ± .001
FOR CHORD ± .005
FOR ANGLES 1/5 DEGREE

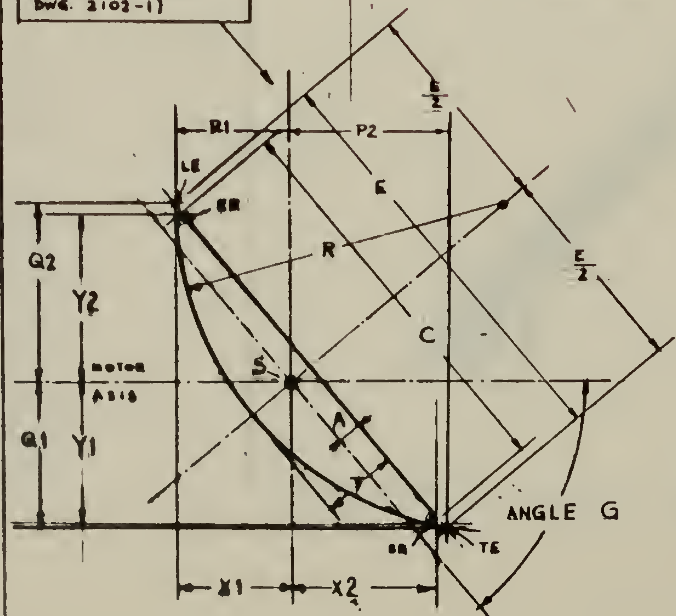

TYPICAL BLADE PROFILE (NO SCALE)
(PRESSURE SIDE IS STRAIGHT LINE)
(SUCTION SIDE IS A CIRCULAR ARC)

STACK POINTS S MUST LIE ON RADIAL STACKING LINE OF DWG. 2102-1

NAVAL POSTGRADUATE SCHOOL DEPT. OF AERONAUTICS, TURBO PROPULSION LABORATORY	
DRAWN M. H. VAVRA 7/28/66	USED ON 2102-1
CHECKED	SHEET 2 OF 2
APPD.	SCALE AS NOTED
TRANSONIC COMPRESSOR TEST RIG	
BLADING DATA OF TRANSONIC ROTOR	2102-2

DO NOT SCALE DRAWING

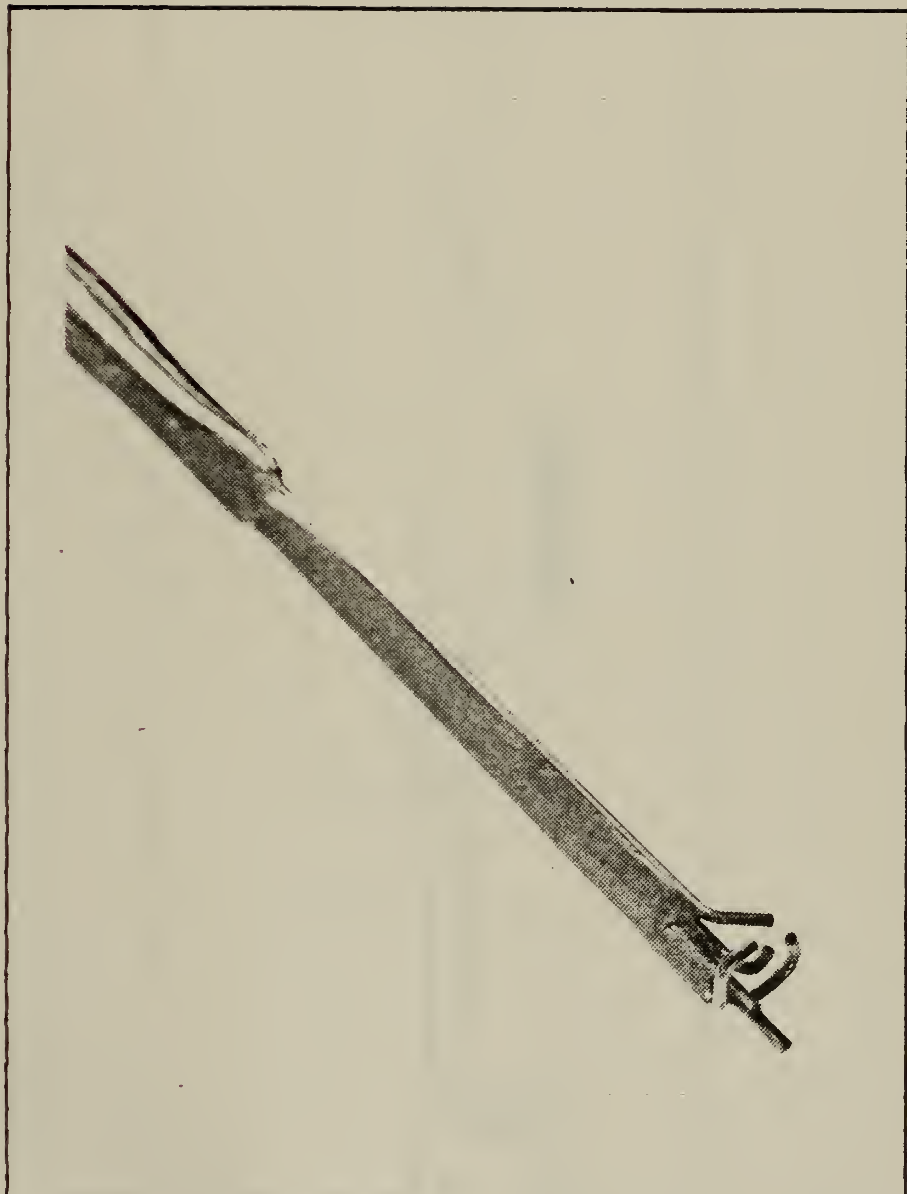

FIG. 4 COMBINATION PROBE (SHOWN WITH THERMO-
COUPLE REMOVED)

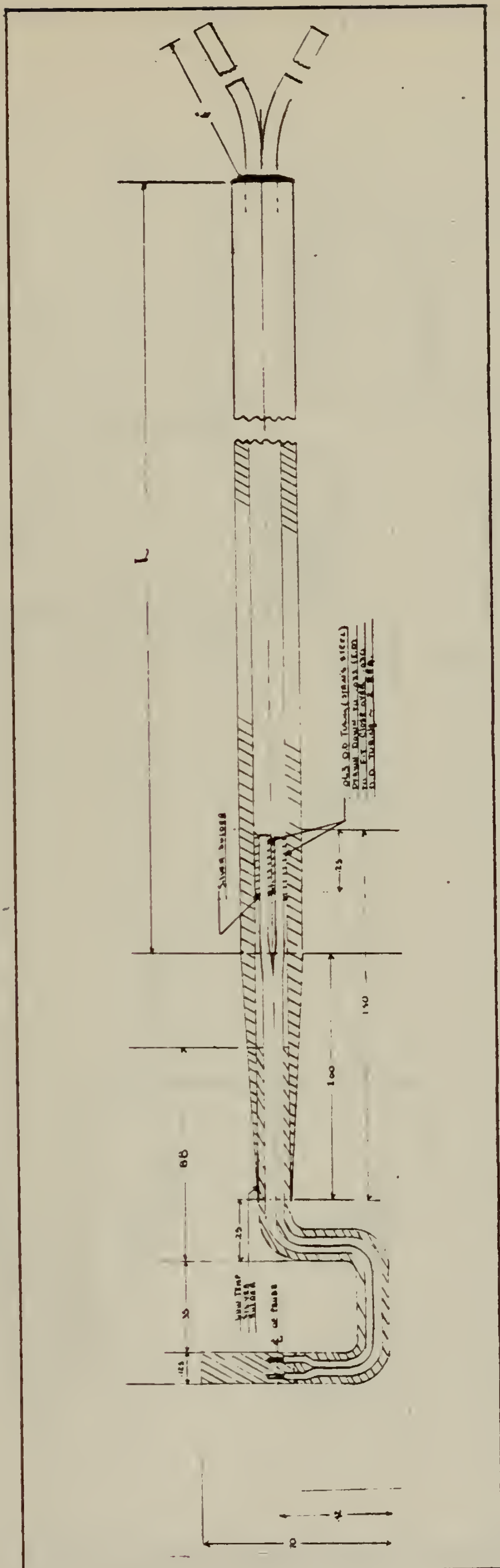

FIG. 5 WEDGE PROBE

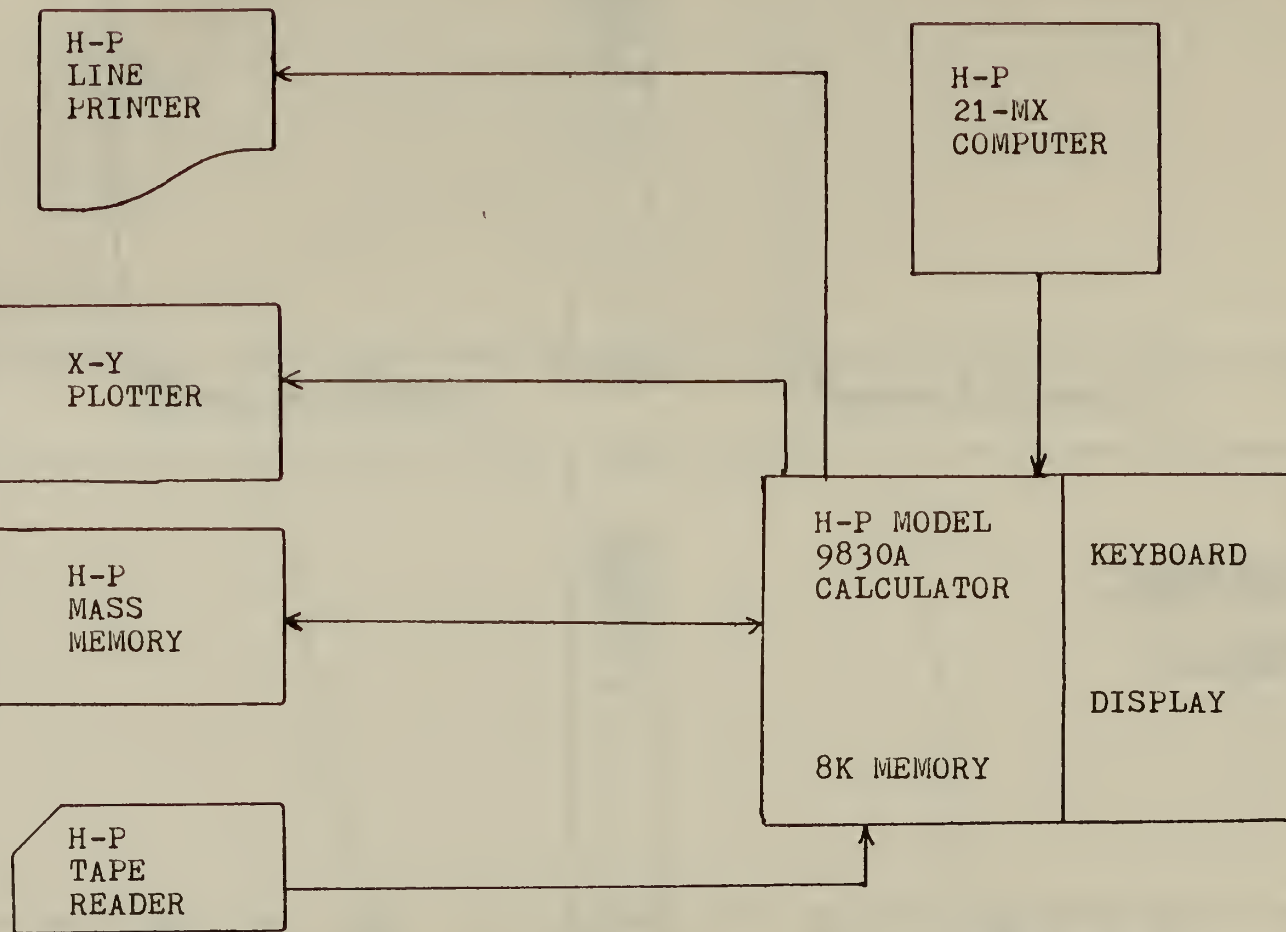

FIG. 6 SCHEMATIC OF THE HEWLETT-PACKARD MODEL 9830A CALCULATOR DATA REDUCTION SYSTEM

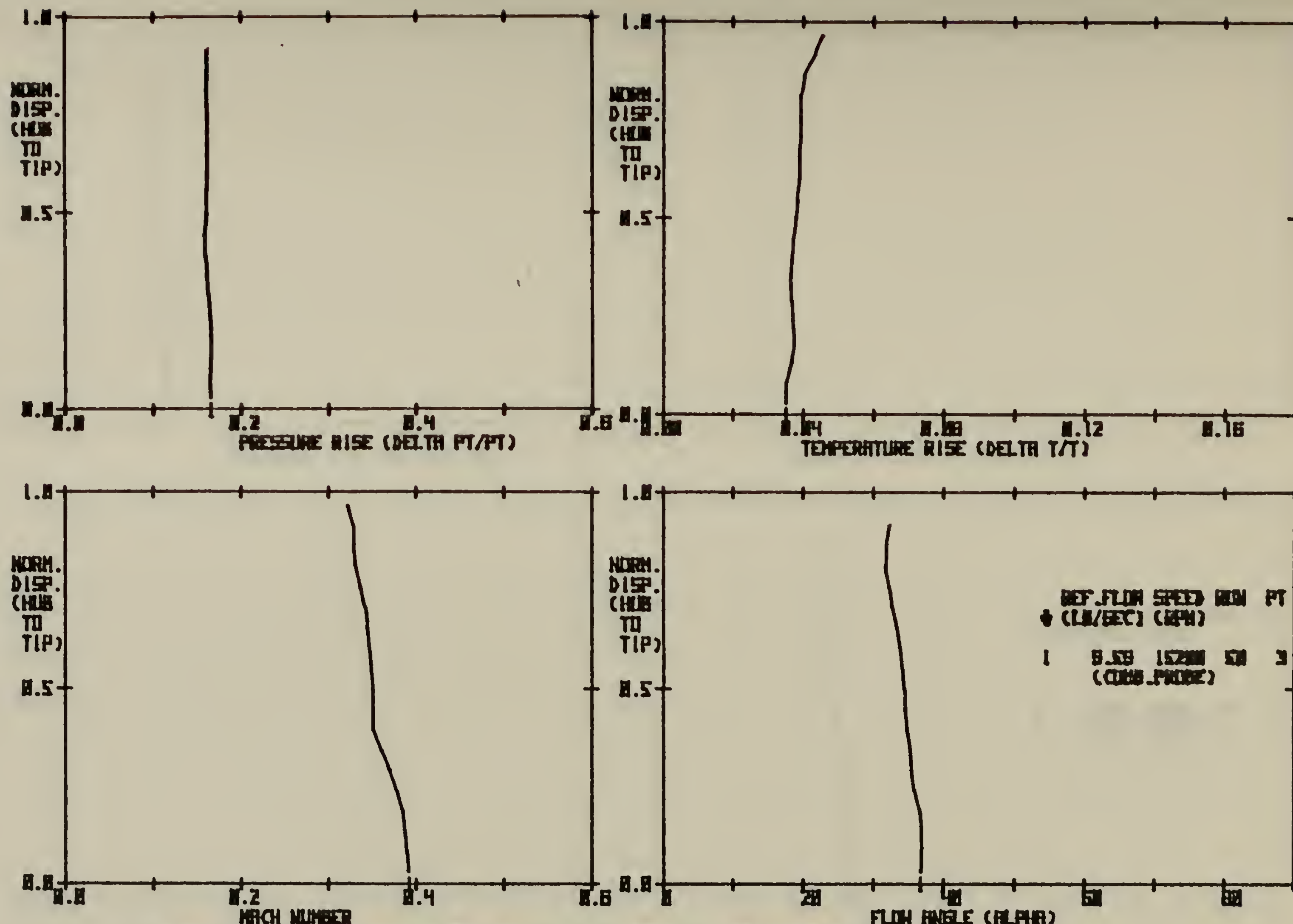

FIG. 7 RESULTS OF PROBE SURVEYS DOWNSTREAM OF THE TRANSONIC COMPRESSOR ROTOR

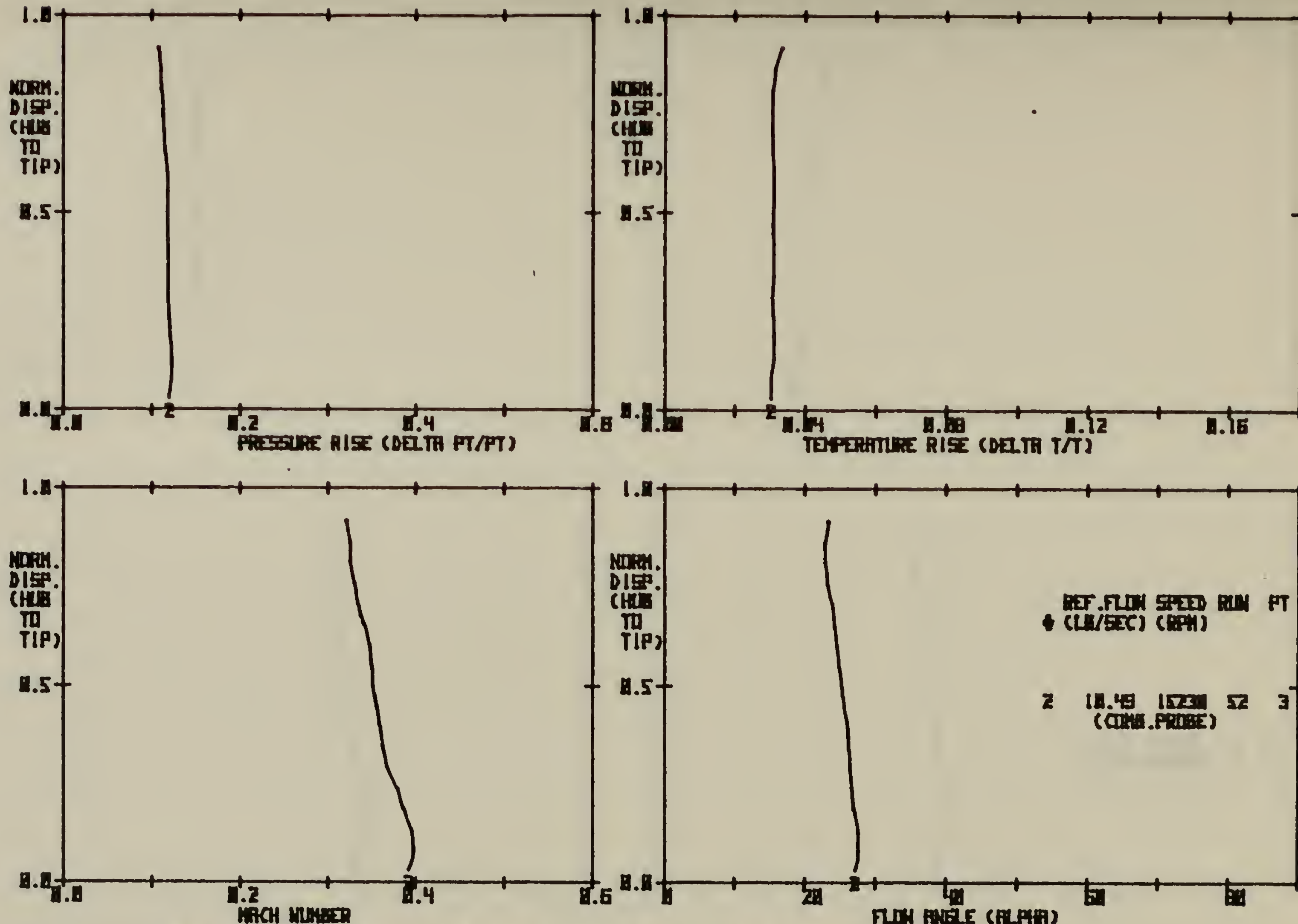

FIG. 8 RESULTS OF PROBE SURVEYS DOWNSTREAM OF THE TRANSONIC COMPRESSOR ROTOR

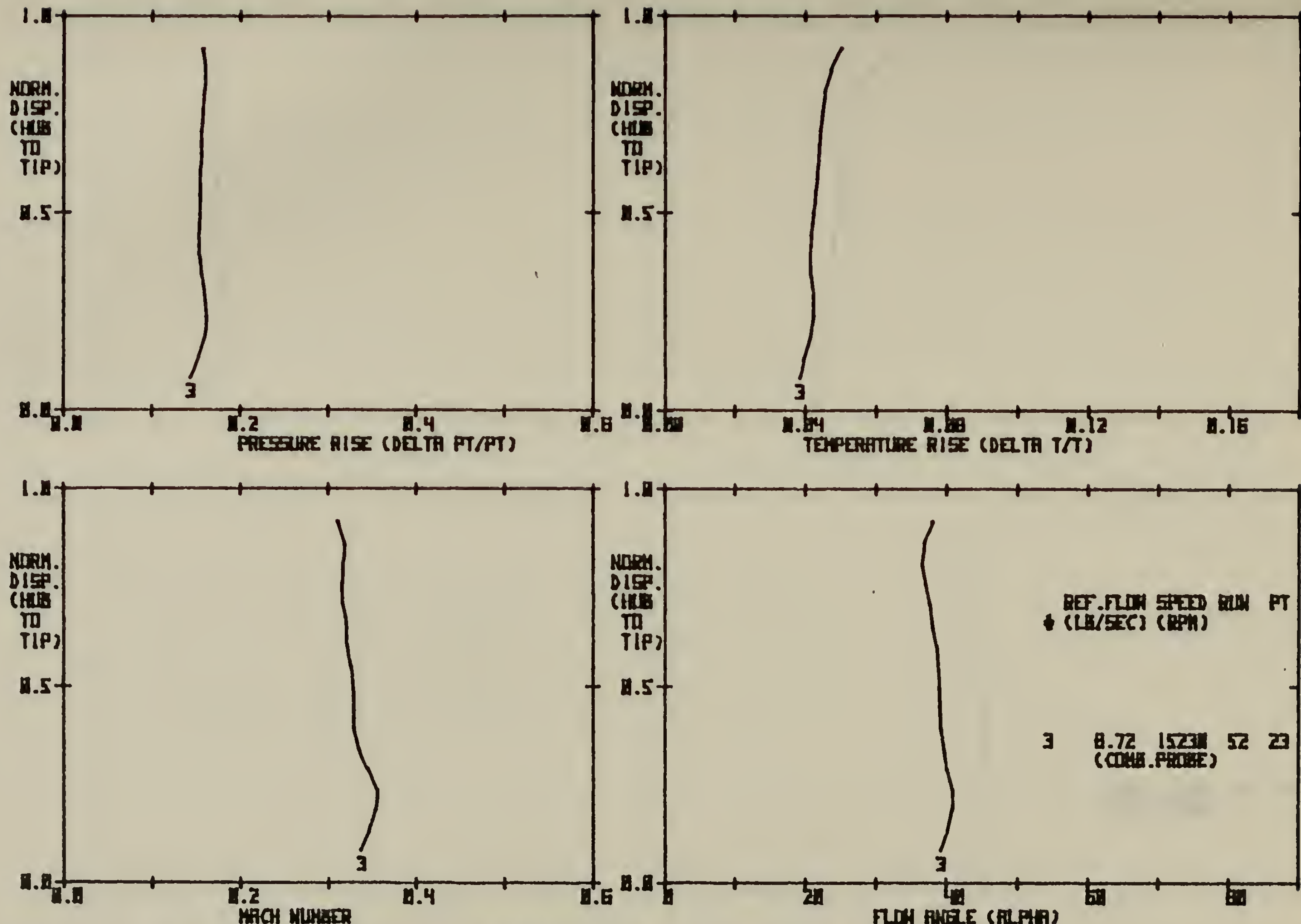

FIG. 9 RESULTS OF PROBE SURVEYS DOWNSTREAM OF THE TRANSONIC COMPRESSOR ROTOR

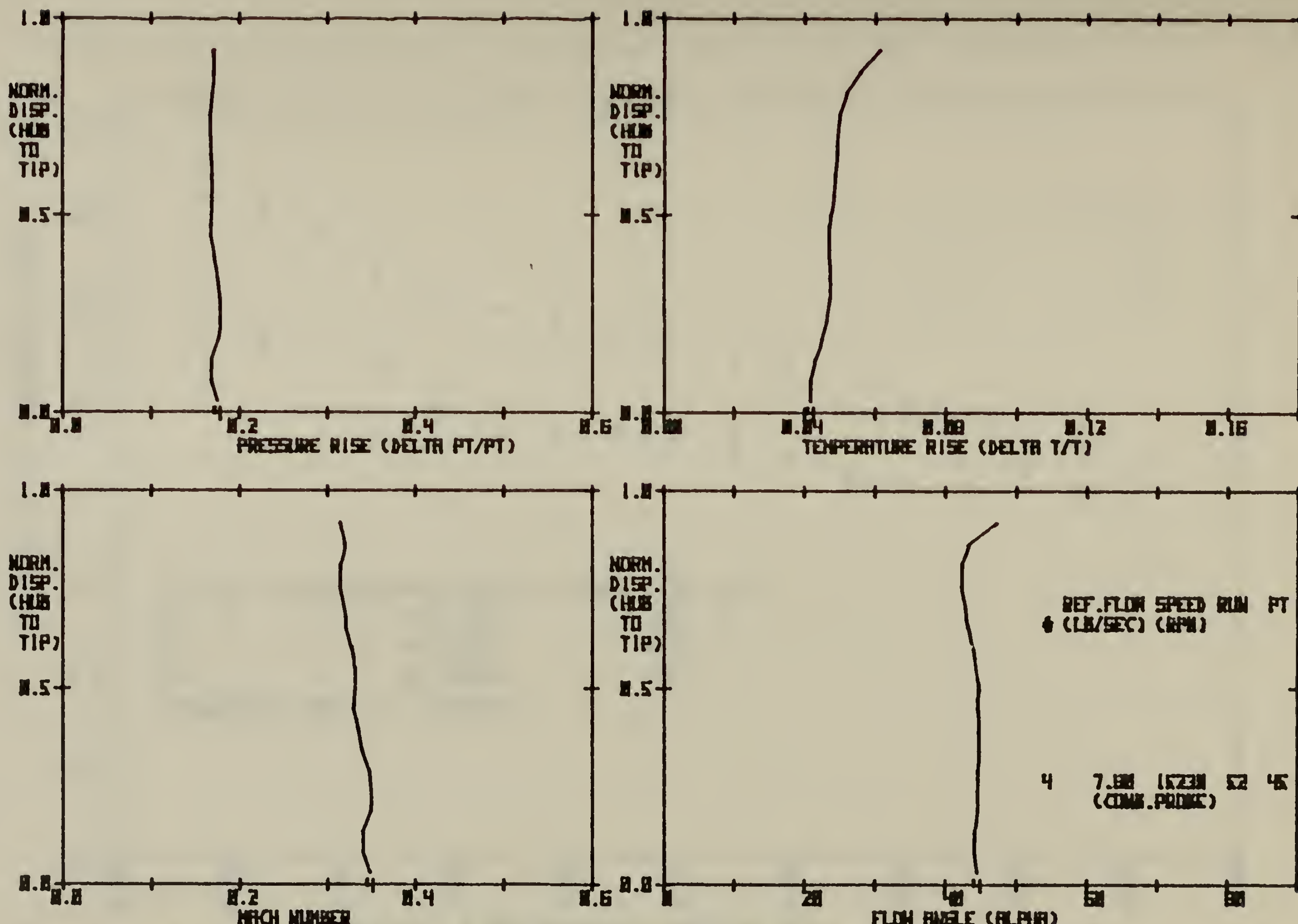

FIG. 10 RESULTS OF PROBE SURVEYS DOWNSTREAM OF THE TRANSONIC COMPRESSOR ROTOR

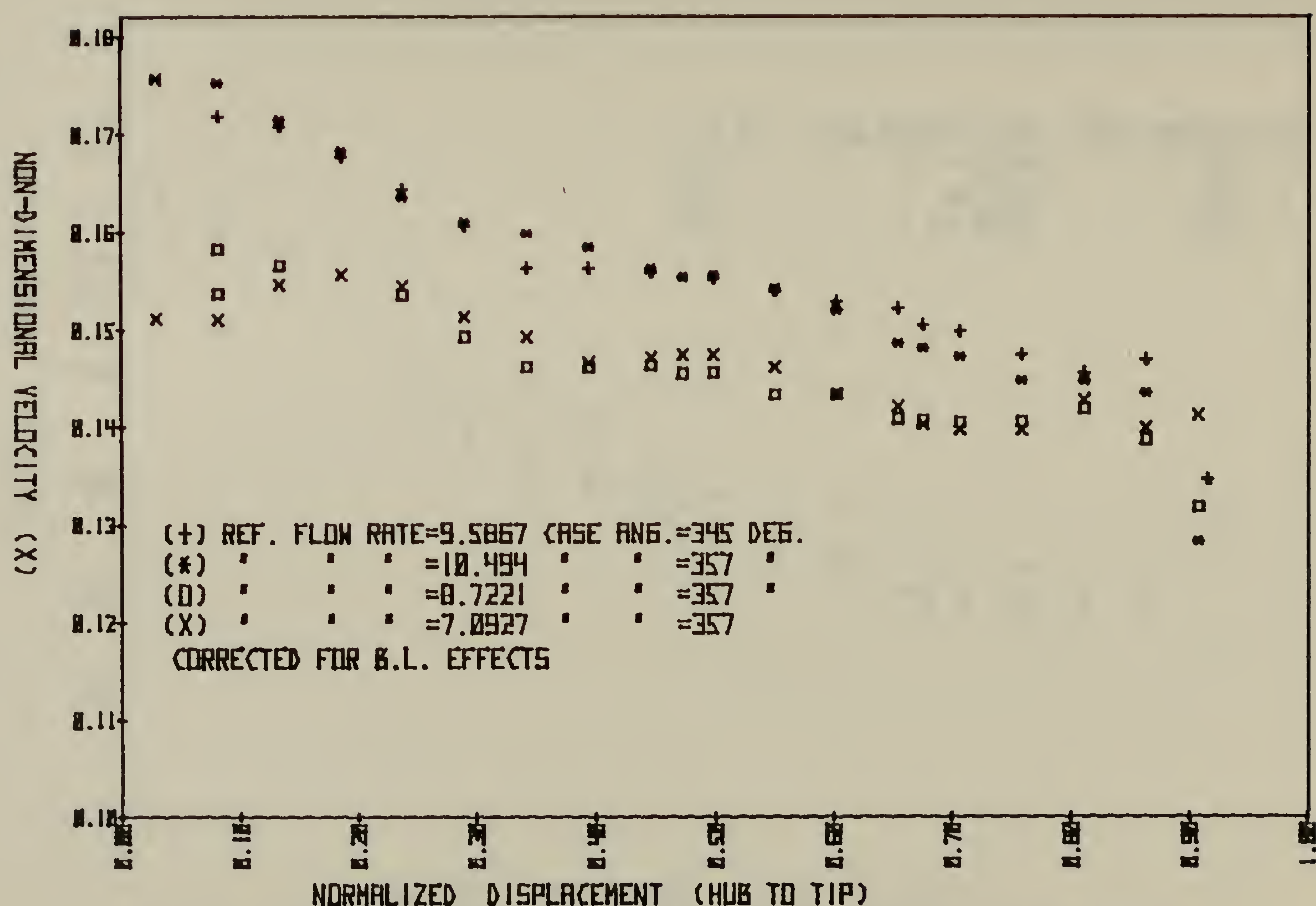

FIG. 11 VELOCITY DISTRIBUTION DOWNSTREAM OF THE ROTOR USING THE COMBINATION PROBE

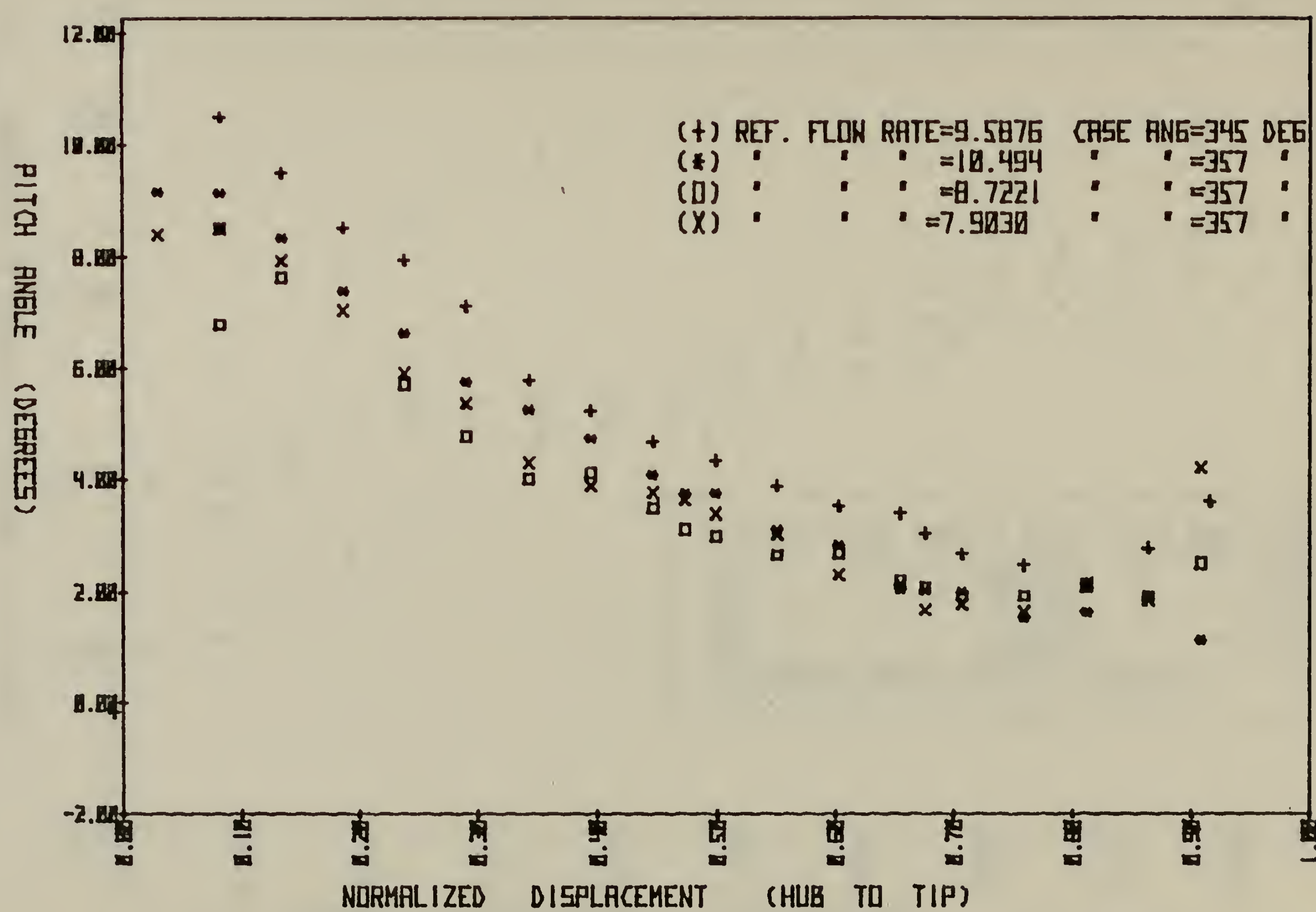

FIG. 12 PITCH ANGLE DISTRIBUTION DOWNSTREAM OF THE ROTOR
USING THE COMBINATION PROBE

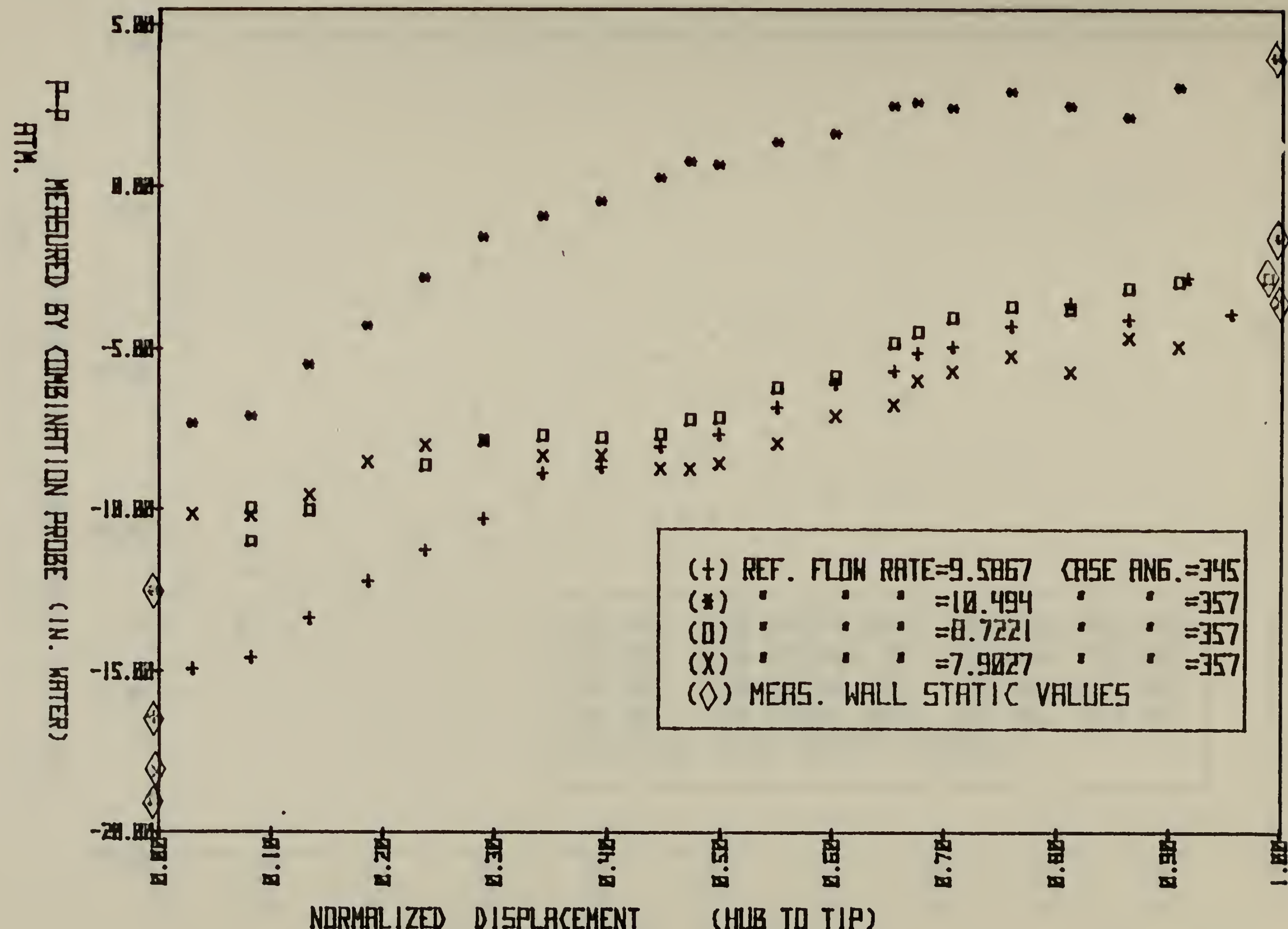

FIG. 13 STATIC PRESSURE DISTRIBUTIONS DOWNSTREAM OF THE ROTOR DERIVED USING THE COMBINATION PROBE CALIBRATION AND IMPACT PRESSURE MEASUREMENT

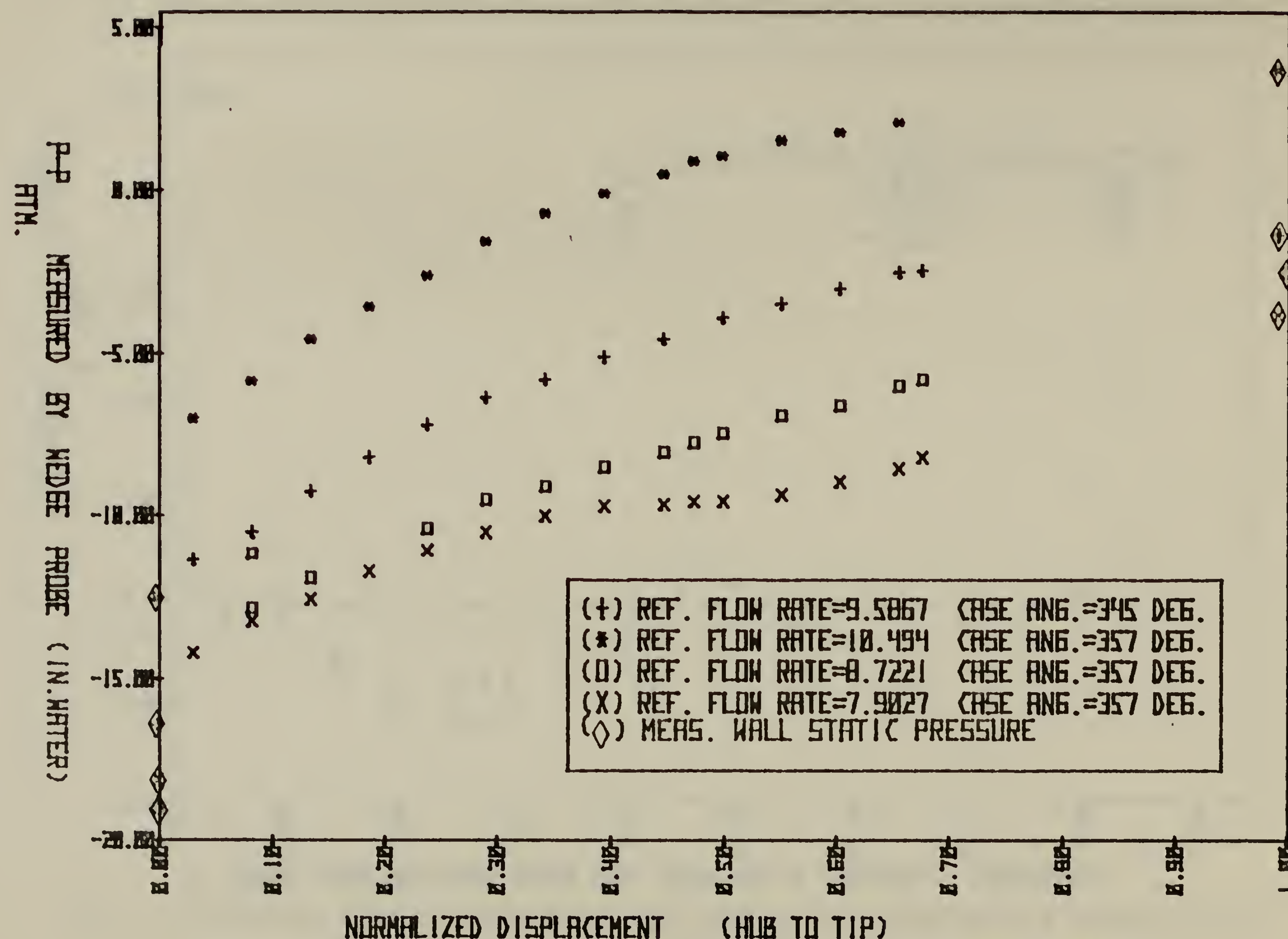

FIG. 14 STATIC PRESSURE DISTRIBUTIONS MEASURED DOWNSTREAM OF THE ROTOR USING THE WEDGE STATIC PROBE

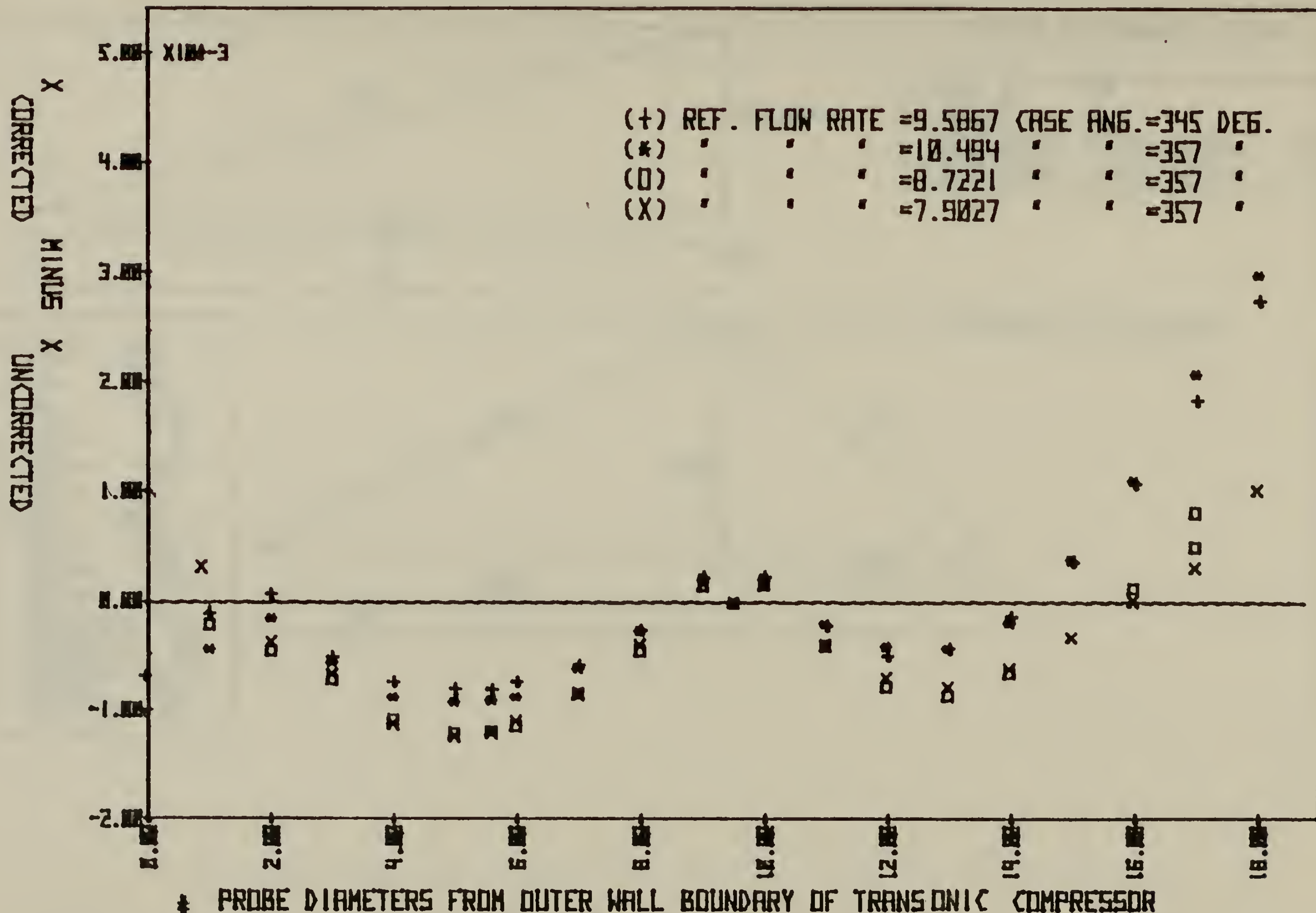

FIG. 15 BOUNDARY EFFECT CORRECTION APPLIED TO THE COMBINATION PROBE RESULTS

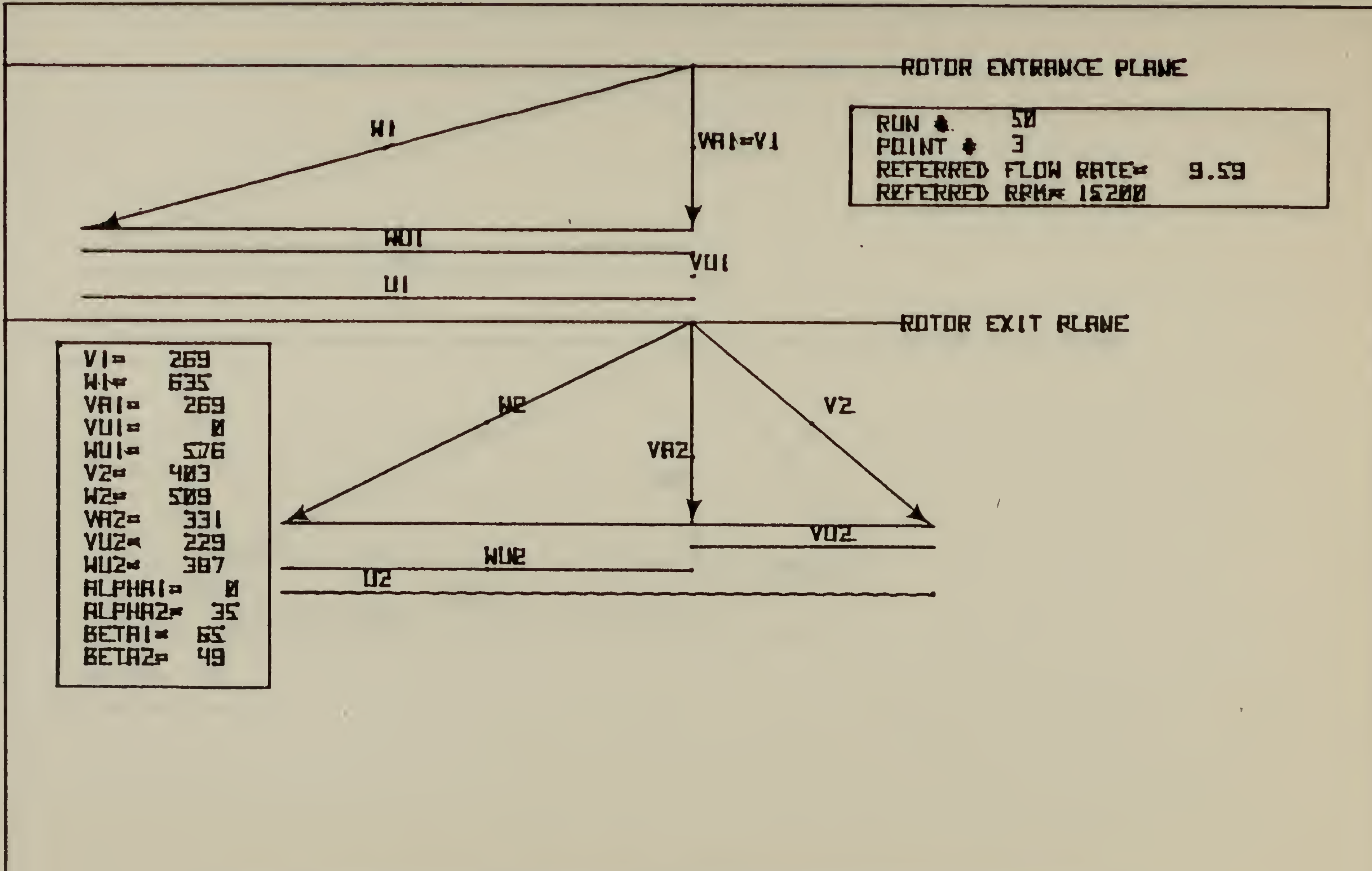

FIG. 16a VELOCITY TRIANGLES AT MIDSTREAM FOR RUN 50 POINT 3

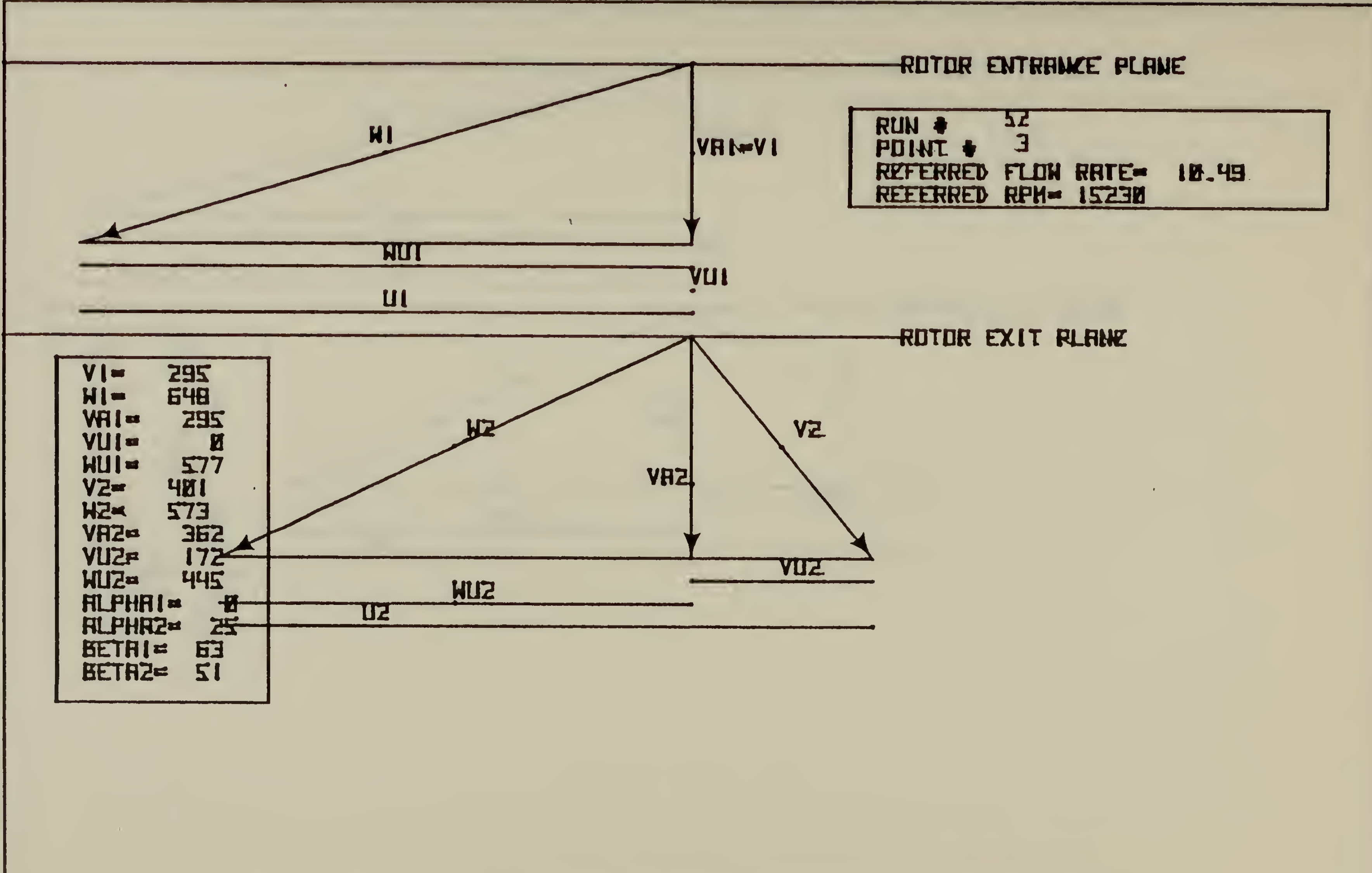

FIG. 16b VELOCITY TRIANGLES AT MIDSTREAM FOR RUN 52 POINT 3

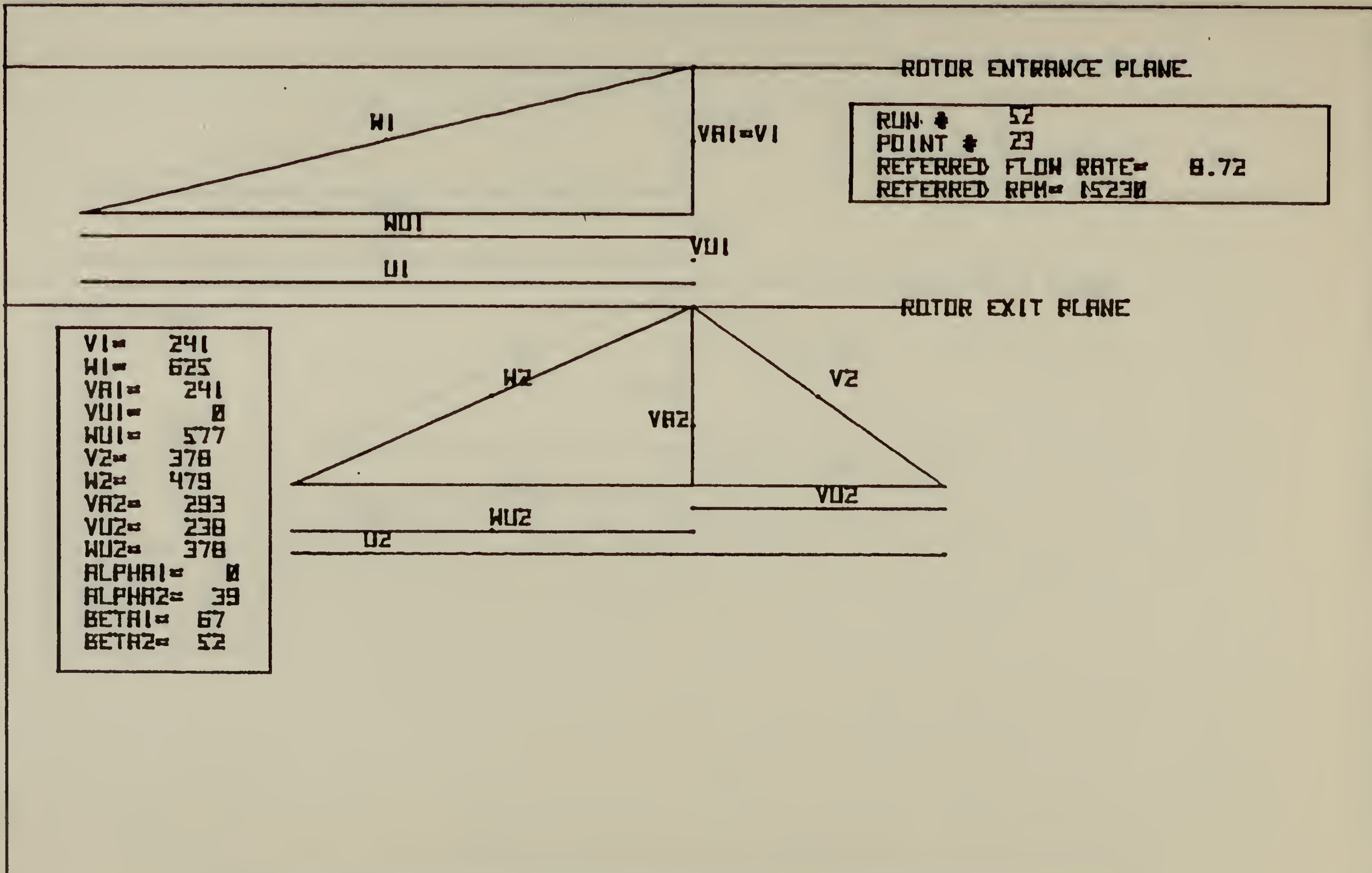

FIG. 16c VELOCITY TRIANGLES AT MIDSTREAM FOR RUN 52 POINT 23

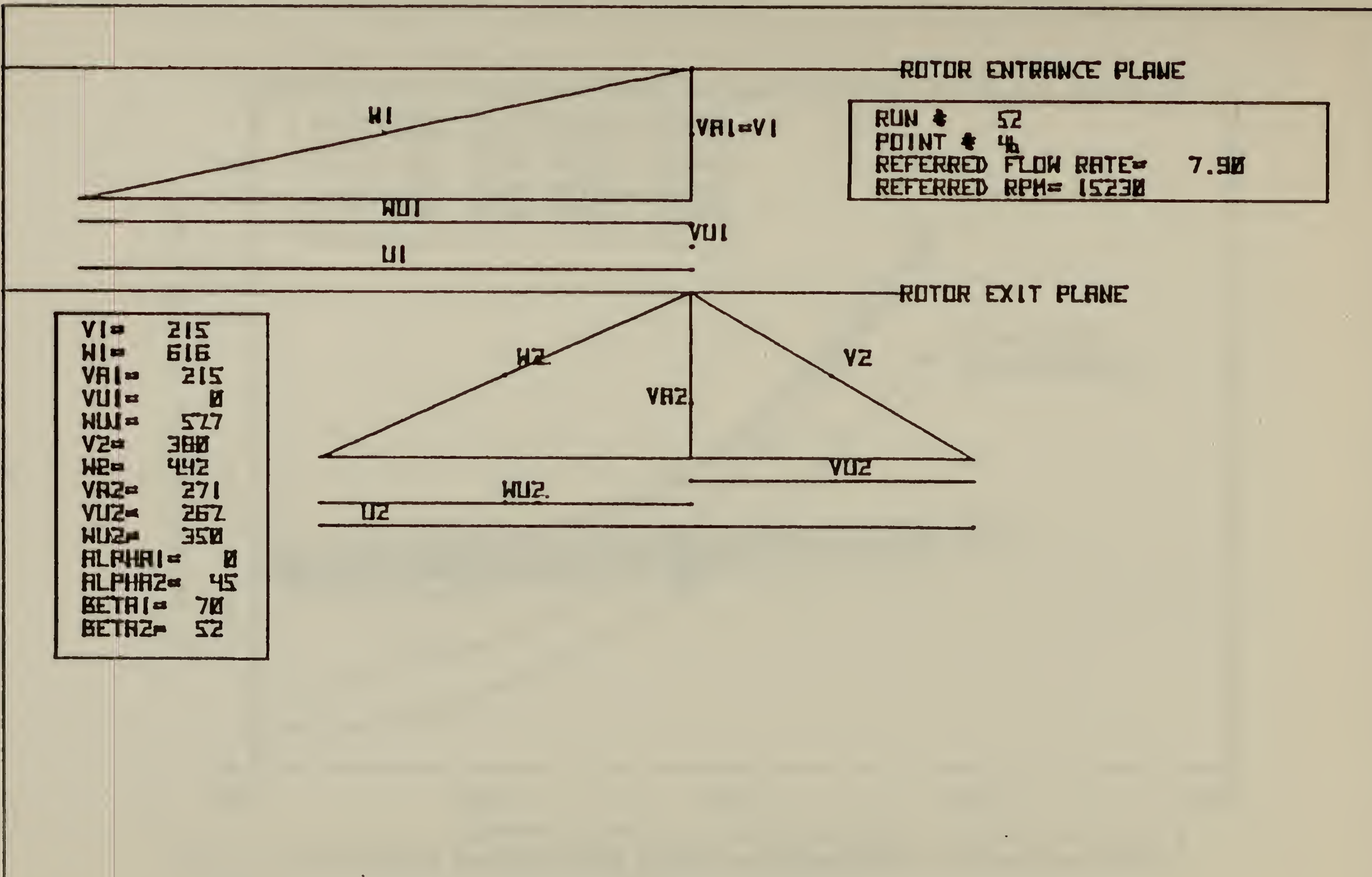

FIG. 16d VELOCITY TRIANGLES AT MIDSTREAM FOR RUN 52 POINT 46

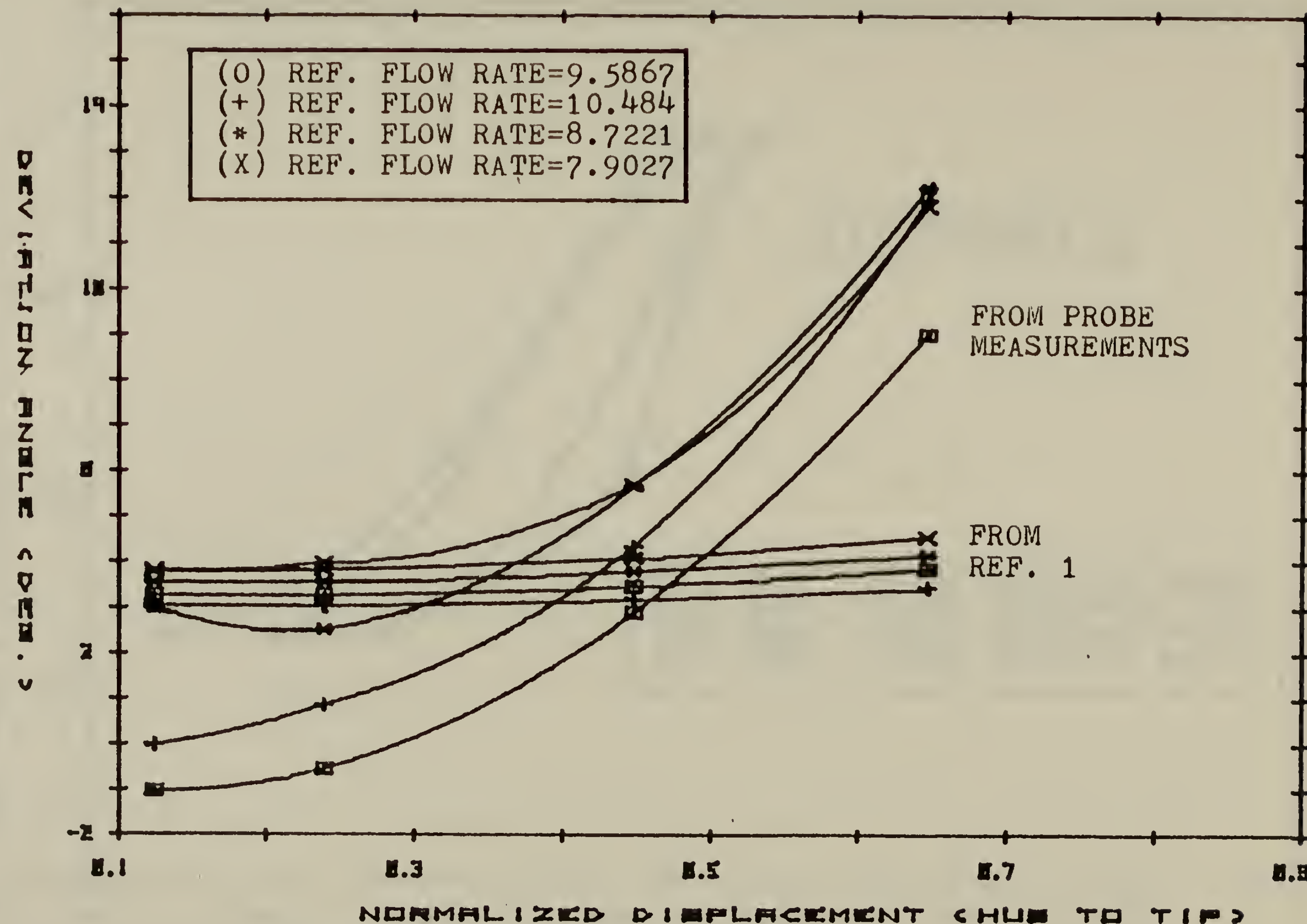

FIG. 17 DEVIATION ANGLES FROM PROBE MEASUREMENTS AND CALCULATIONS

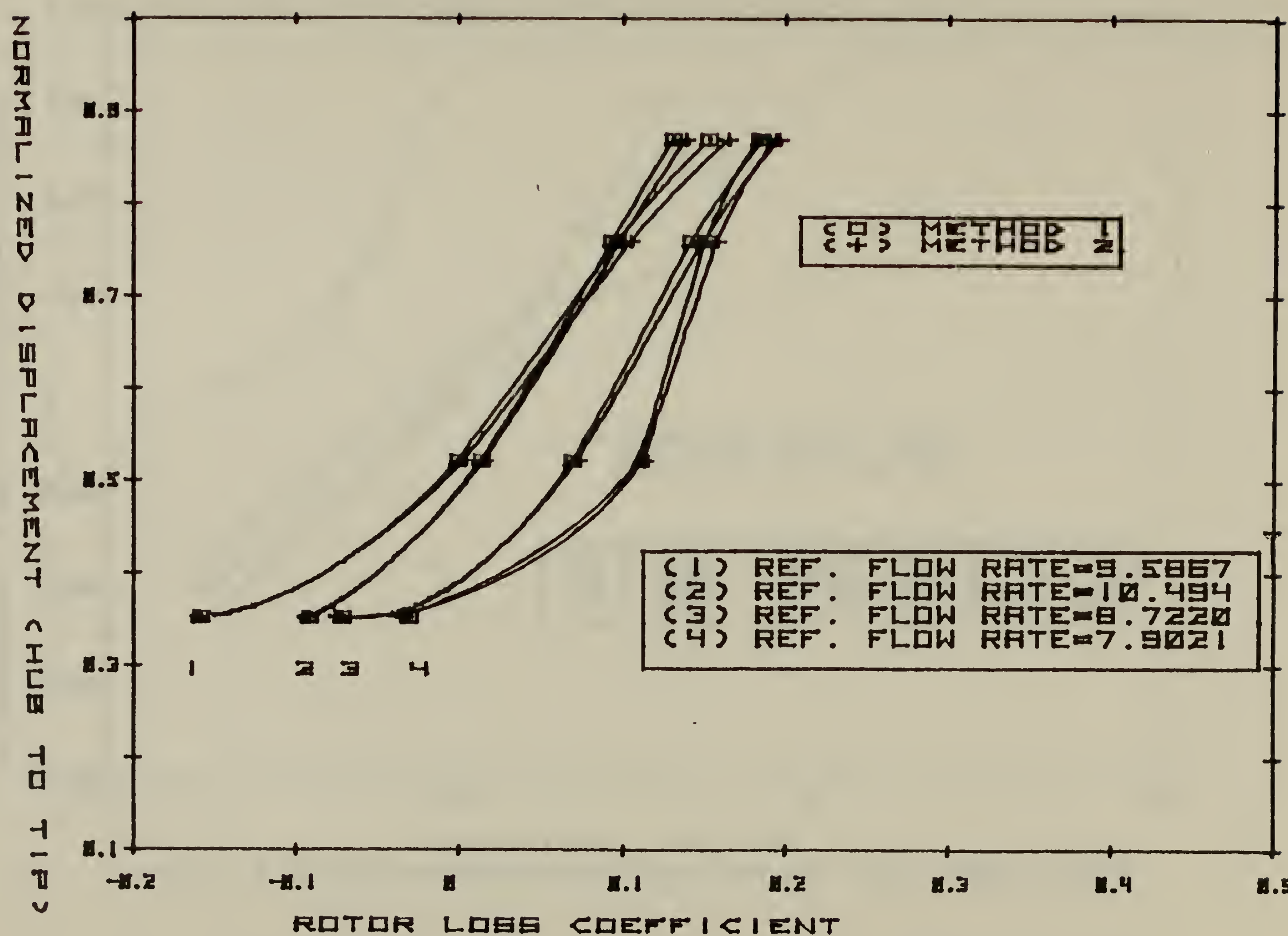

FIG. 18 LOSS COEFFICIENTS FOR THE TRANSONIC COMPRESSOR ROTOR

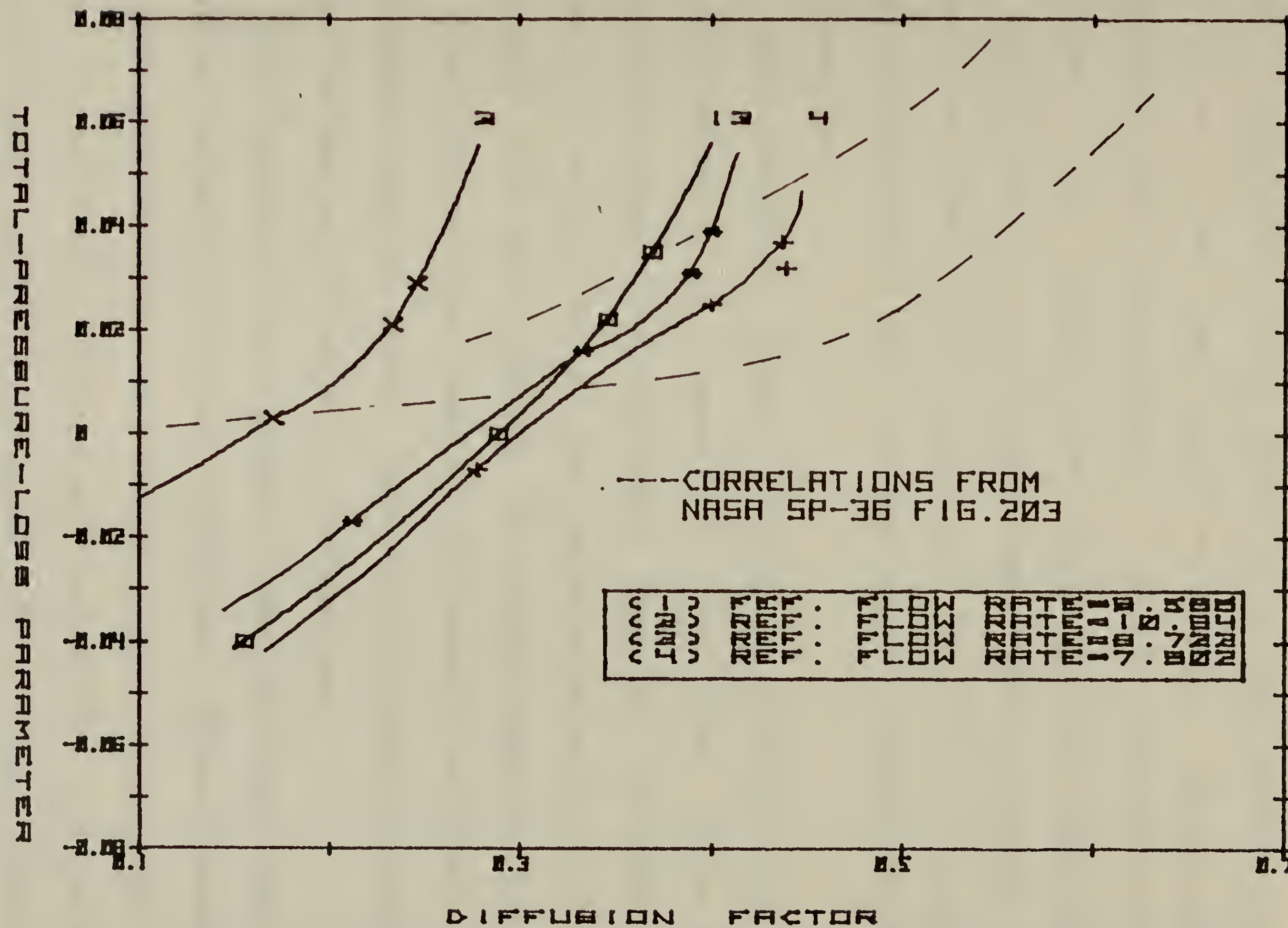

FIG. 19 DIFFUSION FACTOR CORRELATION OF LOSS COEFFICIENTS

APPENDIX A: BLADE ELEMENT PERFORMANCE PREDICTION

A1. INTRODUCTION

Flow through the blading of an axial-flow compressor is an extremely complicated three-dimensional process. As a result, simplified design models have been devised that permit the use of two-dimensional techniques. The approach is described fully in Reference 1. Involved is first the calculation of the "through-flow" assuming axial symmetry, then the calculation of the "blade-element flow" assuming approximately two-dimensional behaviour. The latter calculation, based on Chapters 6 and 7 of Reference 1, is the subject of this section.

Five quantities shown in Figure A1 determine the aerodynamic behaviour of a cascade in ideal flow. Three of these define the geometry of the blade; they are, the shape of the blade, the orientation of the blades with respect to the cascade axis, and the solidity. The fourth quantity identifies the direction of flow ahead of the cascade and finally, the Mach number must be known. When these quantities are specified, the inviscid flow may be determined.

Real cascade flows however, experience many other influences including friction, turbulence, three-dimensional and unsteady effects, and boundary layer interaction. The procedure outlined in Reference 1 correlates cascade and compressor blade element performance data. Various correction factors are introduced which account empirically for the effects which can not be predicted analytically. The result

is a method of calculating the performance of compressor blading. The method can be applied to both rotors and stators over a fairly wide range of Mach numbers. The method is limited however to the calculation of performance close to design point.

NASA SP-36 has become a reference text in the axial compressor industry. A brief summary of the method is presented here, followed by a computerized solution which uses the extensive correlations of data presented in this manual.

The main thrust was to develop a program to calculate the blade element performance of a blade design of arbitrary geometry. The program would provide a very powerful design tool, and would provide the basis for a program to predict the performance of a transonic compressor rotor. Reference 6 reports an extension of this was used with considerable success up to a Mach number of about 1.5.

A2. METHOD OF BLADE ELEMENT PREDICTION

A2.1 Two-Dimensional Incidence Angle. Any cascade of aerodynamic blading behaves qualitatively as shown in Figure A2 where Δ i is the "range" of performance and the mid-point of the curve is defined as the reference minimum loss incidence angle ($i_{ref.}$). For blading with a given camber (ϕ'), thickness distribution, and maximum thickness ratio (t/c), the solidity (σ) and blade angle (γ) complete the definition of the cascade geometry. Given β_1 and the inlet velocity the method in Reference 1 allows the determination minimum loss incidence angle, the deviation angle, and the loss coefficient.

The reference incidence angle for any blade element can be calculated from correlations of two-dimensional cascade measurements. Two-dimensional reference incidence angle for 10% thick blades is given as

$$i_{2-D} = K_i (i_0)_{10} + n\phi' \qquad A(1)$$

where K_i is a function of blade thickness distribution and $(i_0)_{10}$ is the zero-camber incidence angle (function of β_1 and σ). n is a slope factor given by

$$n = (i - i_0) / \phi'_{2-D} \qquad A(2)$$

which is also a function of β_1 and σ.

In Ref. 1, $(i_0)_{10}$ is given in Fig. 137 and n is given in Fig. 138. K_i has the value 0.7 for double circular-arc aerofoil shapes.

<u>A2.2 Two-Dimensional Deviation Angle</u>. As in the analysis of reference incidence angle, the correlation of blade-element deviation angle is expressed in terms of blade geometry by

$$\delta^o_{2-D} = K_\delta \, (\delta_0{}^o)_{10} + (m / \sigma^b) \phi' \qquad A(3)$$

where K_δ is a function of blade type (0.7 for double circular arc). $(\delta_0{}^o)_{10}$ is the zero-camber deviation angle (function of β_1 and σ), m is a function of β_1, for the different basic camber distribution, and b is an exponent that is also a function of β_1.

Since deviation angle varies somewhat with incidence angle, a corrected deviation angle is defined as

$$\delta_{2-D}{}^o = K_\delta \, (\delta_0{}^o)_{10} + \frac{m}{\sigma^b} \phi' + (i_c - i_{2-D})\left(\frac{d\delta^o}{di}\right)_{2-D} \qquad A(4)$$

where $(d\delta/d_i)_{2-D}$ is the slope of the two-dimensional variation of deviation angle with incidence angle at reference incidence, and i_c is the actual incidence angle.

Camber and turning angle are related by the equation:

$$\phi' = \beta_1 - \beta_2 + \delta + i$$

or

$$\Delta\beta = \phi' + i - \delta \qquad A(5)$$

Once the two-dimensional deviation and incidence angles have been established, the turning angle can be computed.

<u>A2.3 Corrections for Three-Dimensional Effects</u>. The next step in the procedure is to correct reference deviation and reference incidence angles for three-dimensional effects. This is accomplished by defining the three-dimensional reference angles

$$(i_{ref})_{3-D} = i_{2-D} + (i - i_{2-D})deg \qquad A(6)$$

and

$$(\delta_{ref})_{3-D} = \delta_{2-D} + (\delta - \delta_{2-D}) \qquad A(7)$$

where $(i - i_{2-D})$ and $(\delta - \delta_{2-D})$ are functions of Mach number.

In summary, the desired turning angle is given by Eq. 288 of Ref. 1.

$$\Delta\beta = \phi'\left[1 - \frac{m}{b} + n\right] - \left[(\delta_c^o - \delta_{2-D}) - (i_c - i_{2-D})\left[1.0 - \left(\frac{d\delta^o}{d_i}\right)_{2-D}\right] - K_i(i_0)_{10} + K_\delta(\delta_0^o)_{10}\right] \qquad A(8)$$

<u>A2.4 Loss Coefficient</u>. The loss coefficient for a blade element can be calculated from the correlation given in

Fig. 203 of Ref. 1. Here the "total loss parameter" is correlated in terms of "Diffusion Factor". The calculation of losses is given in Appendix D.

A3. POLYNOMIAL REPRESENTATION OF CORRELATIONS

All values on the right side of Eq. A(8) may be determined using data given in Figures in Ref. 1 once the geometry of the blade has been given and the inlet velocity calculated.

Each of the unknown values of Eq. A(8) are functions of blading geometry and air inlet angle or blading geometry and Mach number, and are described by well-behaved families of curves. Fig. 168 of Ref. 1 has been chosen to illustrate the process of computerizing the solution, which involved reducing the data correlations given in figures to analytical expressions.

Eleven values of air inlet angle (β_1) were chosen for each solidity given in Fig. 168. The values were plotted as slope factor (m) vs. air inlet angle (β_1) for constant solidity. The data points for each solidity were fit by a third order polynomial curve using the Hewlett-Packard 9830A calculator and X-Y plotter. For simplicity, a fifth order plotting routine was always used with the higher order coefficients equal to zero if a lower order resulted in a more appropriate fit. The plot and polynomial curve fits for each solidity are shown in Fig. A3. The polynomial curve fit for each set of data points gave six soefficients for each curve. Thus for each m vs. β_1 plot, the six coefficients A_0, A_1,.....,A_5 were calculated for the polynomial

expression for m as a function of β_1:

$$m = A_0 + A_1\beta_1 + A_2\beta_1^2 + A_3\beta_1^3 + A_4\beta_1^4 + A_5\beta_1^5 \qquad A(11)$$

at each value of solidity with β_1 converted to radians to minimize the error in higher order terms. The coefficients $A_0, A_1, \ldots, A_5$ derived from the curve fits of Fig. A3 were plotted against each of twelve values of solidity as follows:

$$\begin{aligned} &A_0\ (I)\ \text{vs.}\ \sigma(I)\ldots\ldots\ldots 12\text{points} \\ &A_1\ (I)\ \text{vs.}\ \sigma(I)\ldots\ldots\ldots 12\text{points} \\ &\vdots \\ &A_5\ (I)\ \text{vs.}\ \sigma(I)\ldots\ldots\ldots 12\text{points} \end{aligned} \qquad A(12)$$

This produced curves of the form

$$\begin{aligned} A_0 &= a_0 + a_1\sigma + a_2\sigma^2 + a_3\sigma^3 + a_4\sigma^4 + a_5\sigma^5 \\ A_1 &= a_0^1 + a_1\sigma^1 + a_2^1\sigma^2 + a_3^1\sigma^3 + a_4^1\sigma^4 + a_5^1\sigma^5 \\ &\vdots \\ A_5 &= a_0^5 + a_1^5\sigma + a_2^5\sigma^2 + a_3^5\sigma^3 + a_4^5\sigma^4 + a_5^5\sigma^5 \end{aligned} \qquad A(13)$$

which resulted in polynomial curve fits shown in Fig. A4. In this case the higher order coefficients A_4 and A_5 are set equal to zero. When all the coefficients in Eq. A(13) are known, the slope factor m, for any given σ and β_1 can be calculated from:

$$\begin{aligned} m = &(a_0 + a_1\sigma + a_2\sigma^2 + a_3\sigma^3 + a_4\sigma^4 + a_5\sigma^5) \qquad A(14) \\ &+ (a_0^1 + a_1^1\sigma + a_2^1\sigma^2 + a_3^1\sigma^3 + a_4^1\sigma^4 + a_5^1\sigma^5)\beta_1 \ldots + \\ &\ldots + (a_0^5 + a_1^5\sigma + a_2^5\sigma^2 + a_3^5\sigma^3 + a_4^5\sigma^4 + a_5^5\sigma^5)\beta_1^5 \end{aligned}$$

This procedure resulted in a single equation (Eq. A(14))for m in which the coefficients were analytic functions of β_1.

The coefficients are given in Tables A1 and A2. Due to the well-behaved nature of the curves, the slope factor m could be calculated to well within the accuracy of the original data contained in Ref. 1.

All data necessary to predict performance for circular-arc blading was reduced to polynomials using a similar procedure. The polynomials were included in a computer program to calculate blade element performance for specified input geometry and flow conditions.

A4. COMPUTER PROGRAM

A4.1 Description. Program "NASA36" was written for the Hewlett-Packard 9830A calculator to calculate the incidence and deviation angles for a rotor with meridional inlet velocity. The program follows the method of Ref. 1 through the equations given in Section A2. Where a value from a Figure in Ref. 1 is required, it is calculated using a polynomial approximation to the data as described in Section A3.

The program is self-explanatory through the listing given in Table A3. The symbols are defined in Table A4. The program performs the blade element calculations for a specified compressor operating condition. The inputs are referred flow rate and speed, and temperatures upstream and downstream of the rotor. Through the method given in Appendix C, these inputs define the inlet velocity as a function of the radial position. It should be noted therefore that the present version of the program includes a description

of the transonic compressor inlet flow-field, while it allows changes in blading geometry to be input.

A4.2 Operation. Detailed information on the operating procedures for the HP-9830 calculator, mass memory and associated equipment are found in Ref. 9 and Ref. 10. The following is a step-by-step operating procedure for the program called "NASA36".

1. After loading "NASA36" into the Hewlett-Packard 9830A calculator press "Run" and "Execute".

2. The calculator will then display a series of inputs required to determine the geometry of the blading. These are shown in Fig. 3 and are:

a) Stagger angle

b) Chord with sharp leading and trailing edges

c) Tip radius

d) Hub radius

e) Diameter of cone through stacking radius

f) Maximum Profile Thickness

g) Radius of Profile Contour

h) Blade camber angle

i) Profile chord

j) Angle of cone thru stacking radius

3. The operating parameters of the compressor rotor are now required. These are:

a) Revolutions per minute

b) Total temperature upstream of rotor

c) Temperature downstream of rotor

d) Referred flow rate

Outputs include deviation and incidence angles, Mach number before and after the rotor, and referred flow function (Φ).

Table A1

Coefficients for Eq. A(11)

Value of Solidity	A_0	A_1'	A_2	A_3	A_4	A_5
.4	.60422074	-.00172689	.05745331	-.0686459	0	0
.5	.48957429	-.002457967	.07365157	-.05157576	0	0
.6	.40879632	.01587984	.024863524	-.0072702	0	0
.7	.349811725	.025196542	.02439882	-.00063945	0	0
.8	.30978144	.03080154	-.00434522	.0243992	0	0
.9	.280292	.02295859	-.0005187	.03103606	0	0
1.0	.24934145	.03885258	-.0253336	.043310059	0	0
1.2	.2093762	.04138388	-.040108605	.05919224	0	0
1.4	.181571948	.02853839	-.03145125	.0626165	0	0
1.6	.160653459	.013581617	-.013581617	.056440537	0	0
1.8	.14262652	.02473965	-.0389736	.0715060	0	0
2.0	.12848536	.02868824	-.0346697	.0655224	0	0

Table A2

Coefficients for Eq. A(13)

Coefficient	a_0	a_1	a_2	a_3	a_4	a_5
A_0	1.1078294	-1.70264568	1.070834595	-.23258418	0	0
A_1	.12218714	-.18703165	.06354814	-.0044876	0	0
A_2	-.25565987	.628179584	-.38691079	.08008022	0	0
A_3	0	0	0	0	0	0
A_1	0	0	0	0	0	0

TABLE A3 PROGRAM LISTING

```
10 REM --PROGRAM---****NASA36****---W.R.HAWKINS----1/7/76--------
20 REM----PROGRAM TO CALCULATE COMPRESSOR BLADING PERFORMANCE
30 REM----BASED UPON EMPIRICALLY DERIVED DATA (REFERENCED BY
40 REM-----"AERODYNAMIC DESIGN OF AXIAL COMPRESSORS",NASA,1965)
50 REM-----INPUTS REQUIRED ARE AIR INLET ANGLE(B1),CHORD LENGTH,
60 REM-----CAMBER ANGLE,THICKNESS/CHORD RATIO,STAGGER ANGLE,& SOLIDITY
70 DIM A[6],B[6],C[6],D[6],E[6],F[6],G[6],Z[6]
80 PRINT
90 RAD
100 DISP "ENTER STAGGER ANGLE(G),DEG.,MIN.)";
110 INPUT G,E9
120 E9=E9/60
130 G=G+E9
140 PRINT "STAGGER ANGLE(G)-----------------------------------"G"DEG"
150 DISP "ENTER E";
160 INPUT E
170 PRINT "CHORD WITH SHARP LEAD.&TRAILING EDGES(E)-----    "E
180 DISP "ENTER DIA. OF CONE THRU STACK RADIUS";
190 INPUT D0
200 R1=D0/2
210 REM     DISP "INPUT TIP RADIUS R0";
220 REM    INPUT R0
230 R0=5.5
240 REM     DISP "INPUT HUB RADIUS(R3)";
250 REM    INPUT R3
260 R3=3.58
270 PRINT "RADIUS AT ROTOR INLET(R1)--------------------------    "R1
280 PRINT "RADIUS AT ROTOR TIP  (R0)--------------------------    "R0
290 PRINT "RADIUS AT ROTOR HUB  (R3)--------------------------    "R3
300 DISP "ENTER THICKNESS(T)";
310 INPUT T
320 PRINT "THICKNESS(T)---------------------------------------    "T
330 DISP "ENTER RADIUS OF PROFILE CONTOUR(R9)";
340 INPUT R9
```

```
350 PRINT "ENTER RADIUS OF PROFILE CONTOUR(R9)-----------"R9
360 X=E/(2*R1)
370 P0=ATN(X/SQR(1-X↑2))
380 P0=P0*180/PI
390 PRINT "BLADE CAMBER ANGLE(P0)------------------------"P0"DEG"
400 DISP "ENTER PROFILE CHORD(C0)";
410 INPUT C0
420 S=(PI*2*R1)/18
430 PRINT "SPACING(S)------------------------------------"S
440 S0=C0/S
450 PRINT "SOLIDITY(S0)----------------------------------"S0
460 DISP "ENTER ANGLE OF CONE THRU STACK, RAD(DEG)";
470 INPUT H
480 H=H*PI/180
490 DISP "ENTER RPM";
500 INPUT R
510 PRINT "RPM(R)----------------------------------------"R
520 H1=((D0-1.376*TAN(H))/5.5)+1
530 H2=(D0+2.624*TAN(H)-7.16)/3.84
540 D3=(D0/2-0.688*TAN(H))*2
550 D4=(D0/2+1.312*TAN(H))*2
560 U1=(PI*R*D3)/(30*24)
570 U2=(PI*R*D4)/(30*24)
580 DISP "INPUT T1 TOTAL";
590 INPUT T1
600 T1=T1+459.688
610 DISP "ENTER T(TOTAL)2";
620 INPUT T2
630 T2=T2+459.688
640 GOSUB 3150
650 GOSUB 3430
660 T8=(1-Y1↑2)*T2
670 V8=109.62*(SQR(T8))
680 V3=Y1*V8
690 B1=ATN(U1/V3)
```

TABLE A3 (CONTINUED)

```
700 PRINT "BETA1(B1)------------------------------------------ "B1*180/PI"DEG"
710 B1=B1*180/PI
720 I=B1-P0/2-G
730 B1=B1*PI/180
740 PRINT "PROFILE CHORD(C0)------------------------------- "C0
750 T0=T/C0
760 PRINT "THICKNESS/CHORD RATIO----------------------------"T0
770 PRINT
780 PRINT
790 PRINT
800 REM----CALCULATE ZERO CAMBER INCIDENCE ANGLE(I0) FROM FIG. 137
810 X1=S0
820 REM-----COEFFICIENTS FIG.137
830 DATA 0.000636,-0.001466,0.000087,0,0,0
840 DATA 0.000671,0.086416,0.000831,0,0,0
850 DATA -0.002147,-0.008859,-0.000475,0,0,0
860 DATA 0,0,0,0,0,0
870 DATA 0,0,0,0,0,0
880 DATA 0,0,0,0,0,0
890 I0=FNZ(B1)
900 I0=180*I0/PI
910 PRINT "ZERO CAMBER INCIDENCE ANGLE -----FIGURE 137--   "I0"DEG"
920 PRINT "   "
930 REM-----CALCULATE SLOPE FACTOR(N) FROM FIGURE 138
940 X1=S0
950 REM-----COEFFICIENTS FIG.138
960 DATA 0.013041,-0.376566,0.774974,-0.708297,0.306622,-0.050579
970 DATA -0.879264,3.402177,-5.761135,4.962811,-2.053883,0.325004
980 DATA 0.384817,-2.637453,4.778125,-4.148041,1.706835,-0.267415
990 DATA 0,0,0,0,0,0
1000 DATA 0,0,0,0,0,0
1010 DATA 0,0,0,0,0,0
1020 N=FNZ(B1)
1030 PRINT "SLOPE FACTOR(N)-----FIGURE 138---------------------    "N
1040 PRINT "   "
```

TABLE A3 (CONTINUED)

```
1050 REM----CALCULATE CORRECTION FACTOR(K1) FROM FIGURE 142
1060 DATA -0.000137,19.138403,-125.752414,343.82285,0,0
1070 MAT READ A
1080 K1=FNP(T0)
1090 PRINT "CORRECTION FACTOR(K1)---FIGURE 142----------  "K1
1100 PRINT "   "
1110 K0=0.7
1120 REM***CALCULATE 2-DIM REFERENCE ANGLE***
1130 I1=K0*K1*I0+N*P0
1140 PRINT "****2-DIM. REFERENCE INCIDENCE ANGLE(I1)***  "I1"DEG"
1150 PRINT "   "
1160 PRINT "   "
1170 REM----CALCULATE ZERO CAMBER DEVIATION ANGLE(D1) FROM FIG. 161
1180 X1=S0
1190 REM----COEFFICIENTS FIG.161
1200 DATA -0.453433,2.579382,-5.217276,4.780341,-2.031498,0.324804
1210 DATA 4.926602,-25.689873,53.480056,-48.402612,20.021683,-3.071158
1220 DATA -8.271574,44.385592,-86.271767,74.424845,-29.602908,4.347884
1230 DATA 1.912247,-7.995133,12.803662,-5.827965,0.105506,0.370343
1240 DATA 0,0,0,0,0,0
1250 DATA 0,0,0,0,0,0
1260 D1=FNZ(B1)
1270 PRINT "ZERO CAMBER DEVIATION  ANGLE(D1)--FIGURE 161-  "D1"DEG"
1280 PRINT "     "
1290 REM----CALCULATE SLOPE FACTOR(M) FROM FIGURE 168
1300 X1=S0
1310 REM----COEFFICIENTS FIG. 168
1320 DATA 1.6515028,-4.463623015,6.105404369,-4.416738437,1.610496857,-0.2327375
1330 DATA 0.182868,-0.428030048,0.339064375,-0.060885158,-0.059347634,0.02260378
1340 DATA -0.569236,2.18965113,-3.158964364,2.3046766,-0.819050758,0.111924774
1350 DATA 0,0,0,0,0,0
1360 DATA 0,0,0,0,0,0
1370 DATA 0,0,0,0,0,0
1380 M=FNZ(B1)
1390 PRINT "SLOPE FACTOR(M)----FIGURE 168-------------  "M
```

TABLE A3 (CONTINUED)

```
1400 PRINT "   "
1410 REM----CALCULATE CORRECTION FACTOR(K ) FROM FIG. 172
1420 DATA -0.001662,8.248814,-6.181318,231.64355,0,0
1430 MAT READ A
1440 K2=FNP(T0)
1450 PRINT "CORRECTION FACTOR(K2)----FIGURE 17  --------  "K2
1460 PRINT "   "
1470 REM****CALCULATE 2-DIM REFERENCE DEVIATION ANGLE(D2)****
1480 D2=K0*K2*D1+M*F0
1490 PRINT "***2-DIM. REFERENCE DEVIATION ANGLE(D2)****   "D2"DEG"
1500 PRINT "   "
1510 PRINT "   "
1520 REM-----CALCULATE SLOPE AT REFERENCE INCIDENCE(K9) FROM FIG. 177
1530 X1=B1
1540 DATA 0.96354267,0.11284222,-0.29700206,0.19853914,0,0
1550 DATA -2.30672898,-0.3060019,1.03794406,-0.16526256,0,0
1560 DATA 1.83870369,0.31632269,-1.05984846,-0.00904133,0,0
1570 DATA -0.477233144,-0.10789486,0.33398654,0.02129055,0,0
1580 DATA 0,0,0,0,0,0
1590 DATA 0,0,0,0,0,0
1600 K9=FNZ(S0)
1610 PRINT "SLOPE AT REF. INCIDENCE ANG.(K9)--FIGURE 177  "K9
1620 PRINT "   "
1630 REM****CALCULATE DEVIATION ANGLE(D)****
1640 D=D2+(I-I1)*K9
1650 PRINT "****2-DIM.DEVIATION ANGLE(D)**** -----------  "D"DEG"
1660 PRINT "   "
1670 PRINT "   "
1680 REM---BEGIN CALCULATIONS FOR 3-DIM. EFFECTS--------------
1690 REM-----CALCULATE VARIATION OF AVERAGE REF. INCIDENCE ANGLE MINUS LOW-
1700 REM-----SPEED 2-DIM.-CASCADE-RULE REF. INCIDENCE ANGLE(I9)--FIG.201--
1710 W1=SQR(V3↑2+U1↑2)
1720 A0=SQR(1.402*32.174*53.35*T8)
1730 M1=V3/A0
1740 M8=W1/A0
```

TABLE A3(CONTINUED)

```
1750 PRINT "RELATIVE MACH# ------------------------------ "M9
1760 REM-----CAL. % BLADE HEIGHT FROM COMPRESSOR TIP ----
1770 07=(1-H1)
1780 PRINT "% BLADE HEIGHT FROM COMPRESSOR TIP-------------- "07*100
1790 07=07*PI/180
1800 PRINT
1810 X1=07
1820 DATA 3.1904866,2.63303497,0.59823692,-0.25517487,0,0
1830 DATA -33.02330069,-75.74313142,9.42464303,0.410693,0,0
1840 DATA 54.18997981,65.30572852,-26.18918077,1.65947664,0,0
1850 DATA -22.16945937,-34.57348169,13.04161503,-0.37704419,0,0
1860 DATA 0,0,0,0,0,0
1870 DATA 0,0,0,0,0,0
1880 I9=FNZ(M8)
1890 PRINT "DEDUCED VARIATION OF AVER. ROTOR REF.INCIDENCE ANGLE MINUS LOW-"
1900 PRINT "SPEED 2-DIM.-CASCADE-RULE REF.INCIDENCE ANGLE(I9) FIG.20)-------"
1910 PRINT "------------------------------------------------ "I9"DEG"
1920 PRINT " "
1930 REM-----CAL. 3-DIM. REF. INCIDENCE ANGLE-----
1940 I6=I1+I9
1950 PRINT "****3-DIM. REF. INCIDENCE ANGLE(I6)****--- "I6"DEG"
1960 PRINT " "
1970 PRINT " "
1980 REM-----CALCULATE DEDUCED VARIATION OF AVERAGE ROTOR DEVIATION ANGLE
1990 REM-----MINUS LOW SPEED 2-DIM.-CASCADE-RULE DEVIATION ANGLE AT ------
2000 REM-----COMPRESSOR REFERENCE INCIDENCE ANGLE -----
2010 X1=07
2020 DATA -2.134354,4.383126,-3.93633,1.696049,0,0
2030 DATA 1.36E+00,-1.019E+01,1.182E+01,-4.506E+00,0,0
2040 DATA -1.253E+00,9.18E+00,-1.014E+01,3.886E+00,0,0
2050 DATA 0,0,0,0,0,0
2060 DATA 0,0,0,0,0,0
2070 DATA 0,0,0,0,0,0
2080 D9=FNZ(M8)
2090 PRINT "DEDUCED VARIATION OF AVERAGE ROTOR DEVIATION ANGLE-----------"
```

TABLE A3 (CONTINUED)

```
2100 PRINT "--AINOS LOW SPEED 2-DIM. CASCADE-RULE DEVIATION ANGLE AT ----"
2110 PRINT "COMPRESSOR REFERENCE INCIDENCE ANGLE ------- "D9"DEG"
2120 PRINT "  "
2130 REM----CAL. 3-DIM. REF. DEVIATION ANGLE-----------------------------
2140 D6=D+D9
2150 PRINT "****3-DIM. DEVIATION ANGLE(D6)****------------- "D6"DEG"
2160 PRINT "  "
2170 PRINT "  "
2180 B1=B1*180/PI
2190 B2=B1-(P0+I6-D6)
2200 PRINT "  "
2210 PRINT "U1-------------------------------------------- "U1"FT./SEC."
2220 PRINT "U2-------------------------------------------- "U2"FT./SEC."
2230 B1=B1*PI/180
2240 B2=B2*PI/180
2250 W3=W1*SIN(B1)
2260 V5=0
2270 A1=ATN(V5/V3)
2280 V1=SQR(V5↑2+V3↑2)
2290 V4=V3
2300 W2=V4/(COS(B2))
2310 W4=W2*SIN(B2)
2320 V6=U2-W4
2321 A2=ATN(V6/V4)
2322 V2=V4/(COS(A2))
2330 V9=109.62*SQR(T2)
2340 Y2=V2/V9
2350 T9=(1-Y2↑2)*T2
2380 A1=A1*180/PI
2390 A0=SQR(1.402*32.174*53.35*T9)
2400 M2=V2/A0
2420 PRINT "BETA1----------------- "B1*180/PI
2430 PRINT "ALPHA1---------------- "A1
2440 PRINT "V1-------------------- "V1
2450 PRINT "VA1------------------- "V3
```

```
2460 PRINT "VU1-----------------------"V5
2470 PRINT "W1------------------------"W1
2480 PRINT "WU1-----------------------"W3
2490 PRINT "M1------------------------"M1
2500 PRINT "X1------------------------"Y1
2520 PRINT
2530 PRINT
2540 PRINT "V(TOTAL 1)----------------"V8
2550 PRINT "PHI-----------------------"P1
2560 PRINT "PHI(C-LINE VALUE)---------"I5
2570 PRINT "T TEMP(1)-----------------"T8-459.688
2580 PRINT "REFERRED FLOW RATE--"I4
2590 PRINT "NON-DIM RADIUS(HUB TO TIP)"H1
2600 PRINT
2601 REM--- CALCULATION OF COMPLETE VELOCITY TRIANGLES ASSUMES
2602 REM--- AXIAL THROUGH FLOW VELOCITY CONSTANT---------------
2610 PRINT
2620 PRINT "BETA2---------------------"B2*180/PI
2630 PRINT "ALPHA2--------------------"A2*180/PI
2640 PRINT "V2------------------------"V2
2650 PRINT "VA2-----------------------"V4
2660 PRINT "VU2-----------------------"V6
2670 PRINT "W2------------------------"W2
2680 PRINT "WU2-----------------------"W4
2690 PRINT "T (TEMP 2)----------------"T9-459.688
2700 PRINT "M2------------------------"M2
2710 PRINT "X2(CAL)-------------------"Y2
2740 PRINT "V(TOTAL2)-----------------"V9
2770 PRINT "NON-DIM RADIUS(HUB TO TIP)"H2
2780 PRINT
2790 PRINT
2800 DISP "DRAW VEL. DIA.? YES=1,NO=0";
2810 INPUT N9
2820 PRINT "  "
2830 DEG
```

```
2840 IF N9=0 THEN 2860
2850 CHAIN "BPLOT"
2860 PRINT
2870 PRINT
2880 STOP
2890 END
2900 DEF FNZ(X0)
2910 MAT READ B
2920 MAT READ C
2930 MAT READ D
2940 MAT READ E
2950 MAT READ F
2960 MAT READ G
2970 MAT A=B
2980 Z[1]=FNP(X1)
2990 MAT A=C
3000 Z[2]=FNP(X1)
3010 MAT A=D
3020 Z[3]=FNP(X1)
3030 MAT A=E
3040 Z[4]=FNP(X1)
3050 MAT A=F
3060 Z[5]=FNP(X1)
3070 MAT A=G
3080 Z[6]=FNP(X1)
3090 MAT A=Z
3100 X2=FNP(X0)
3110 RETURN X2
3120 DEF FNP(X2)=A[1]+A[2]*X2+A[3]*X2↑2+A[4]*X2↑3+A[5]*X2↑4+A[6]*X2↑5
3130 STOP
3140 END
3150 REM---SUBROUTINE TO CALCULATE X BASED ON REFERRED FLOW RATE
3160 DISP "ENTER REFERRED FLOW RATE";
3170 INPUT I4
3180 I5=-0.005809+0.011326*I4
```

TABLE A3 (CONTINUED)

```
3190 REM --- COEFFICIENTS FOR FLOW COEFF.
3200 REM --THIS SCHEME TAKES THE VALUE OF REFERRED FLOW RATE
3210 REM -- AND OBTAINS THE CLOSEST CURVE APPROX. FIT
3220 IF I4<9.165 THEN 3290
3230 IF I4>9.165 AND I4 <= 10.135 THEN 3310
3240 IF I4>10.135 AND I4 <= 11.035 THEN 3330
3250 IF I4>11.035 AND I4 <= 11.3 THEN 3350
3260 IF I4>11.3 AND I4 <= 12.625 THEN 3370
3270 IF I4>12.625 AND I4 <= 14.065 THEN 3390
3280 IF I4>14.065 THEN 3410
3290 P1=(0.896413+0.347221*H1-0.220228*(H1)↑2-0.119712*(H1)↑3)*I5
3300 GOTO 3420
3310 P1=(0.857467+0.496957*(H1)-0.40696*(H1)↑2-0.03361*(H1)↑3)*I5
3320 GOTO 3420
3330 P1=(0.920532+0.299275*H1-0.258236*(H1)↑2-0.044748*(H1)↑3)*I5
3340 GOTO 3420
3350 P1=(0.954823+0.082347*(H1)+0.163275*(H1)↑2-0.294517*(H1)↑3)*I5
3360 GOTO 3420
3370 P1=(0.964092+0.119941*H1-0.01897*(H1)↑2-0.154942*(H1)↑3)*I5
3380 GOTO 3420
3390 P1=(0.98905-0.017937*H1+0.219834*(H1)↑2-0.28032*(H1)↑3)*I5
3400 GOTO 3420
3410 P1=(1.009099-0.088129*H1+0.290343*(H1)↑2-0.300944*(H1)↑3)*I5
3420 RETURN
3430 REM---SUBROUTINE TO CAL NON-DIM VELOCITY(X)------
3440 G0=1.402
3450 Y1=0.15
3460 P2=Y1*(1-Y1↑2)↑(1/(G0-1))
3470 P4=(1-Y1↑2)↑(1/(G0-1))
3480 P4=P4+(-2*Y1↑2)*(1/(G0-1))*(1-Y1↑2)↑(1/(G0-1)-1)
3490 IF ABS(P2-P1)<0.000001 THEN 3520
3500 Y1=Y1+(P1-P2)/P4
3510 GOTO 3460
3520 RETURN
```

PROGRAM:

TABLE A4

	ARRAY	SIMPLE VARIABLE "NASA36" SUBSCRIPT										
			0	1	2	3	4	5	6	7	8	9
A	⊠		a_1	α_1	α_2							
B	⊠			β_1	β_2							
C	⊠		C									
D	⊠	δ		$(\delta_o)_{10}$	δ^{2-0}_{ref}	D_{m1}	D_{m2}		δ_{3-0}			⊠
E	⊠	E								⊠	⊠	⊠
F	⊠											
G	⊠	γ	$\gamma'_{(air)}$	$\frac{\gamma}{\gamma-1}$								
H		H		⊠	⊠							
I		i	$(i_o)_{10}$	$i_{ref.\,2-0}$			$\dot{\omega}^*$	Φ_{CL}	i_{3-0}			⊠
J												
K		$(K_i)_{SH}$	$(K_i)_t$	$(K_s)_t$								⊠
L												
M		m	a_a	M_1	M_2						M_{u1}	M_{u2}
N		n										⊠
O										⊠	⊠	⊠
P		$P_{ref.}$	ϕ'	Φ	⊠		$\frac{d\Phi}{dx}$				P_{t1}	P_{t2}
Q												
R		RPM	R_{Tip}	R	R_{Hub}							⊠
S		S	σ									
T		t	t/c	T_{t1}	T_{t2}						T_1	T_2
U				U_1	U_2							
V				V_1	V_2	V_{a1}	V_{a2}	V_{u1}	V_{u2}		V_{t1}	V_{t2}
W				W_1	W_2	W_{u1}	W_{u2}					
X		⊠	⊠	⊠	⊠							
Y				X_1	X_2			X_{u1}	X_{u2}			⊠
Z	⊠											

SCORE SHEET: RECORD OF VARIABLES USED.

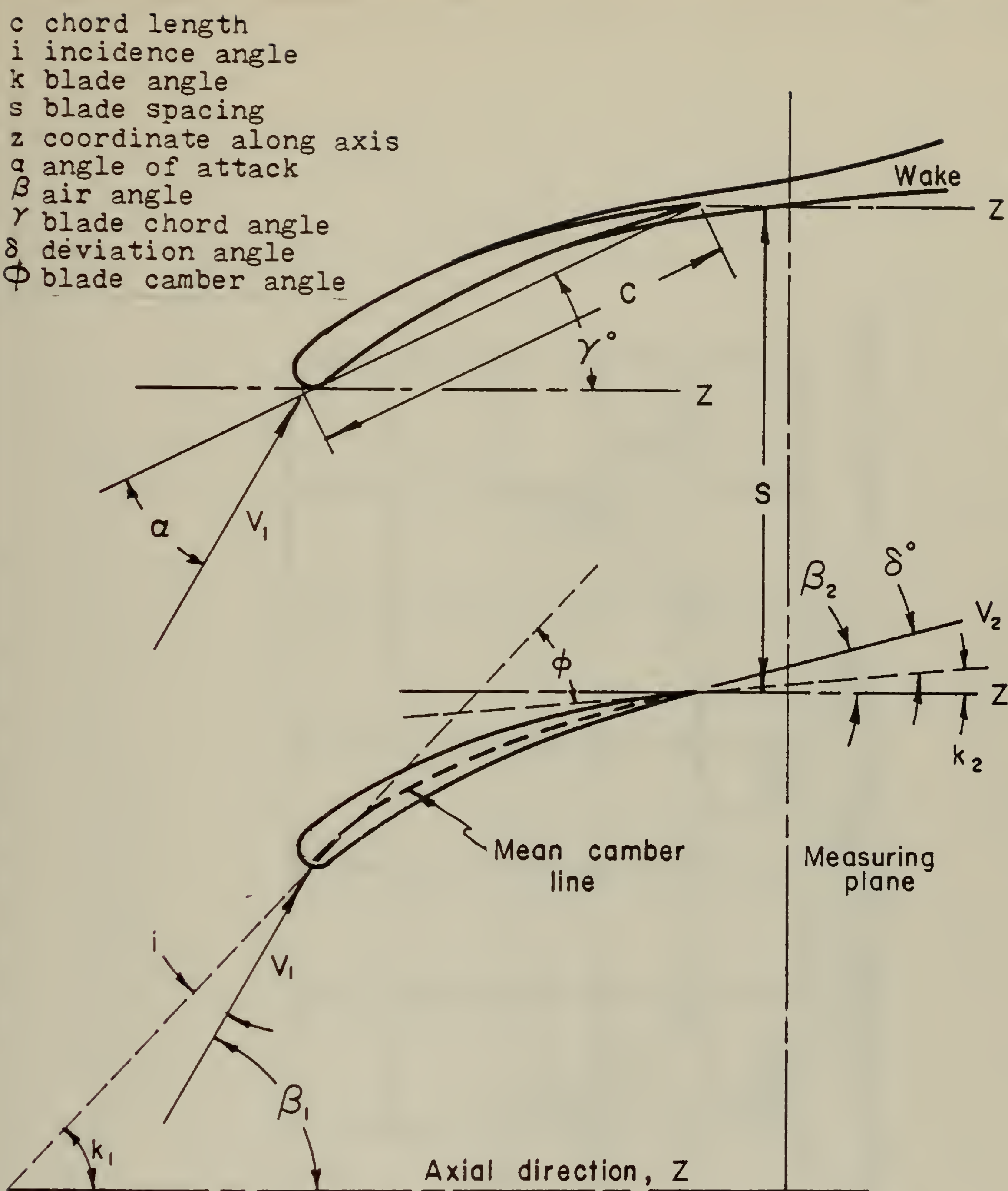

FIG. A1 NOMENCLATURE FOR CASCADE BLADE

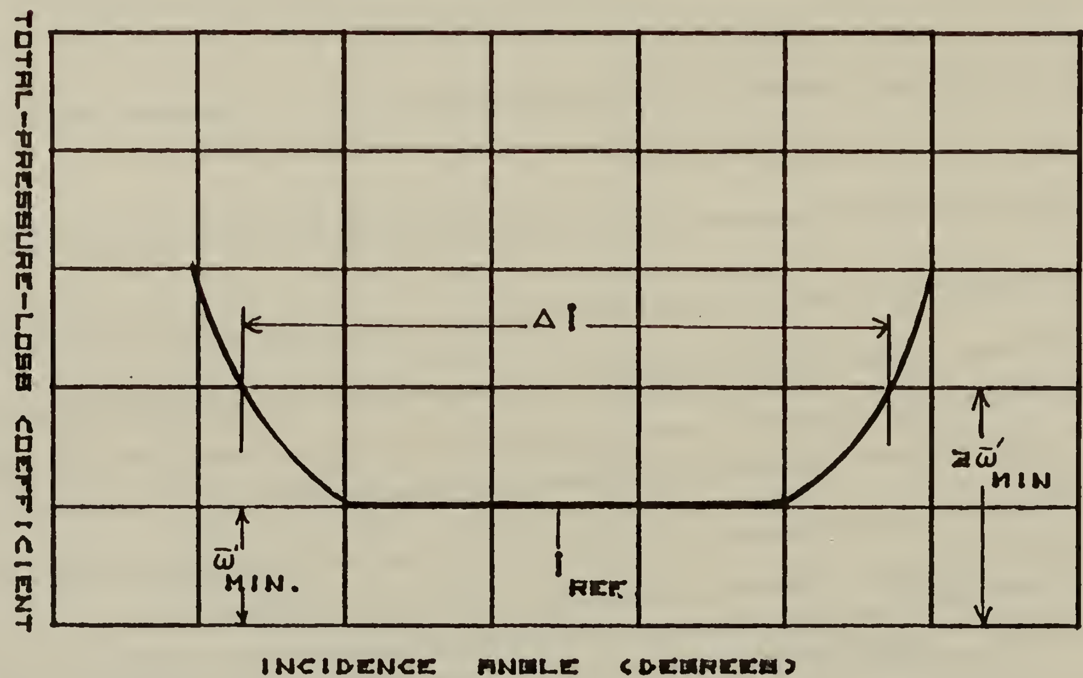

FIG. A2 TOTAL-PRESSURE-LOSS COEFFICIENT VS. INCIDENCE ANGLE

FIG. A3
DEDUCED VARIATION OF SLOPE FACTOR M IN DEVIATION-ANGLE RULE FOR CIRCULAR-ARC-MEAN-LINE BLADES

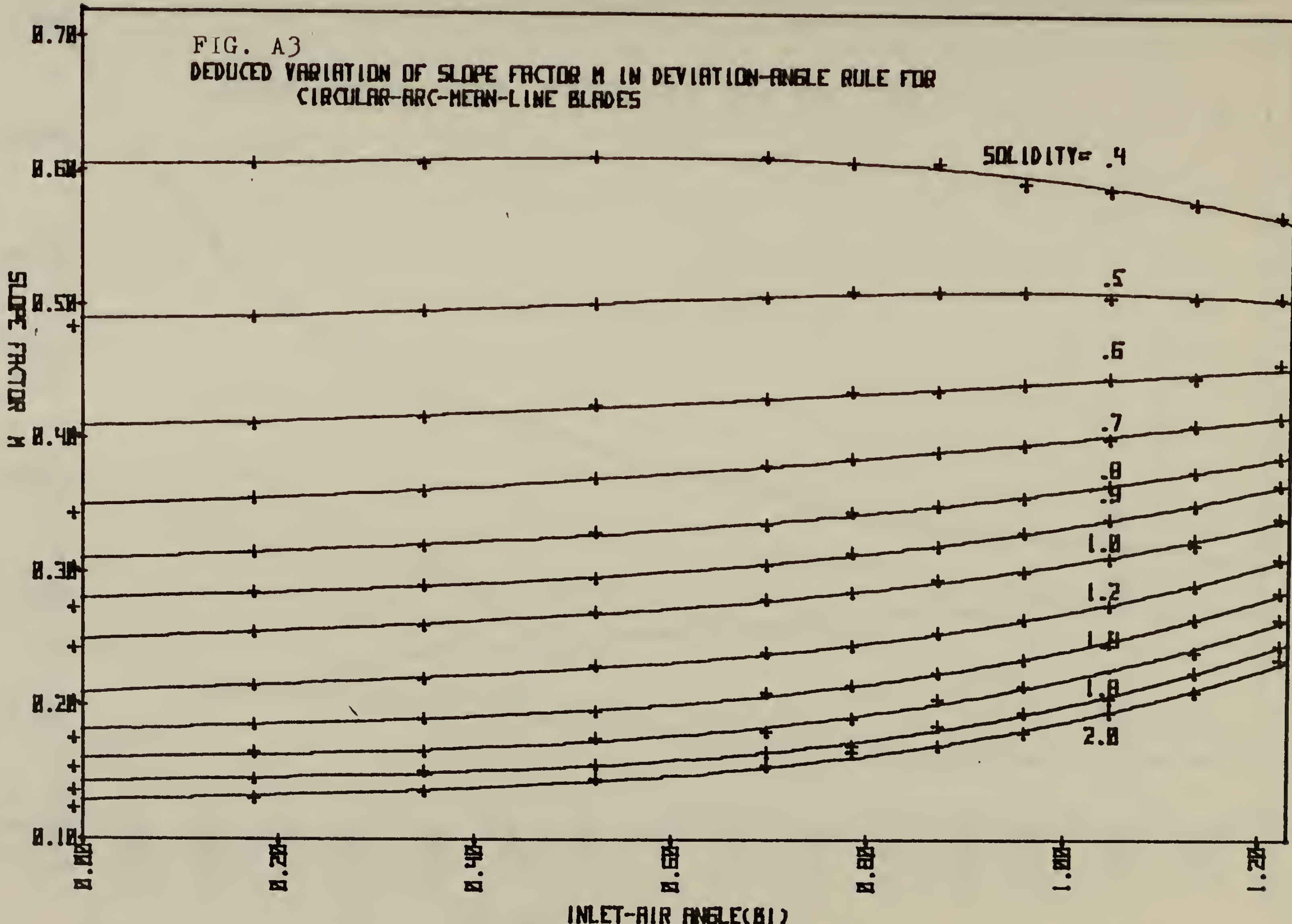

FIG.

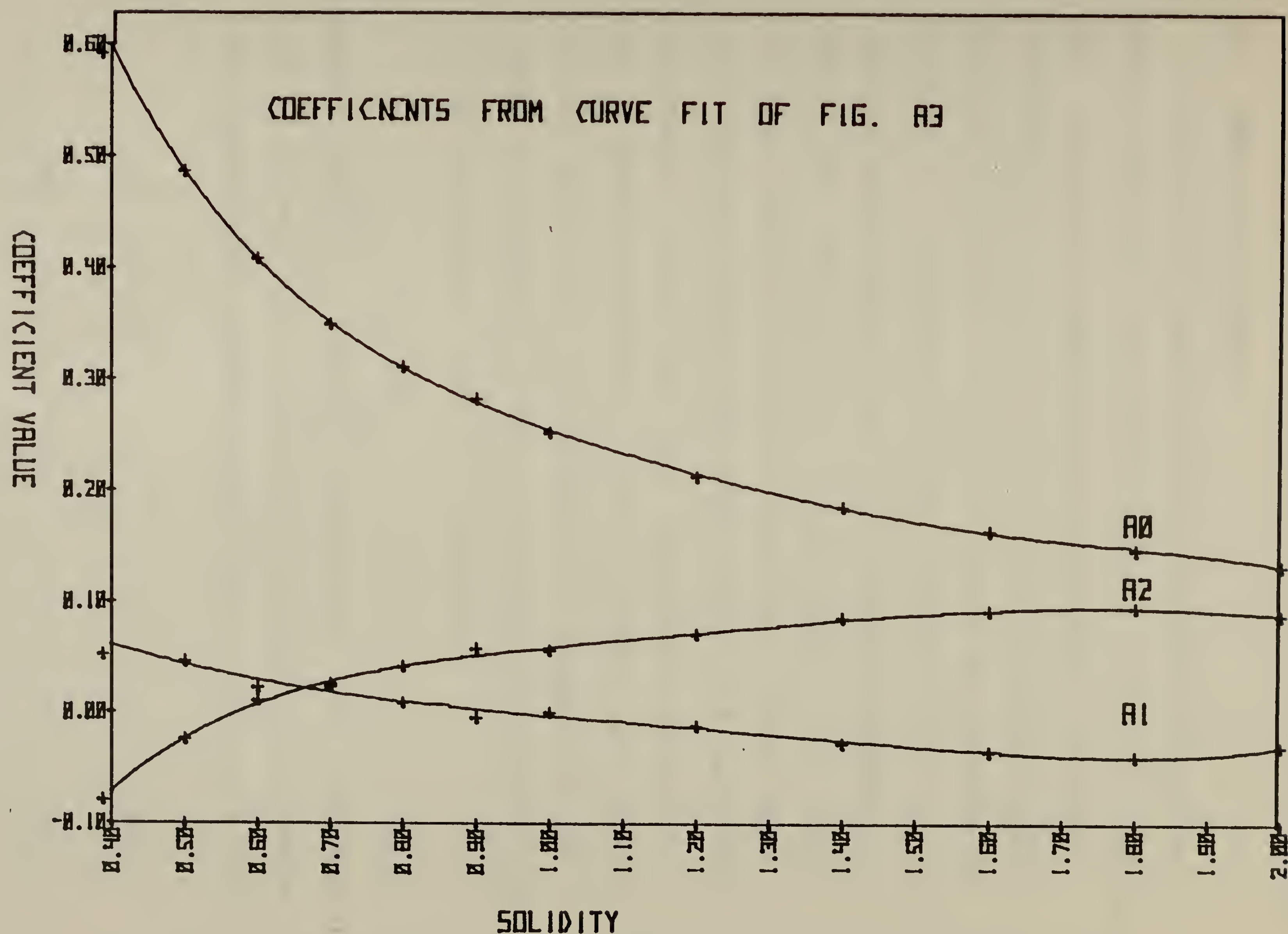

FIG. A4 VARIATION OF OCEFFICIENTS OF POLYNOMIAL CURVES IN FIG. A3

APPENDIX B: CALIBRATION AND CORRECTION OF PNEUMATIC PROBES

B1. FREE-JET APPARATUS

The free-jet apparatus used to calibrate probes is shown in Fig. B1. The device consisted of a 8 inch diameter pipe with the air supplied by the laboratory's central Allis-Chalmers Compressor. A 4.2 inch converging nozzle was used to increase velocity and attain Mach numbers up to about .9. To determine if the exiting velocity was uniform and undisturbed by the probe mounting arrangement, surveys were conducted with a Prandtl probe over a range of 5 Mach numbers at two axial locations. Surveys were also conducted with the same probe mounted and traversed from opposite sides of the jet. The results shown in Fig. B2 indicated that the velocity profiles were uniform over the core of the jet extending to a diameter of 3.8 inches. As suggested in Ref. 11, the non-dimensional velocity (X) appearing in Fig. B2 is defined by

$$X = V/V_t \qquad \mathrm{B(1)}$$

where $V_t = \sqrt{2C_pT_t} = 109.62\sqrt{T_t}$ when T_t is in ^{o}R. Following Ref. 11 further, the relationships for stagnation pressure, total temperature, and Mach number are, in terms of X given by

$$\frac{T}{T_t} = 1 - X^2 \qquad \mathrm{B(2)}$$

$$\frac{P}{P_t} = (1 - X^2)^{\gamma/(\gamma-1)} \qquad \mathrm{B(3)}$$

$$M = \frac{V}{\sqrt{\gamma RT}} = \frac{2}{\sqrt{\gamma - 1}} \cdot \frac{X}{\sqrt{1 - X^2}} \qquad B(4)$$

The values of X in Fig. B2 were calculated using the measurement of stagnation pressure and the assumption of atmospheric static pressure in Eq. B(3).

B2. CALIBRATION OF THE COMBINATION PROBE

Calibration of the pneumatic probe reported in Ref. 2 can be represented by defining two functions of the nondimensional velocity, X, and the pitch angle, ϕ. If P_1 and $P_{2/3}$ are indicated stagnation and indicated static pressure of the probe respectively, then define

$$F_\theta = F_\theta\,(X,\phi) = \frac{P_1 - P_{2/3}}{P_1} \qquad B(5)$$

$$F_\phi = F_\phi\,(X,\phi) = \frac{P_1 - P_4}{P_1} \qquad B(6)$$

to be calibration functions when the probe is rotated to balance $P_2 = P_3$. P_4 is the fourth, off axis pressure measured by the probe.

The complete calibration procedure is given in detail in Ref. 3. The probe was recalibrated to confirm the results given in Ref. 2 before investigating corrections for boundary effects. A range of Mach numbers (X = .13 to .4) and pitch angles (-20° to 20°) were used. With true static pressure taken to be atmospheric and true impact pressure that measured by a reference Prandtl probe, the value of X was calculated from Eq. B(3). As in Ref. 2, polynomial

representations were found for the calibration equations written in the form

$$X = X(F_{\theta}, \phi) \tag{B(7)}$$

and

$$F_{\phi} = F_{\phi}\ (X, \phi) \tag{B(8)}$$

where F_{θ}, and F_{ϕ} are the ratios of probe pressure measurements defined in Eq. B(5) and Eq. B(6). It is noted that Eq. B(6) departs from the definition used by Dodge in Ref. 2. The present method was found to give more accurate results. The coefficients in Eq. B(7) and Eq. B(8) derived from the calibration test results are given in Table B1.

As a test of the analytical representation of the calibration, the calibration data were used to calculate values of X and ϕ to compare with the actual values. Table B2 shows the results of this comparison for the velocity. The error in X is generally less than 1% and only reaches higher values at high positive or negative pitch angles (16° or -8°) or at higher Mach numbers (.88). At this point the error increases to about 2%.

Fig. B3 shows the error in the pitch angle in the range of pitch angle from -4° to $+12^{\circ}$. The error is seen to be $\pm 1\frac{1}{2}^{\circ}$ and is not a simple function of either pitch angle or Mach number (or X). There appears to be a limit to the capability of resolving ϕ. The error was larger at high negative and positive values of pitch angles but these were outside the intended range of use.

B3. BOUNDARY EFFECT ON COMBINATION PROBE MEASUREMENTS

In application, the probe is not in plane flow away from all boundaries. The indicated velocity and pitch angle will depend upon several factors including boundary layer and stem immersion effects. The method of approach assumed here was that the probe always obeys the calibrations established and that errors are induced due to the perturbation of the probe itself on the flow near the boundary. Thus, in any flow the probe measures a velocity, X, and a pitch angle, ϕ, which are the sum of the actual and an "induced" component.

Three surveys were conducted in a 10 inch pipe up to the maximum attainable Mach number of .55. The results of calculating velocity applying the free jet calibration given above are shown in Fig. B4.

Introducing subscripts a(actual), i(induced), and m(measured), the velocity, X, may be represented by

$$X_m = X_a + X_i = X_a \left[1 + \frac{X_i}{X_a}\right] = X_a \, (1 + \epsilon_x) \qquad \text{B(9)}$$

where the fractional 'error' in X, ϵ_x, which is induced by the presence of the wall, is given by

$$\epsilon_x = \frac{X_m - X_a}{X_a} \qquad \text{B(10)}$$

X_m is determined from the probe calibration in the usual way. X_a is the required, correct velocity, and ϵ_x is the error to be established by calibration tests.

The measured velocity is corrected using

$$X_a = \frac{X_m}{1 + \epsilon_x} \tag{B(11)}$$

when the error ϵ_x is known.

In the same manner actual pitch angle may be represented by

$$\phi_a = \phi - \epsilon_\phi \tag{B(12)}$$

In the 10 inch pipe tests, the actual velocity was calculated from the probe impact pressure and pipe wall static pressure using Eq. B(3) and the actual pitch angle was zero. Thus the "induced" error in X was calculated using Eq. B(10) and the "induced" error in ϕ was calculated using Eq. B(12). The two errors, ϵ_x and ϵ_ϕ, were then examined as a function of distance from the pipe walls expressed as a number of probe diameters; (the characteristic dimension of the probe was taken to be 0.1 inches). It was found that the errors became negligible at about 9.5 probe diameters from the boundary. In order to derive an expression of a suitable form, the errors were plotted as a function of (9.5-D), where D is the displacement as a number of probe diameters. The velocity error was then approximated by a polynomial of the form

$$\epsilon_x = A_0 + A_1\ (9.5 - D) + A_2\ (9.5 - D)^2 \tag{B(13)}$$

where D is measured from the wall through which the probe was inserted. The result is shown in Fig. B5. The error was less than 2% at distances greater the 0.25 inches from

the wall. In order to extrapolate the correction to larger values of velocity, the error was represented as a function of X. The coefficients in Eq. B(13) were plotted as a function of X, and the result is shown in Fig. B6. A_0, A_1 and A_2 were seen to be almost linear functions of X and were therefore approximated by

$$A_0 = B_0 + B_1 X_{.95} + B_2 X_{.95}^2$$

$$A_1 = C_0 + C_1 X_{.95} + C_2 X_{.95}^2$$

$$A_2 = D_0 + D_1 X_{.95} + D_2 X_{.95}^2$$

where $X_{.95}$ was the value of X at D = 9.5. Values of X(corrected) minus X(uncorrected) verses immersion depth are shown in Fig. B7. Because of the aerodynamic design of the probe, the corrections necessary for boundary effects are small.

Results for the induced pitch angle error are shown in Fig. B8. Since these errors were within the resolution capability of the probe ($1\frac{1}{2}^{\circ}$), no correction was made.

B4. COMBINATION PROBE MEASUREMENTS IN STEADY SWIRLING FLOW

Additional errors may be present when a pneumatic probe is immersed in a swirling flow. Fig. B9 shows the apparatus which was constructed to investigate this possibility. The apparatus consisted of an annulus with a channel height of $1\frac{1}{2}$ inches (10 inches in outer diameter). A total of 40 static wall readings were available and a provision was made for probe surveys at different axial stations. The

swirl velocity was generated by a single stage of stator blading at the entrance to the annulus. Initial measurements suggested the possibility of boundary layer separation and reverse flow near the hub. In an effort to correct this problem, a plate was constructed to decrease the channel height at the exit, isolating the pressure at the hub wall from the surrounding atmosphere, and blocking backflow.

Results are given in Fig. B10 which shows the static pressure derived from the probe calibration. Agreement is very close near the hub with a moderate departure near the tip at the highest Mach number.

B5. CALIBRATION OF THE WEDGE PROBE

A type of probe which is reported to give a good indication of static pressure over a wide range of Mach number is the wedge static probe illustrated in Fig. 5. The probe has a hatchet-shaped head with small pressure taps in each face of the wedge. In principle, if the leading edge is sharp and the wedge angle is small, the flow past the sensing orifice will be almost unperturbed, and the measured pressure will be close to the static pressure in the undisturbed flow.

The static pressure may thus be determined by

$$P_S = (P_{2/3} - P_A) + P_A \qquad B(11)$$

where it is assumed the probe is aligned in the flow with P_2 and P_3 equal, and P_A is the reference atmospheric pressure.

The wedge probe shown in Fig. 5 was traversed in both the free jet and the swirling annular flows through the same range of Mach numbers reported for the combination probe. However, the characteristics of the probe in swirling flow were not fully determined. It was found in analyzing the results of the tests in the swirl annulus that the radial gradient in the flow angle gave rise to probe readings which were in error when the probe was rotated to balance. This was explained by the difference in the radial position of the sensors on the two faces of the wedge. It was therefore necessary to use the combination probe to sense flow direction in the compressor measurements and to set the wedge to the measured angle.

Table B1

Probe Calibration Coefficients for $F\phi = F\phi(X,\phi)$

Order of Coefficient	$a_i^0(X)$	$a_i^1(X)$	$a_i^2(X)$	$a_i^3(X)$	$a_i^4(X)$	$a_i^5(X)$
Zeroth	-.031966	.007201	.430296	0	0	0
First	.356675	.024152	-5.78223	0	0	0
Second	1.065658	-7.67746	29.28679	0	0	0
Third	-.6217505	5.75709	-31.33828	0	0	0
Fourth	0	0	0	0	0	0
Fifth	0	0	0	0	0	0

Probe Calibration Coefficients for $X = X(Fe,\phi)$

Order of Coefficient	$b_i(\phi)$	$b_i^1(\phi)$	$b_i^2(\phi)$	$b_i^3(\phi)$	$b_i^4(\phi)$	$b_i^5(\phi)$
Zeroth	.049479	3.060194	-16.7985	64.17796	0	0
First	-.096216	5.92345	-76.79957	377.5630	0	0
Second	-.023244	.43807	-73.94789	578.1631	0	0
Third	.465854	-17.54476	138.16714	-187.4164	0	0
Fourth	0	0	0	0	0	0
Fifth	0	0	0	0	0	0

Table B2

Error Analysis of Limiting
Velocity From Combination Probe Calibration

ϕ	%E	X	X_1	%E	X	X_1
-8	1.240859	.131396	.133026	1.294396	.164529	.166658
-4	..179254	.131396	.131631			
0	.278352	.131396	.131761	.500537	.164718	.165542
4	-1.363128	.131396	.129604	1.408336	.164718	.016703
8	-1.530939	.131396	.129384	.203496	.164718	.165053
12	-0.680858	.131396	.130501	.651461	.164718	.165791
-8	1.000402	.19477	.196718	.233878	.220488	.221003
-4	-0.117261	.194314	.194086	.152853	.220744	.221081
0	.169147	.104618	.194947	-.114982	.220616	.220362
4	-0.214012	.194161	.193745	-.092819	.221253	.221047
8	-0.358790	.194466	.193768	-1.029916	.220871	.218596
12	.376707	.19477	.195503	-.646592	.220616	.219189
-8	-1.239331	.246923	.243862	.237152	.287457	.288138
-4	-0.034597	.247245	.247159	1.076403	.287457	.290551
0	-0.146786	.247138	.246775	1.024665	.28754	.290486
4	-0.515128	.24703	.245757-	.471649	.287872	.289229
8	-1.285034	.24703	.243855	-1.434447	.287872	.283742
12	-1.132503	.246923	.244126	.699168	.287872	.289884
-8	4.327326	.330596	.344901	.274718	.342723	.343664
-4	-3.051296	.330723	.340814	-1.857185	.342664	.336300
0	1.741821	.329579	.335319	-1.009610	.34284	.339378
4	2.010646	.330343	.336985	-.969406	.342488	.339167
8	2.250762	.330089	.337518	-1.002690	.342488	.339053
12	-0.449206	.330089	.328606	-1.115949	.342547	.338724

ϕ = Pitch Angle X = Actual Value

X_1 = Computed Value %E = % Error

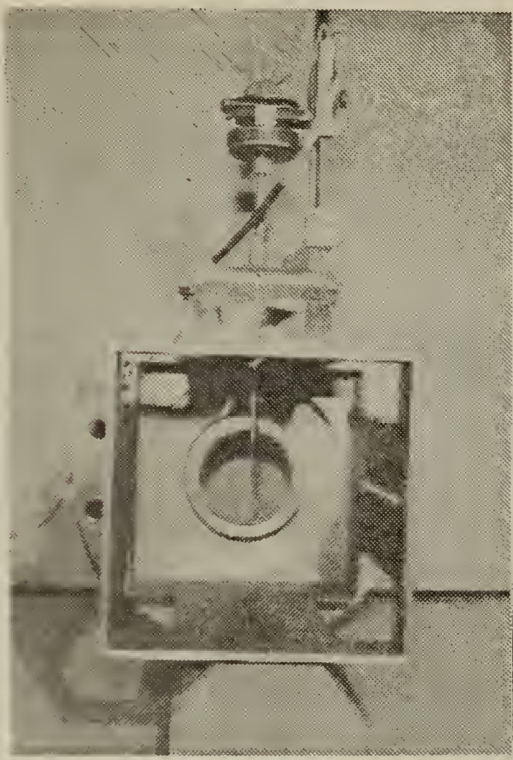

END VIEW

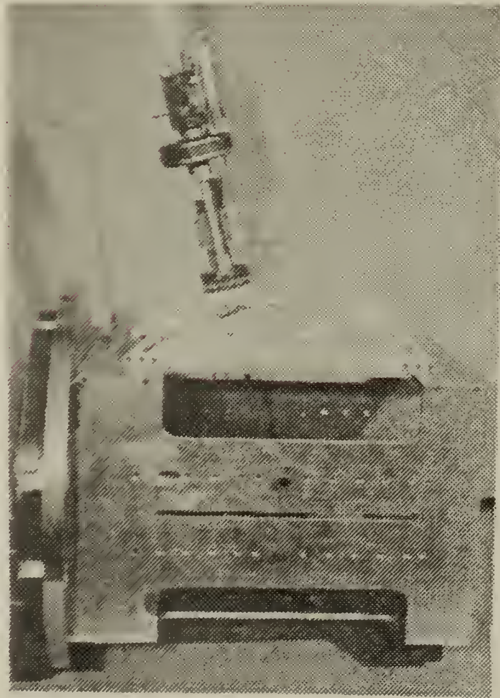

SIDE VIEW

FIG. B1 FREE-JET APPARATUS USED TO CALIBRATE PROBES

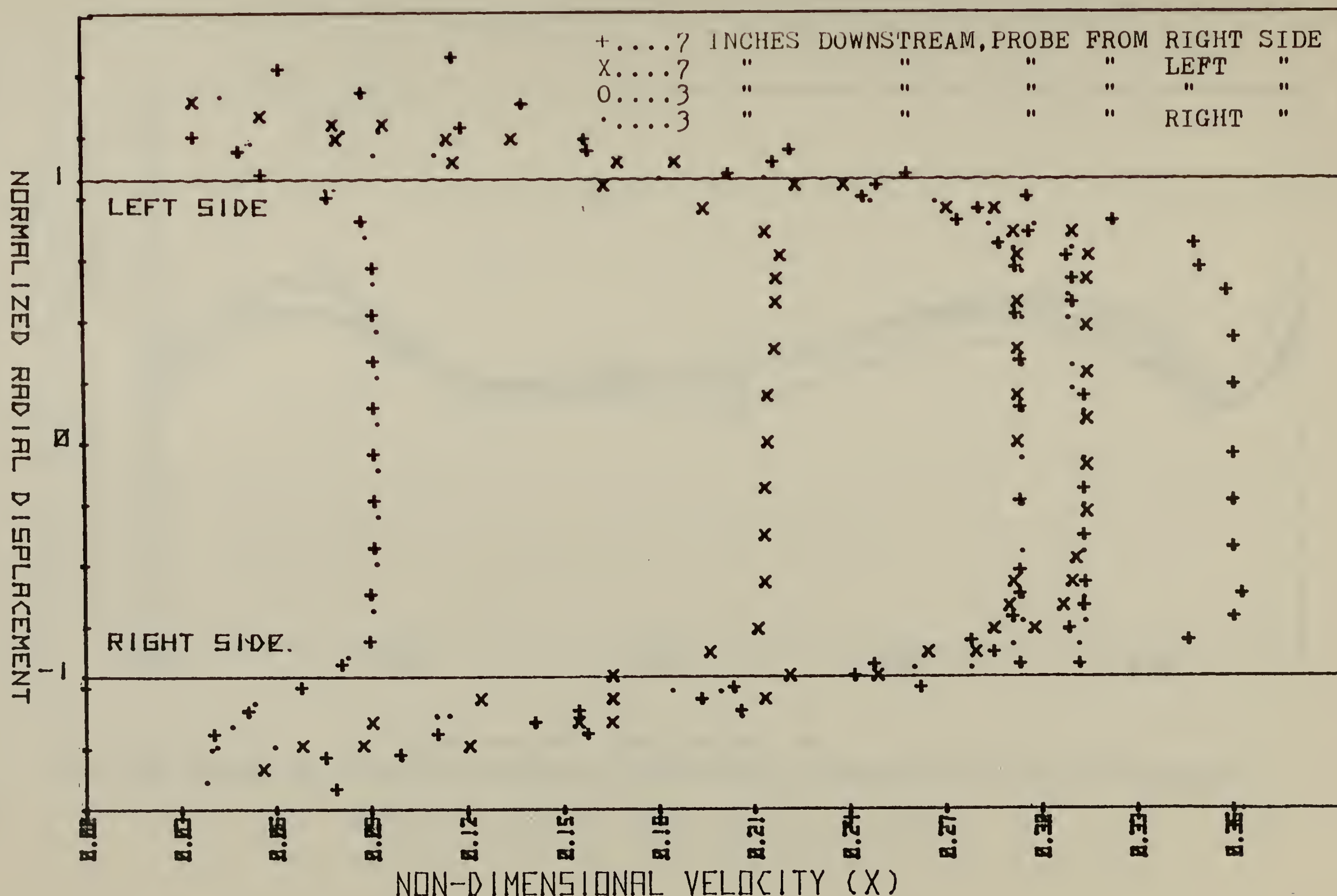

FIG. B2 VELOCITY PROFILES FOR VARIOUS MACH NUMBERS MEASURED IN A 4.2 INCH FREE-JET

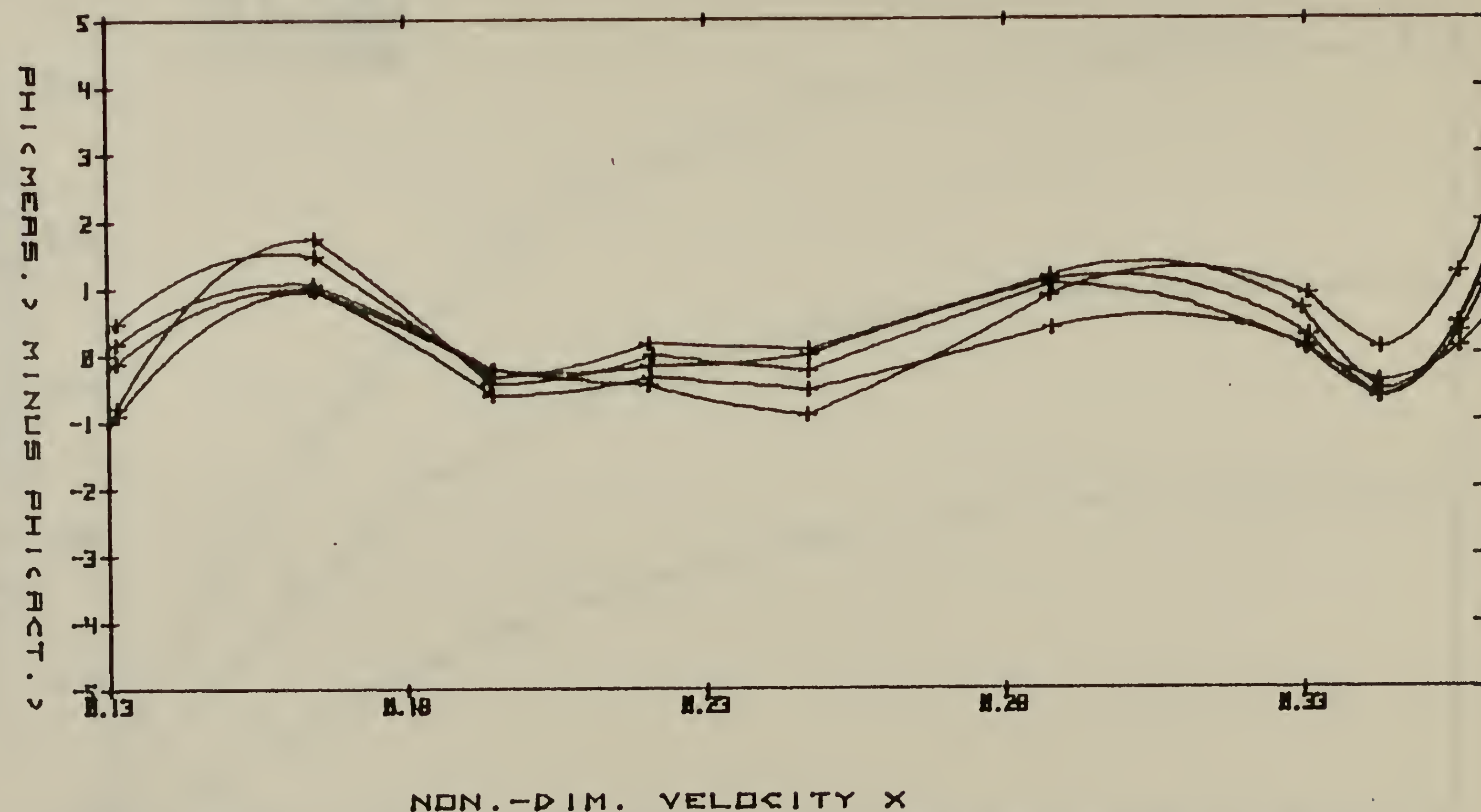

FIG. B3 ERROR IN PITCH ANGLE DERIVED FROM THE COMBINATION PROBE CALIBRATION

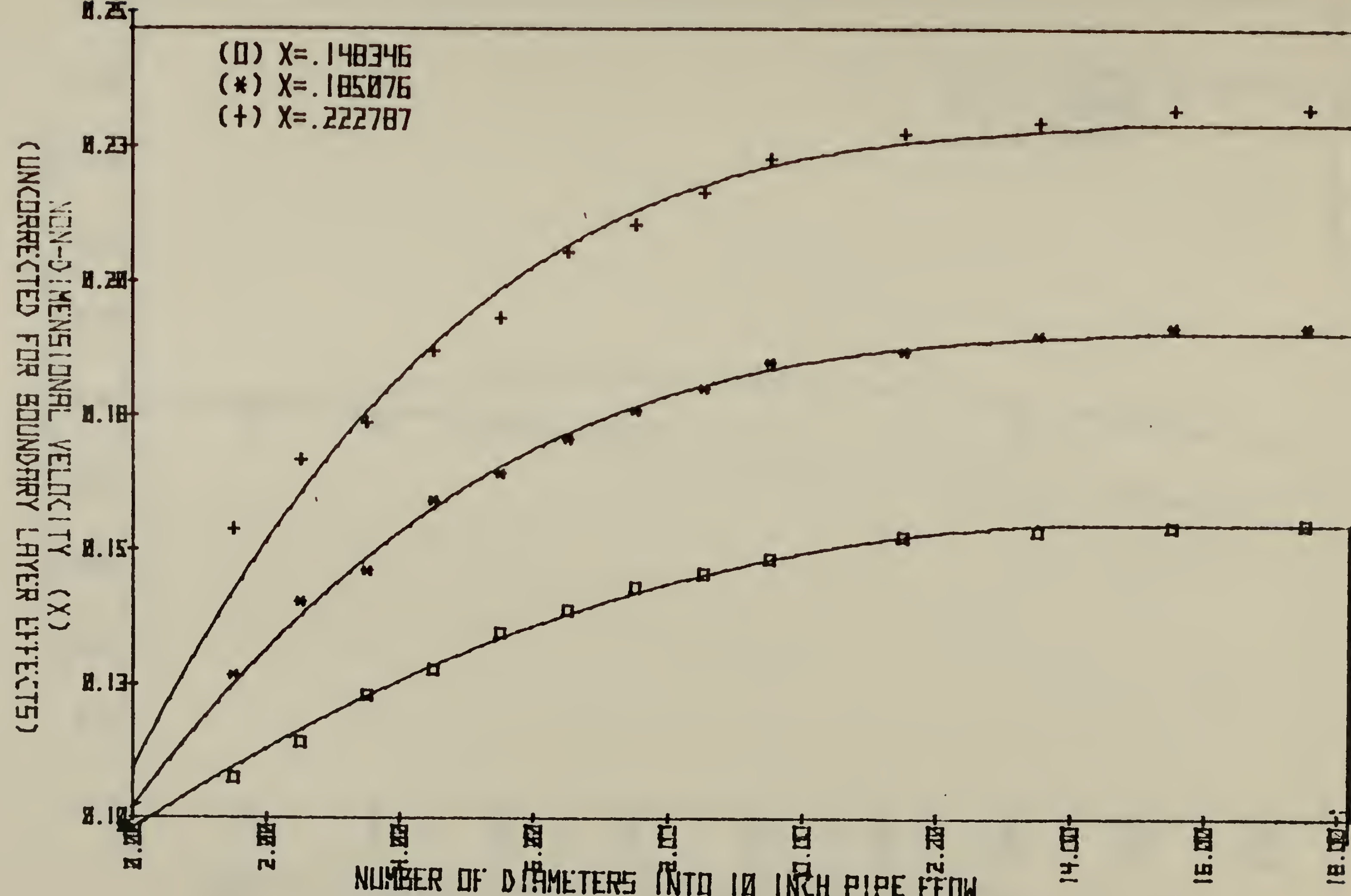

FIG. B4 DISTRIBUTION OF VELOCITY MEASURED IN A 10 INCH PIPE FLOW

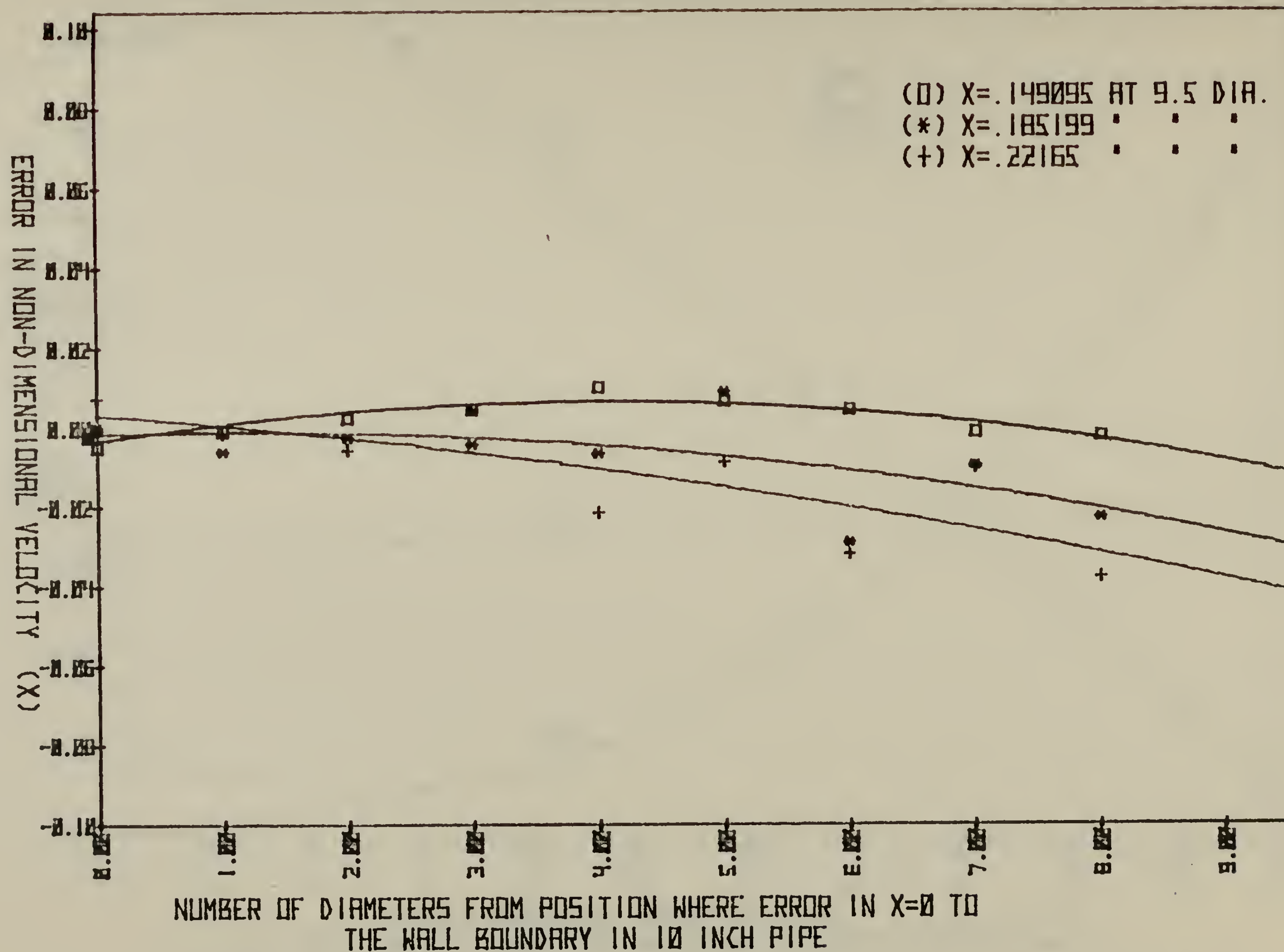

FIG. B5 ERROR IN VELOCITY DUE TO BOUNDARY EFFECTS IN A 10 INCH PIPE FLOW

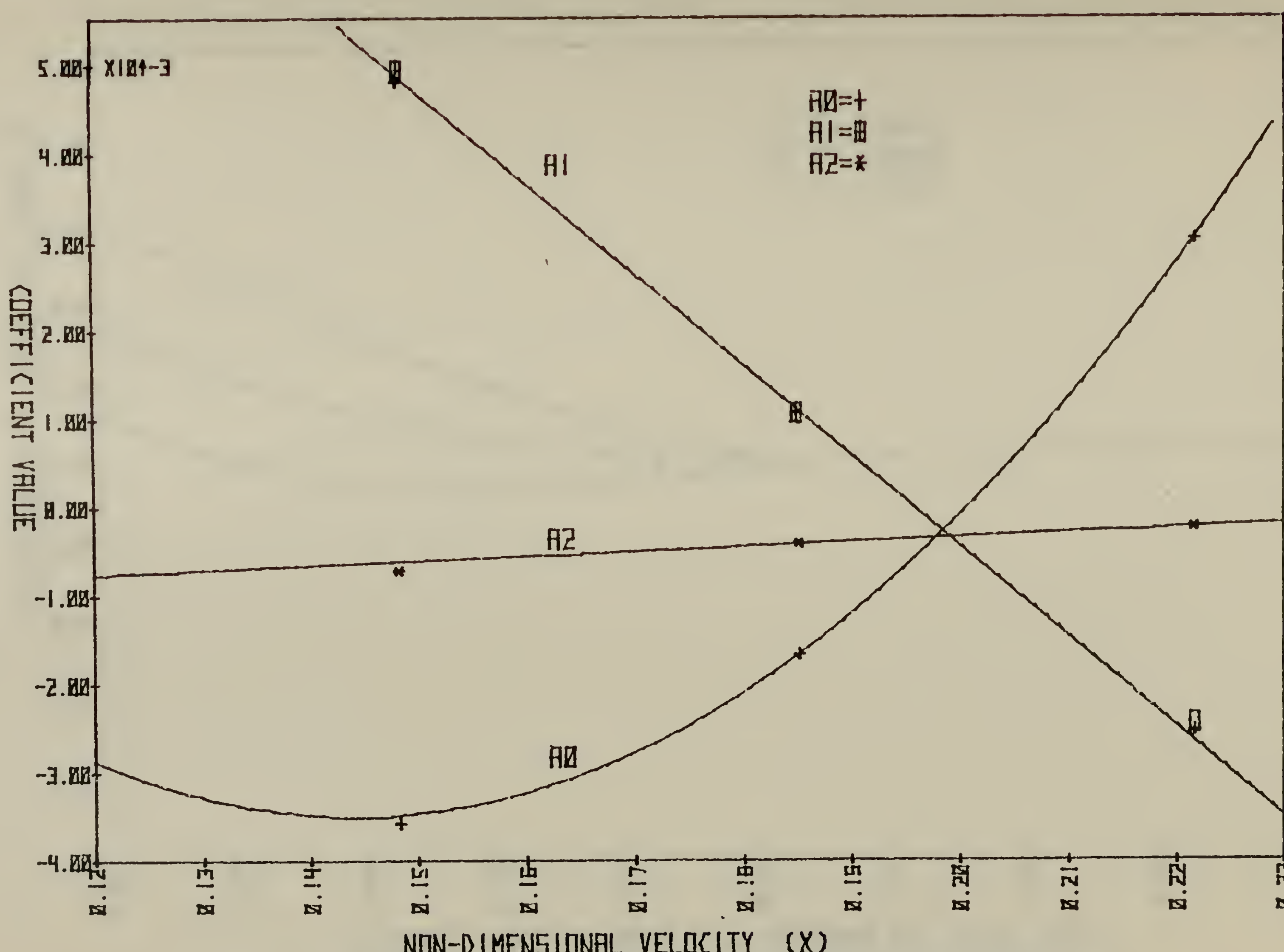

FIG. B6 COEFFICIENTS FOR BOUNDARY EFFECT CORRECTION

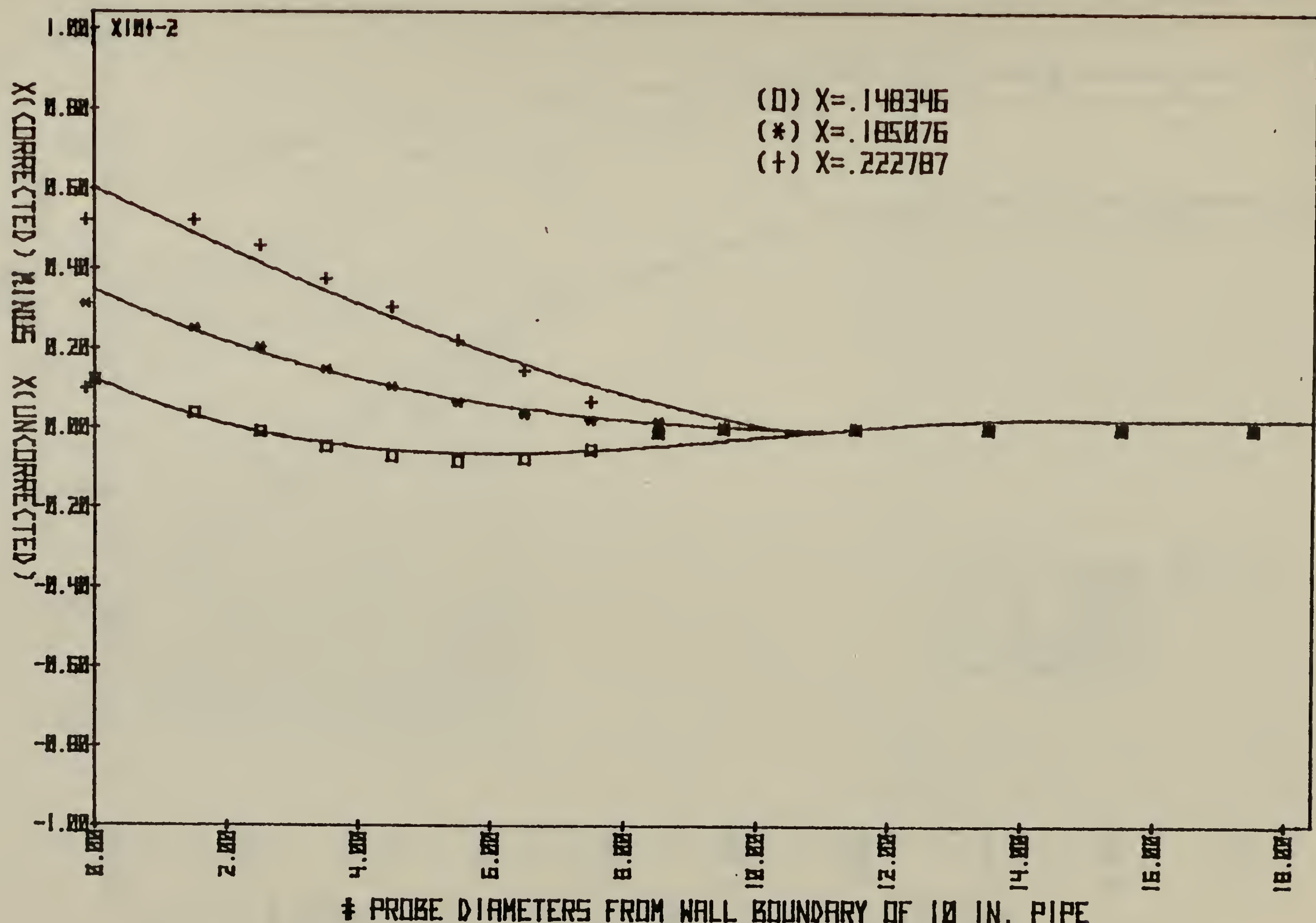

FIG. B7 MAGNITUDE OF THE CORRECTION IN VELOCITY RESULTING FROM BOUNDARY EFFECT

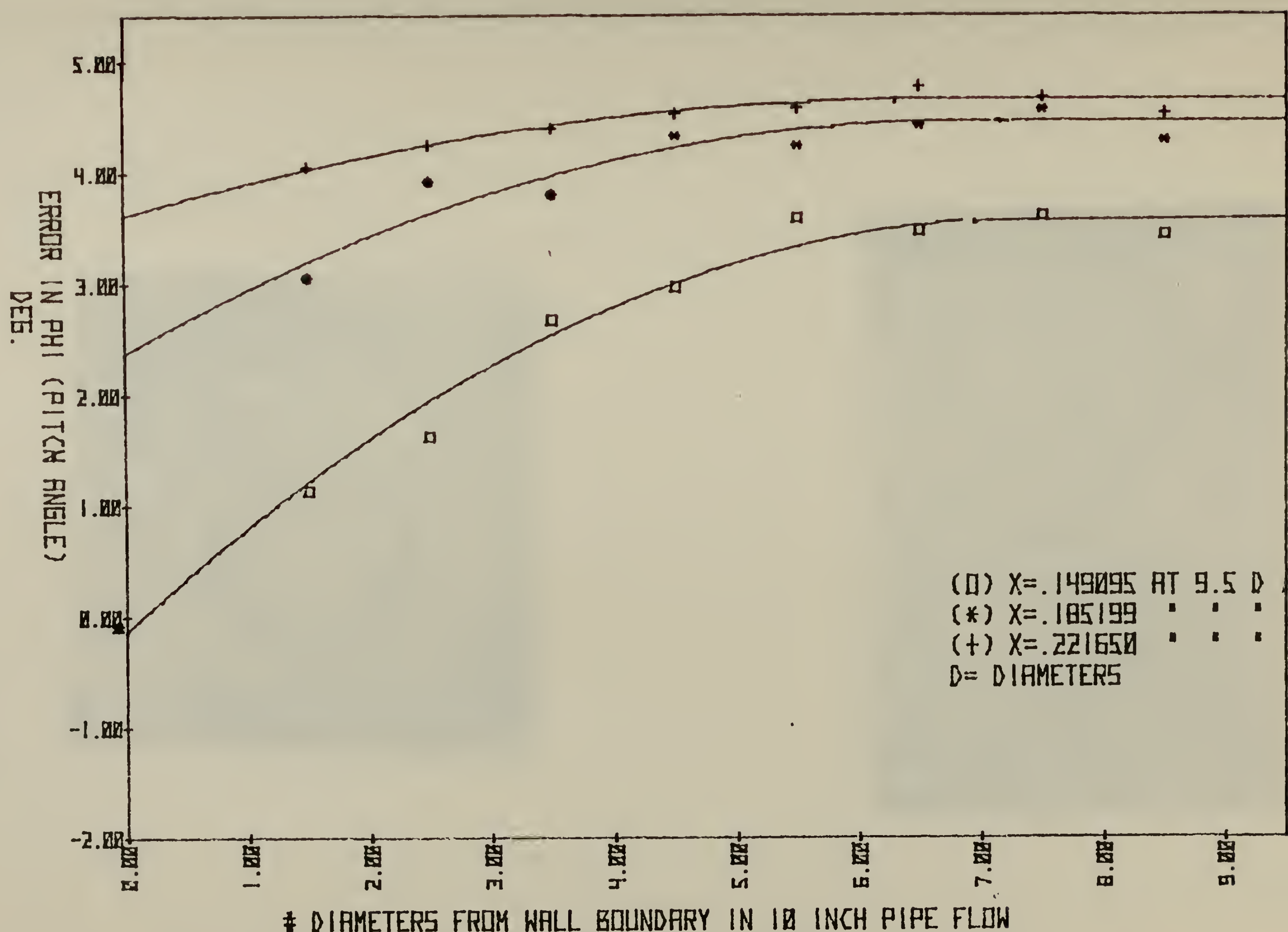

FIG. B8 ERROR IN PITCH ANGLE DUE TO BOUNDARY EFFECT IN A 10 INCH PIPE FLOW

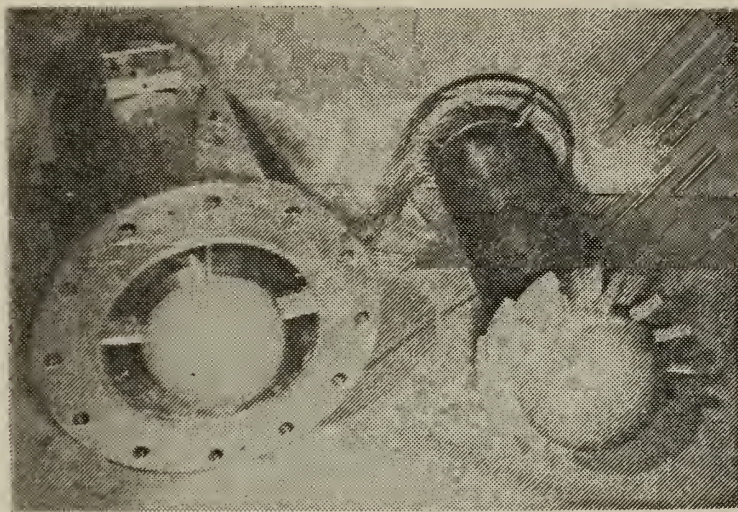

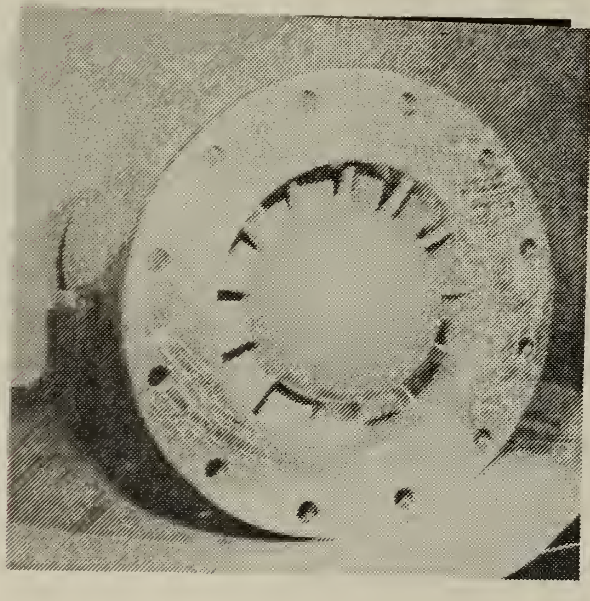

FIG. B9 SWIRL ANNULUS APPARATUS

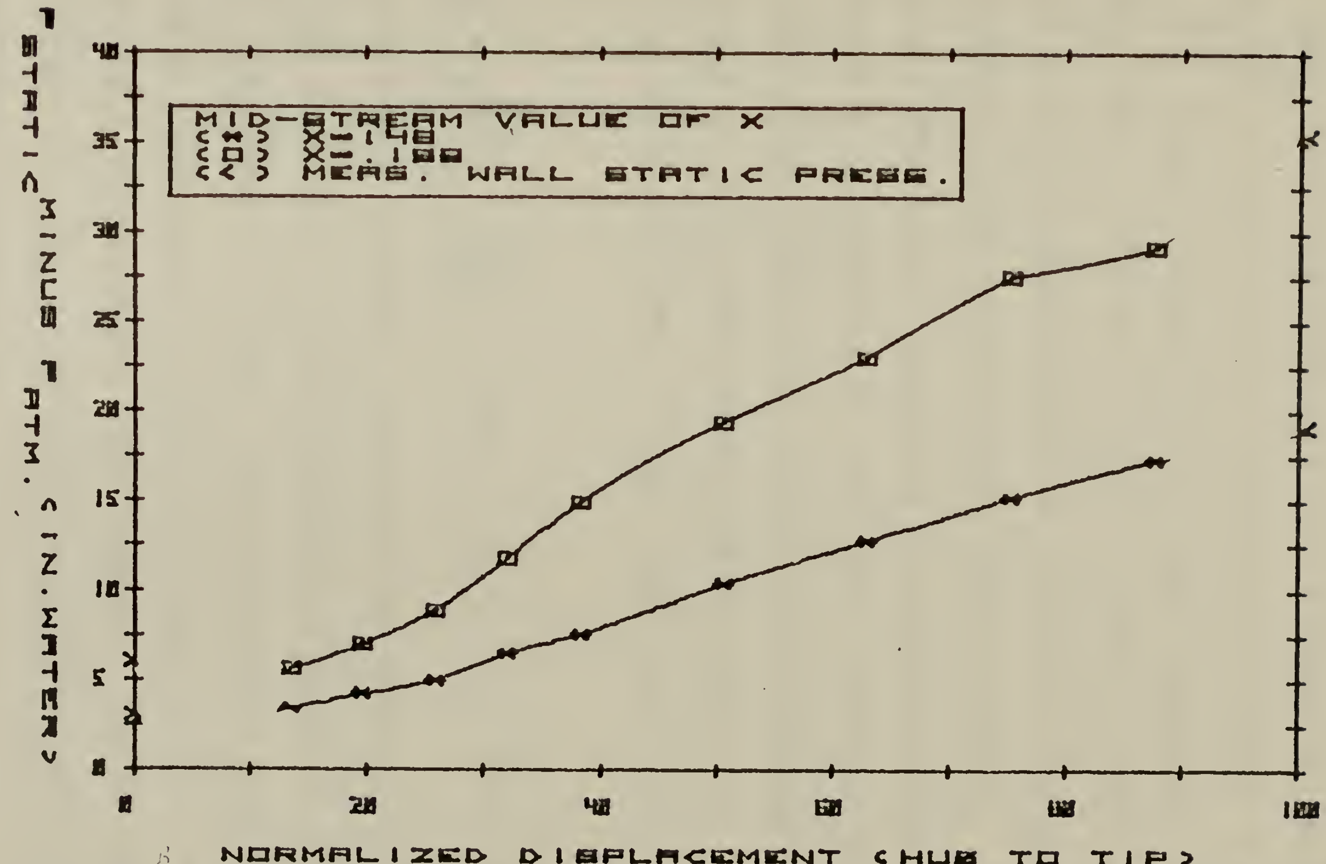

FIG. 10 RESULTS OF SWIRL ANNULUS TEST OF COMB. PROBE

APPENDIX C: INLET FLOW FIELD DETERMINATION

C1. METHOD OF APPROACH

An important consideration in a transonic compressor installation is the velocity profile at the face of the rotor. The profile depends on the inlet shape and the mass flow rate. The following analysis is based on the assumption that a close approximation to the true velocity may be calculated if the referred flow rate is known.

Seven surveys were conducted by Anderson (Ref. 3) in which accurate calculation of the inlet velocity profiles was accomplished using a calibrated United Sensor Probe over a range of flow rates tabulated in Table C1.

Reference 11 defines a "total flow function," , given by

$$\Phi = \frac{\rho \bar{V}}{\rho_t V_t} = \frac{\dot{W}/A}{\rho_t V_t} = F(X) = X(1 - X^2)^{1/(\gamma-1)} \qquad C(1)$$

The flow function provides the means of replacing density in the equation with the non-dimensional velocity (X) for internal compressible flows. For each survey conducted in Ref. 3, Φ was calculated at each point and plotted versus the normalized displacement (hub to tip). The results are shown in Fig. C1. Each curve was then fitted with a suitable polynomial of the form

$$\Phi = a_0 + a_1 H + a_2 H^2 + a_3 H^3 + \ldots \qquad C(2)$$

where H = normalized displacement (hub to tip) and a_1, a_2,..

are determined by a polynomial regression curve fitting routine. The value of the total flow function at the centerline (Φ_{cL}) was evaluated for each case. Values of Φ/Φ_{cL} for each survey were then calculated and plotted against H. The resulting curves shown in Fig. C2 were then approximated by a family of polynomials having the form

$$\bar{\Phi} = \Phi/\Phi_{cL} = A_0 + A_1 H + A_2 H^2 \dots \qquad C(3)$$

which is then called the 'normalized flow function.'

The referred flow rate is defined as

$$\dot{W}^* = \frac{\dot{\omega}\sqrt{\theta}}{\delta'} \qquad C(4)$$

where

$$\Theta = \frac{T_{t_0}}{T_{ref}} \qquad C(5)$$

and

$$\delta' = \frac{P_{t_0}}{P_{ref}} \qquad C(6)$$

and $\dot{\omega}$ = mass flow rate.

A plot of Φ_{cL} versus $\dot{W}^*$ shown in Fig. C3 yielded the following linear relationship:

$$\Phi_{cL} = b_0 + b_1 \dot{W}^* \qquad C(7)$$

Thus, Eq. C(3) and Eq. C(7) provide an analytical representation of the inlet flow profile in terms of the referred flow rate only.

C2. APPLICATION

For each run of the transonic compressor, $\dot{W}^*$ is calculated and Φ_{cL} is then evaluated from Eq. C(7). Φ can then be evaluated from Eq. C(3).

X is then evaluated as the subsonic solution of the flow function given by Eq. C(1) using Newton's method as follows:

1) Guess $X = X_0$
2) Calculate

$$\Phi_2 = X\,(1 - X^2)^{1/(\gamma-1)} \qquad C(8)$$

$$\frac{d\Phi}{dX} = \Phi_2 \left[\frac{1}{X} - \frac{2}{(\gamma-1)}\left(\frac{X}{1-X^2}\right)\right] \qquad C(9)$$

$$X = X + \frac{\Phi_1 - \Phi_2}{\frac{d\Phi}{dX}} \qquad C(10)$$

3) Now test for convergence of Φ.

If $|\Phi_2 - \Phi_1| < .00001$ then the calculation is complete. If this requirement is not satisfied then the new Φ_2 in Eq. C(8) is calculated using the new X in Eq. C(10).

4) Mach number is calculated using Eq. B(4).

Table C1

Flow Rates Used for Inlet Velocity Determination

Referred Flow Rate	Centerline Value of Flow Function
8.95	.09589
9.38	.101607
10.89	.11693
11.18	.12039
11.42	.122025
13.83	.151239
14.30	.156789

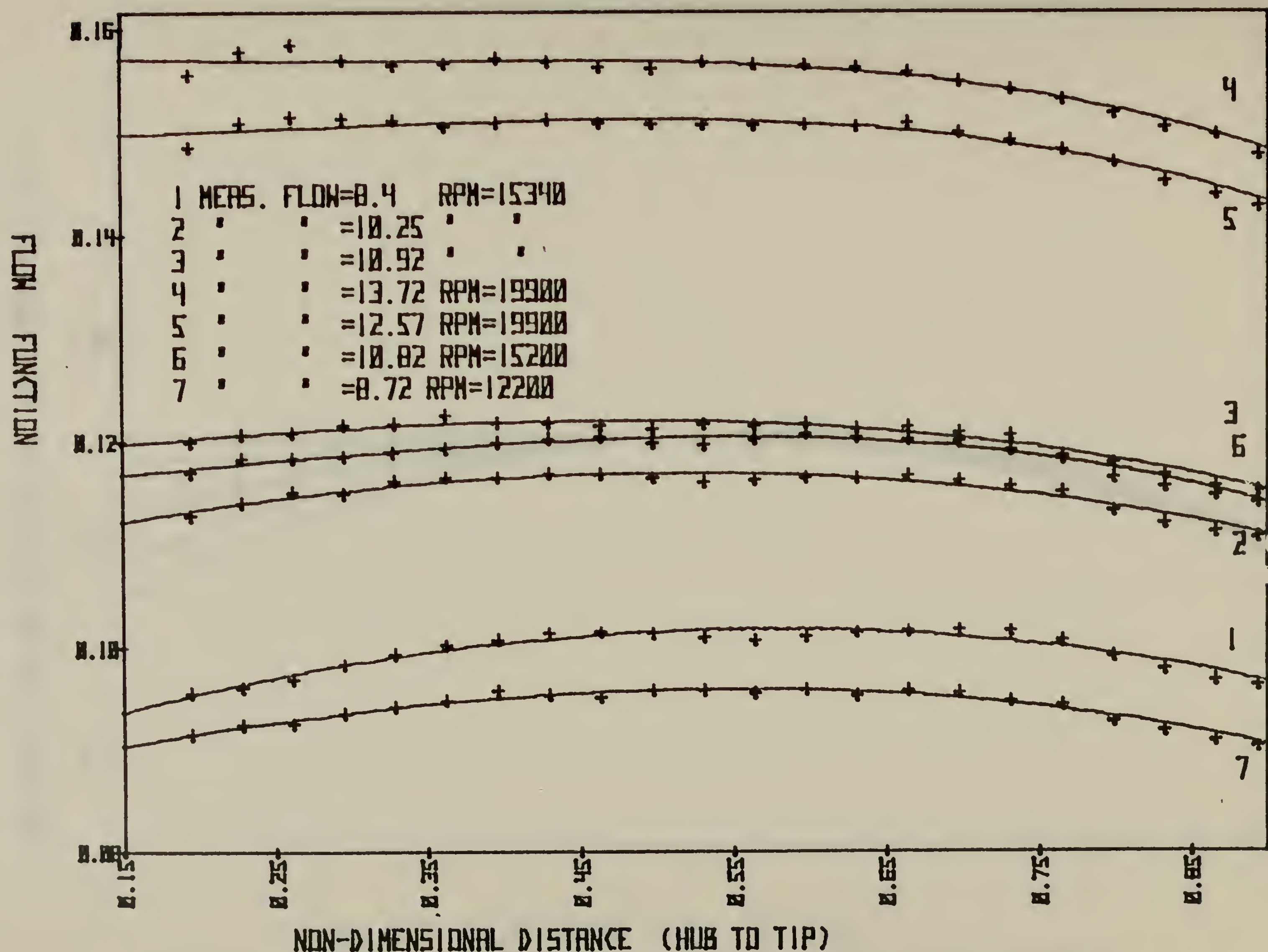

FIG. C1 TOTAL FLOW FUNCTION VS. NORMALIZED DISPLACEMENT UPSTREAM OF THE ROTOR

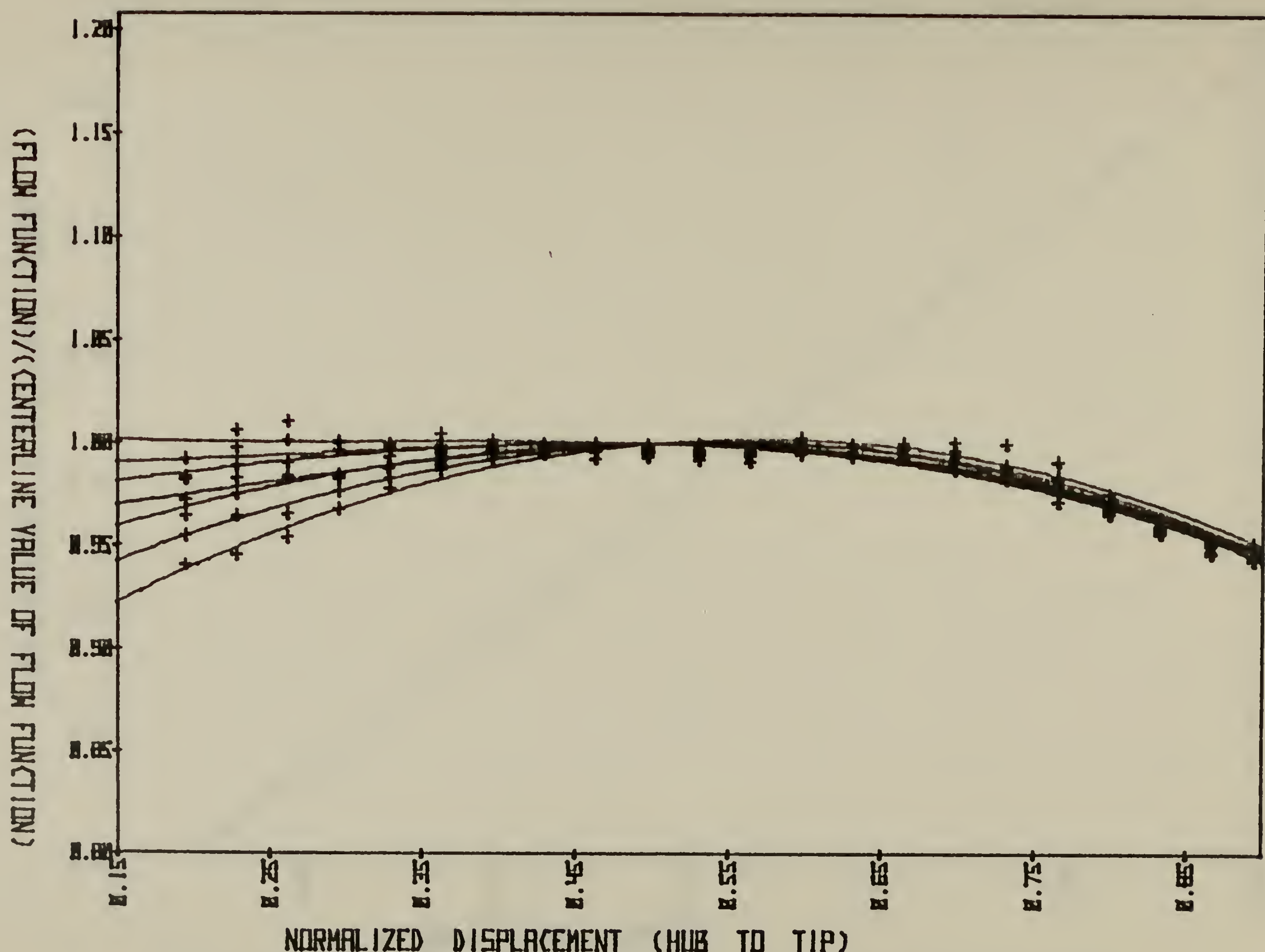

FIG. C2 NORMALIZED FLOW FUNCTION VS. NORMALIZED DISPLACEMENT UPSTREAM OF THE ROTOR

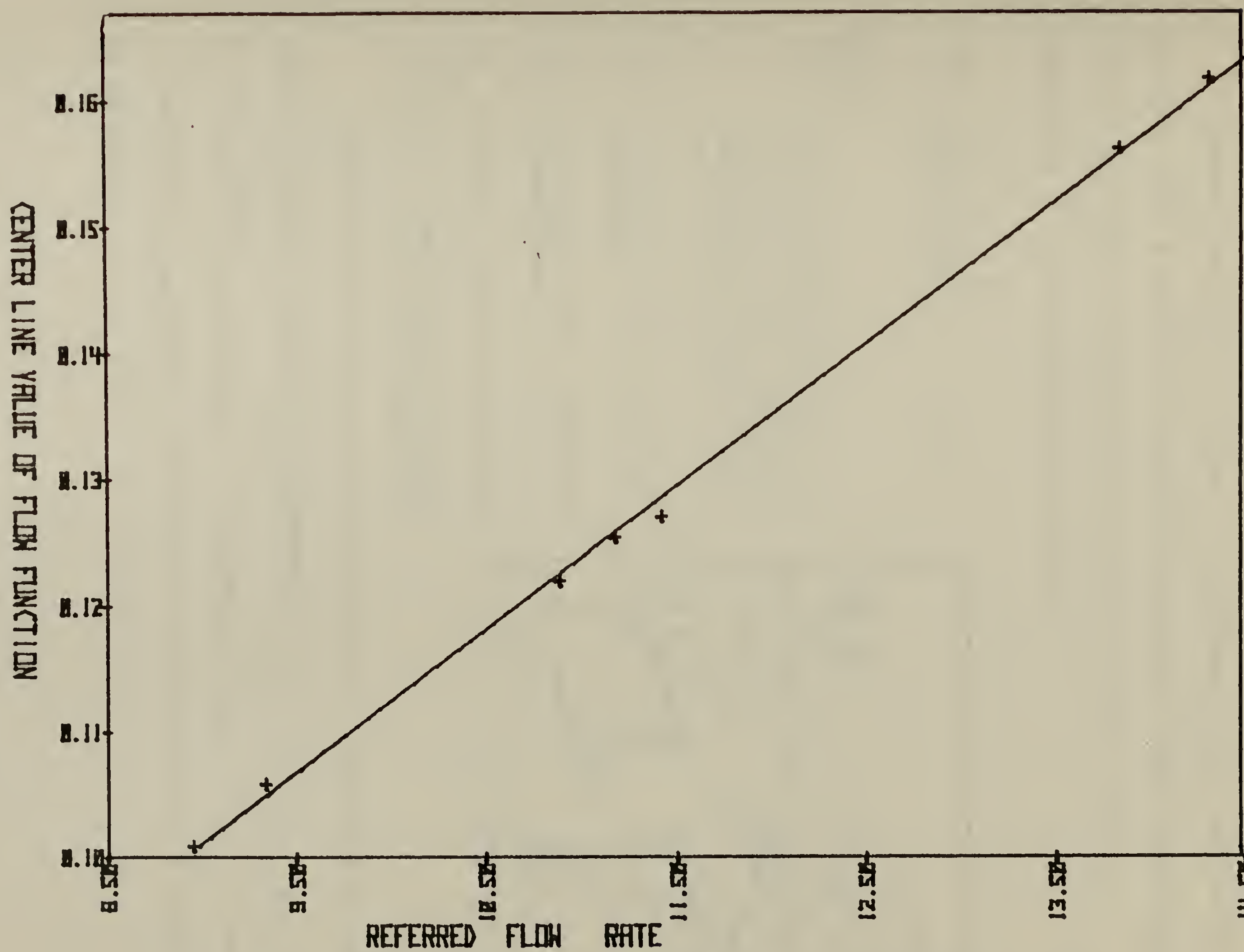

FIG. C3 FLOW FUNCTION AT MID SPAN VS. REFERRED FLOW RATE

APPENDIX D: ROTOR LOSSES

D1. NASA LOSS COEFFICIENT

Losses incurred in flows in turbomachinery may be described with a varity of methods depending upon the measurements available and the specific application. Ref. 1 describes a loss coefficient defined by

$$\bar{\omega}' = \frac{(P_2')_{id} - P_2'}{P_1' - P_1} \qquad D(1)$$

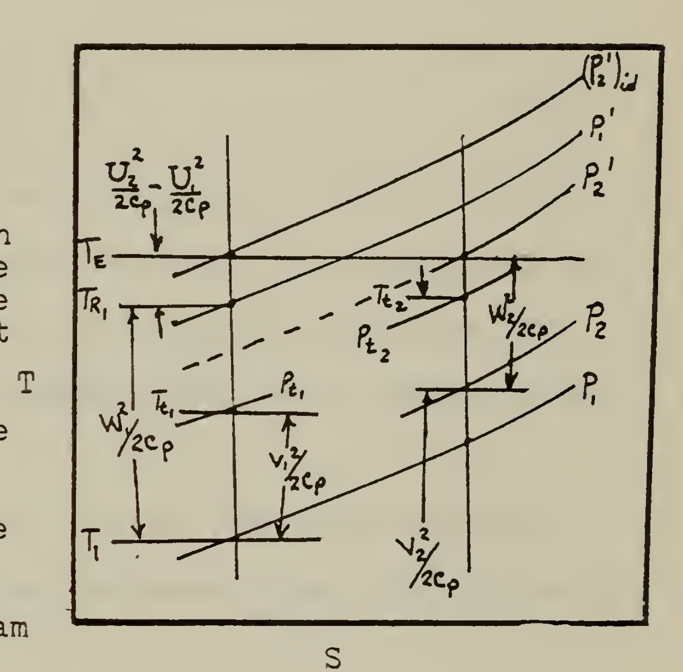

where

$\bar{\omega}'$ = mass-averaged defect in relative total pressure divided by the pressure equivalent of the inlet velocity head

P_1' = relative total pressure upstream

P_2' = relative total pressure downstream

P_1 = static pressure upstream

$(P_2')_{id}$ = ideal relative total pressure downstream

From the measurements obtained and a knowledge of the inlet velocity profile the parameters P_1, P_2, P_{t1}, P_{t2}, X_1, X_2, T_{t1}, and T_{t2} are known. A representation of $\bar{\omega}'$ in terms of measured stagnation conditions and velocities (X or M) is desired.

D1.1 Upstream of the Rotor. The following relations may be written:

$$(P_2')_{id} = P_{t1} \left(\frac{T_E}{T_{t1}}\right)^{\gamma/\gamma-1)} = P_{t1} \left[1 - X_{U_2}^2\right]^{\gamma/\gamma-1)} \qquad D(2)$$

$$T_E = T_1 + \frac{W_1^2}{2C_P} + \frac{U_2^2 - U_1^2}{2C_P} \qquad D(3)$$

$$\frac{T_E}{T_{t1}} = 1 - X_1^2 + X_{W1}^2 + X_{U2}^2 - X_{U1}^2 \qquad D(4)$$

where X is a velocity non-dimensionalized as in Eq. B(1), subscript denotes the relative velocity, and subscript W denotes the wheel speed. The other notation is given in the T-S diagram for the flow through the rotor shown in the above sketch.

Using the above equations, for an "impulse" machine for which there is a meridional entrance flow, the following relations result:

$$\frac{T_E}{T_{t1}} = 1 + X_{U_2}^2 \qquad D(5)$$

$$P_1' = P_{t1} \left(1 + X_{U_1}^2 \right)^{\gamma/(\gamma-1)} \qquad D(6)$$

and

$$P_1 = P_{t1} \left(1 - X_1^2 \right)^{\gamma/(\gamma-1)} \qquad D(7)$$

D1.2 Downstream of the Rotor. Sufficient measurements exist at the machine station 2 to derive P_{t2}' using T_{t2}, T_{t2}, $\bar{X}_2$, α_2, and U_2 where $\bar{X}_2$ is the measured downstream velocity, non-dimensionalized using the downstream limiting velocity

(V_{t2}) in Eq. B(1). Alternatively, since T_E= constant for the flow through the rotor (see diagram), then one of the separate measurements is not needed. Two methods were therefore used. Method 1 used all measurements at station 2. Method 2 did not use the temperature rise at station 2, and thus served as a check on the accuracy of the temperature measurement.

(i) Method I (all measurements at station 2)

$$P_2' = P_{t2} \left(\frac{T_E}{T_{t2}}\right)^{\gamma/(\gamma-1)} \qquad D(8)$$

where $\frac{T_E}{T_{t2}}$ is given by

$$\frac{T_E}{T_{t2}} = 1 - X_{U_2}^2 \left(\frac{T_{t1}}{T_{t2}}\right) - 2\bar{X}_2 X_{U_2}\sqrt{\frac{T_{t1}}{T_{t2}}} \sin\alpha_2 \qquad D(9)$$

Using Eq. D(6), D(7), D(8), and D(9) in Eq. D(1), there results

$$\bar{\omega}' = \frac{\left[1+X_{U2}^2\right]^{\gamma/(\gamma-1)} - \left[1+ \frac{X_{U2}^2}{(T_{t1}/T_{t2})} - \frac{2\bar{X}_2 X_{U_2}\sin\alpha_2}{T_{t2}/T_{t1}}\right]^{\frac{\gamma}{\gamma-1}}\left(\frac{P_{t1}}{P_{t2}}\right)}{\left[1 + X_{U1}^2\right]^{\gamma/(\gamma-1)} - \left[1 - X_1^2\right]^{\gamma/(\gamma-1)}}$$

D(10)

(ii) Method II (Temperature measurement at station 2 not needed)

Temperature measurement downstream may be found using the following relation.

$$\frac{T_E}{T_{t2}} = \left(\frac{T_E}{T_{t1}}\right)/(T_{t2}/T_{t1}) = (1+X_{U2}^2)/(T_{t2}/T_{t1}) \qquad D(11)$$

Define

$$\Psi = \frac{T_{t2}}{T_{t1}} = \left[\bar{X}_2 X_{U_2} \sin\alpha_2 + \sqrt{(\bar{X}_2 X_{U_2} \sin{}_2)^2 + 1}\right]^2 \qquad D(12)$$

Using Eq. D(6), D(7), D(11), and D(12) in Eq. D(1), the loss coefficient is given by

$$\bar{\omega}' = \frac{\left[1+X_{U_2}^2\right]^{\gamma/(\gamma-1)} - \left[(1+X_{U_2}^2)/\Psi^2\right]^{\gamma/(\gamma-1)}}{\left[1+X_{U1}^2\right]^{\gamma/(\gamma-1)} - \left[1-X_1^2\right]^{\gamma/(\gamma-1)}} \left(\frac{P_{t_2}}{P_{t1}}\right) \qquad D(13)$$

D2.. DIFFUSION FACTOR

Ref. 1 reports results of correlating compressor losses in terms of the "diffusion factor". This approach results from the argument that the loss in stagnation pressure depends largely on the suction-surface adverse pressure gradient, of which the diffusion factor can be shown to be an approximate measure. The diffusion factor of Ref. 1 is defined by

$$D = 1 - \frac{W_2}{W_1} + \frac{R_1 W_{U_1} - R_2 W_{U_2}}{\sigma (R_1 + R_2) W_1} \qquad D(14)$$

In this form, changes in axial velocity and radius through the blade row are accounted for.

It is concluded in Ref. 1 that the total-pressure-loss parameter $(\bar{\omega}' \frac{\cos \beta_2}{2\sigma})$ can be correlated in terms of the above diffusion factor. Each family of blade shapes has a somewhat different correlation curve, however, this presents no real problem as the total number of shapes is limited. The correlation for several types of blading is shown in Fig. 203 of Ref. 1.

BIBLIOGRAPHY

1. National Aeronautics and Space Administration Special Report NASA SP-36, Aerodynamic Design of Axial Flow Compressors (NASA SP-36), Edited by Irving A. Johnson and Robert O. Bullock, 1965

2. Naval Postgraduate School Thesis, Development of a Temperature-Pneumatic Probe and Application at the Rotor Exit in A Transonic Compressor, by F. J. Dodge, June 1976.

3. Naval Postgraduate School Thesis, Velocity Measurements in a Transonic Compressor Using a Calibrated Pressure Probe, by D. S. Anderson, March 1975.

4. Naval Postgraduate School Report NPS-57va72091A, A Description of the Turbopropulsion Laboratory in the Aeronautics Department at the Naval Postgraduate School, by M. H. Vavra and R. P. Shreeve, September 1973.

5. Naval Postgraduate School Thesis, Microprogrammable Data Acquisition and Probe Control System (MIDAS IV) With Application to Compressor Testing, by D. D. Patton, March 1976.

6. Naval Postgraduate School Report NPS-57sf74081, Flow Into a Transonic Compressor Rotor Part 1-Analysis, by R. P. Shreeve, August 1974.

7. Bryer, D. W. and Pankhurst, R. C., Pressure-Probe Methods for Determining Wind Speed and Flow Direction, Her Majesty's Stationary Office, 1971.

8. North Atlantic Treaty Organization Advisory Group for Aerospace Research and Development Report AGARD-LS-83, Modern Prediction Methods for Turbomachine Performance, June 1976.

9. Hewlett-Packard 9830A Calculator: Operating and Programming Manual.

10. Hewlett-Packard 9830A Calculator: 9830A/B Mass Memory Operating Manual.

11. Naval Postgraduate School Report NPS-57sf73072A, Calibration of Flow Nozzles Using Traversing Pitot-Static Probes, by R. P. Shreeve, July 1973.

INITIAL DISTRIBUTION LIST

		No. Copies
1.	Defense Documentation Center Cameron Station Alexandria, Virginia 22314	2
2.	Library, Code 0142 Naval Postgraduate School Monterey, California 93940	2
3.	Department Chairman, Code 67 Department of Aeronautics Naval Postgraduate School Monterey, California 93940	1
4.	Assoc. Professor R.P. Shreeve, Code 67Sf Department of Aeronautics Naval Postgraduate School Monterey, California 93940	1
5.	LT W.R. Hawkins 77 Truex Place Middletown, New Jersey 07748	1
6.	Mr. J.E. Hammer, Code 67 Department of Aeronautics Naval Postgrauate School Monterey, California 93940	1
7.	Turbo-Propulsion Laboratory, Code 67 Naval Postgraduate School Monterey, California 93940	8
8.	Mr. H.J. Mueller Code 310A, Naval Air Systems Command Navy Department Washington, D.C. 20360	1
9.	Mr. Karl H. Guttman Code 330C, Naval Air Systems Command Navy Department Washington D.C. 20360	1
10.	Mr. Eric Lister R & T Division Naval Air Propulsion Test Center Trenton, New Jersey 08628	1

Thesis
H3515 Hawkins 160576
c.1 Determination of the
blade-element perform-
ance of a small tran-
sonic rotor.